

Dear editor,

we finally managed our response to the referees. In our feeling, the manuscript improved substantially after addressing the major concerns of the referees.

We implemented the following major changes, which are highlighted in the revised manuscript

- we discussed results for malonic acid in the context of Koehler theory and Kelvin/Frankel Hill Halsey adsorption theory and introduced the new Figure 7
- we implemented a refined analysis of our SMPS data, which led to a more convincing relation between AMS and SPMS results
- we discussed the relation between pure oleic acid and oleic acid films
- we removed all unclear formulations as requested by the referees, especially regarding the experiments at “enhanced” RH and the treatment of multiple charged particles.
- we reformulated section 3.2
- we added clarifying supplementary material in response to major comments by the referee.

With best regards

Thomas Mentel

Cloud Condensation Nuclei Activity of CaCO₃ Particles with Oleic Acid and Malonic Acid Coatings

Mingjin Wang^{1,2}, Tong Zhu^{1*}, Defeng Zhao², Florian Rubach^{2,3}, Andreas Wahner², Astrid Kiendler-Scharr², and Thomas F. Mentel^{2*}

In this paper the effect of coating of oleic acid (low solubility in water) and malonic acid (water soluble) on the activation of particles to cloud drops is investigated. The CCNC experiments seem to be carried out according to present practice and the coating is done with great care.

It is thus disappointing that data evaluation does not meet the same standards. I have mainly identified two areas in which I would have liked to see a deeper analysis:

We thank the reviewer for the positive and critical remarks. We will address the critical remarks in the following.

Tables and Figures for illustration of the responses are given in an appended document.

CI. A full Koehler theory treatment based on the chemical composition of the particles would have been useful. A theoretical consideration of the expected changes in kappa values due to the reactions suggested and bilayer of oleic acid would improve the paper.

Response:

The advantage of using kappa approach (Petters and Kreidenweis, 2007) is that all differences in the (underdetermined) system are mapped to one parameter (i.e. the ratio of the partial molar volumes of water and the solute(s)) and thus CCN activation of differently composed particles becomes comparable. We would like to note, that in Figure 5 and 7 we show the observations in the domain critical supersaturation vs dry diameter relative to fixed kappa lines. For ideal solutions at activation the data in these plots should “parallel” the kappa lines, thus represent one kappa. Deviation from kappa lines indicates non-ideality and other limitations of the kappa approach.

The Koehler theory is described in details by Koehler (1936). For applying Koehler theory to CaCO₃ particles coated with malonic acid at dry condition (RH < 0.7%), we assume that the malonic acid coating will fully dissolve in water when droplets formed. This decreases the activity of water in solution, and thus increases the CCN activity. We assume that at the critical supersaturation (SS_{crit}) the solution is ideal, i.e. water activity coefficient is close to 1, and the partial molar volume of water equals the molar volume of pure water M_w/ρ_w. Since the solubility of CaCO₃ in water is very low (0.00058 g/100 g water, at 298 K), while the solubility of malonic acid (MA) is quite high (62 g/100 g water at 298 K), we apply the linearized approach (e.g. Seinfeld and Pandis 2006), to predict the saturation ratio as a function of the mole solute on a insoluble core:

$$\ln\left(\frac{P_w(D_p)}{P^\circ}\right) = \frac{A}{D_p} - \frac{B}{(D_p^3 - d_u^3)}$$

In this equation A represents the Kelvin effect while B contains the solute effect:

$$A = \frac{4M_w\sigma_w}{RT\rho_w} \cong \frac{0.66}{T} \quad (\text{in } \mu\text{m})$$

$$B = \frac{6n_s M_w}{\pi \rho_w} \cong \frac{3.44 \times 10^{13} v m_s}{M_s} \quad (\text{in } \mu\text{m}^3)$$

Herein $P_w(D_p)$ is the water vapor pressure over the droplet of diameter D_p ; P^o is the water vapor pressure over a flat surface at the same T ; D_p is droplet diameter; d_u is the diameter of insoluble particle fraction, in our case the CaCO_3 core; M_w is water molecular weight; σ_w is the air-water surface tension; ρ_w is the water density; T is in K; R is the universal gas constant; n_s is solute moles; v is the dissociation degree, i.e. the number of ions resulting from the dissociation of one solute molecule; m_s is solute mass per particle; M_s is solute molecular weight.

As the solubility of CaCO_3 in water is very low, activation of CaCO_3 and other mineral dust components is often predicted by a water adsorption approach, wherein the solute term B in the Köhler equation above is replaced by a water adsorption term. The equations show application of the Frenkel Halsey Hill adsorption isotherm (FHH, Sorjamaa and Laaksonen, 2007, Kumar et al. 2009):

$$B = -A_{FHH} \cdot \theta^{-B_{FHH}}$$

Therein we approach the water coverage θ by (Sorjamaa and Laaksonen, 2007):

$$\theta = \frac{D_p - d_u}{2 \cdot 2.75 \cdot 10^{-4}}$$

Therein A_{FHH} is a measure for the intermolecular interaction of water with the substrate surface whereas B_{FHH} characterizes the intermolecular interaction within higher adsorbed water layers. Kumar et al. (2009) gave parameter for CaCO_3 ($A_{FHH}=0.25$ and $B_{FHH}=1.19$, FHH approach) and we will use this later to yield SS_{crit} for bare CaCO_3 particles.

We applied Köhler theory to predict the CCN activation for the malonic acid coatings on the CaCO_3 particles at $T = 293$ K. We neglected the little dissolvable CaCO_3 and assumed that only malonic acid molecules contributed to the dynamic growth. The insoluble CaCO_3 core was set to $d_u = 0.1019 \mu\text{m}$ as measured. We further assume that CaCO_3 doesn't react with malonic acid and that the surface

tension of the solution at activation is that of pure water. The dissociation constants $\text{p}K_{A1}$ and $\text{p}K_{A2}$ of malonic acid are 2.8 and 5.7 in water, respectively. So MA will partly dissociate in water and in the limit of infinite dilute solutions the dissociation degree ν (van' Hoff factor) will be three for full dissociation. The amount of malonic acid coating m_s was taken from the AMS data in Table 1 (revised) in our manuscript and the mole MA solute was calculated applying the dissociation degree of $\nu = 3$ and the molecular mass of malonic acid of $M_s = 104.1 \text{ g mol}^{-1}$. The resulting Koehler curves, equilibrium supersaturation (SS) over the solution droplet as a function of the wet diameter D_p , are shown in Figure S1. In Figure S1, the maximum of each SS curve is the critical supersaturation (theory SS_{crit}). In Table S1 and Figure 2S we compare the SS_{crit} predicted by the Köhler approach (red) with the observed SS_{crit} (black). Köhler theory overpredicts SS_{crit} for thin coatings, but with increasing coating Köhler theory approaches the observed SS_{crit} and the SS_{crit} for a particle with 121 nm diameter composed of pure malonic acid is the limiting case (red filled circle).

In Figure S2 are also shown the $\text{SS}_{\text{crit}} = 1.49$ for bare CaCO_3 particles with $d_{\text{dry}} = 101.9 \text{ nm}$, calculated from the observed κ 's in our study, and the range of κ 's given in the literature for wet generated particles (Tang et al. 2016).

From the Köhler results we derived the predicted water content of the particles at point of activation and we calculated molality and mass fraction of the solute in the solution at the point of activation. The molality at minimum and maximum malonic acid load of $3.3 \cdot 10^{-12} \text{ ug/particle}$ and $610 \cdot 10^{-12} \text{ ug/particle}$ were $0.006 \text{ mol kg}^{-1}$ and $0.0015 \text{ mol kg}^{-1}$, respectively. We used these values in the AIOMFAC model (Zuend et al. 2011) to calculate the deviation from ideality for the solution at point of activation for a flat solution. The both solutions are highly non-ideal with respect to the MA ($a_x = 0.4$), wherein MA was treated as solute with reference state infinite dilution (mole fraction $x_{\text{solute}} \rightarrow 0$). However this did not affect much the activity coefficient of water, which is essentially 1, water treated as solvent with reference state pure liquid (mole fraction $x_{\text{water}} = 1$). Moreover, in this concentration range, the surface tension of aqueous malonic acid solutions is about 70 dyn/cm , thus the nearly same as for water (Table S2). One should expect that Köhler theory would predict SS quite well under such conditions.

One could imagine that a little CaCO_3 will dissolve in water and in the presence of malonic acid, CO_2 should be driven out, and a solution of CaMalonate could be formed. CaMalonate is still slightly soluble in water (0.365 g/100 g water, at 293 K, Linke and Seidell, 1958), ν for CaMalonate is 2. Solubility of CaMalonate converts into about 0.02 mol/kg water, would thus be in a range where the malonate would be fully dissolve. However, because of $\nu = 2$ for CaMalonate while $\nu = 3$ for the pure malonic acid, formation of CaMalonate will decrease the solute effect.

To bring Köhler theory in agreement with the observation for the thinnest coating, *more* solute entities would be required. Thus, disagreement cannot be caused by an ill determined van't Hoff factor as we used already maximum $\nu = 3$ and reducing ν will increase the deviation. (Note, that recent observations point to the importance of the surface effect by organic surface films over the solute effect for water soluble inorganics in presence of organics, including malonic acid (Ruehl et al., 2016). A lower surface tension will bring Koehler prediction and observation punctually in better agreement and still allow for smaller van't Hoff factors. As an example, at point of activation a surface tension of 55% of σ_w and a van't Hoff factor of one will bring Koehler theory and observation in agreement for the thinnest coating. However, a surface tension 55% of σ_w will cause disagreement for the thickest coating, because the solute term gains in importance. Probably, the findings for the mixed solutions of malonic acid and water soluble ammonium sulfate are not directly transferable to our system with insoluble inorganic core, where we expect dilute aqueous solutions of 0.006 mol/kg of malonic acid at the activation point. At such concentrations malonic acid does not reduce σ_w , moreover in the study of Ruehl et al. (2016) malonic acid was one of the more Koehler kappa behaving organics.)

If we turn back to Koehler theory with focus on the solute term, about 4-5 times the measured MA would be needed for the thinnest MA coating to bring prediction and observation in agreement. It cannot be due to a simple calibration error of 4-5, as that would apply to all coating amounts and would lead to mismatches at the thicker coatings. Moreover, a postulated missing mass of $14\text{-}17.5 \cdot 10^{-12}$ ug/particle will be detectable by AMS.

CaCO₃ aerosol in this study was generated by spraying saturated Ca(HCO₃)₂ solutions. The solubility of Ca(HCO₃)₂ in water is with 16.6 g/100g water sufficient that about 1% Ca(HCO₃)₂ would provide the missing amount of solute. However, we dry and temper the aerosol at 300°C and Ca(HCO₃)₂ in dry state is thermodynamically unstable (Zhao et al. 2010). As described in the manuscript, our wet generated CaCO₃ particles are more hygroscopic as Calcite and dry generated CaCO₃ particles. Larger κ for wet generated compared to dry generated CaCO₃ particles is a common phenomenon (e.g. Tang et al. 2016) and possibly related to the formation of Ca(OH)(HCO₃) structures at the surface (see below).

In Figure S2 we show the prediction of SS_{crit} 1.52% for activating CaCO₃ by the Kelvin/FHH theory with the CaCO₃ parameters taken from Kumar et al. (2009). SS_{crit} for our bare CaCO₃ particles is 1.49% and the lower SS_{crit} should be due to a more adsorptive surface, e.g. the presence of Ca(OH)(HCO₃) structures. According to classical Koehler theory the equivalent of $8.5 \cdot 10^{-20}$ moles of dissolvable entities would be needed to explain a drop from 1.52% to 1.3% supersaturation, which is only ¼ of the moles MA in the thinnest MA coating. Therefore, whatever makes our CaCO₃ particles wettable is not sufficient - in terms of Koehler theory - to explain the low SS_{crit} of 0.9 % at the thinnest MA coating.

We estimate monolayer coverage by MA at 2-3% volume fraction (vf), this would be achieved between the third and fourth MA mass load of $13 \cdot 10^{-12}$ - $38 \cdot 10^{-12}$ ug per particle, observed vf 1.5-4.1%. Thus a sub-monolayer coating of $3.3 \cdot 10^{-12}$ ug MA per particle caused a drop of SS_{crit} from 1.49 to 0.9 and increased kappa from 0.0028 to 0.012. Therefore we conclude that CaCO₃/MA coatings show a *non-Koehler* behavior at thin coatings and *approach* Koehler behavior with increasing MA load. This means there must be specific interactions between MA and the CaCO₃ surface which eases water adsorption and CCN activation.

Ca(OH)(HCO₃) structure exists commonly on the surface of CaCO₃ whenever the CaCO₃ surface has been exposed to gaseous water or liquid water. Ca(OH)(HCO₃) exist even at high vacuum condition and act as hydrophilic sites on the surface of CaCO₃ making the CaCO₃ surface more hydrophilic (Stipp, 1999; Stipp and Hochella, 1991; Neagle and Rochester, 1990). CaCO₃ aerosol in our study was generated by

spraying a $\text{Ca}(\text{HCO}_3)_2$ solution, so $\text{Ca}(\text{OH})(\text{HCO}_3)$ structures likely exist on the particle surface. When CaCO_3 particles are coated by malonic acid (or oleic acid) the hydrophilic sides can serve as polar surface active sites for accommodation of the acids. In case of MA there is a second carboxylic group which still could support the adsorption of water films.

If we think in terms of Kelvin/FHH theory to explain the observed low SS_{crit} for thin MA coatings, these coatings must have a net stronger interaction with water (higher A_{FHH}) and/or stronger interaction between the adsorbed water layers (lower B_{FHH}) than bare CaCO_3 . If coatings become thicker the Koehler solute effect starts increasingly to contribute and eventually controls the CCN activation. But our data are not sufficient to determine A_{FHH} and B_{FHH} . (The only system in the literature which comes close - in a far sense - is CaOxalate Monohydrate, with $A_{\text{FHH}} = 0.57$ and $B_{\text{FHH}} = 0.88$ (Kumar et al., 2009). Plug in these parameters will lead to $\text{SS}_{\text{crit}} = 0.53\%$ commensurable with our observed value of 0.56% for $13 \cdot 10^{-12}$ ug MA coating which represents an organic[^]vf of 1.6%, thus is close to monolayer.)

Oleic acid (OA) is not soluble in water. Pure oleic acid particles up to 333 nm do not activate at 0.87% SS. This data sets the upper limit of κ for pure oleic acid to < 0.0005 . With thin coatings of OA, CCN activity is smaller than bare CaCO_3 , however with thick coatings it becomes larger. This is not a classical Koehler behavior. Therefore adsorption e.g. described by Kelvin/FHH theory is a better approach to illustrate what could happen on coating with oleic acid.

Note that we are neither able to perform theoretical calculations nor is our data sufficient to determine e.g. FHH parameters. Both are clearly beyond this experimental work.

We again refer to $\text{Ca}(\text{OH})(\text{HCO}_3)$ structures at the surface which offer polar surface sites to bind the hydrophilic ends (the carboxyl groups) of the oleic acid molecules. Different to malonic acid, only hydrophobic ends of oleic acid molecules (the hydrocarbon chains) are then exposed on the particle surface hence increase the hydrophobicity of the particle surface. Such a formation of a hydrophobic layer

should be occurring until all polar sites are occupied or a monolayer coverage - maybe in form of a self-assembled layer - is reached. This can hinder the uptake of water, and in terms of Kelvin/FHH theory will lower A_{FHH} and/or likely increase B_{FHH} . The formation of a monolayer of OA on black carbon particles with the polar groups pointing outwards was postulated by Dalirian et al. (2017), which lead to increased activation of the black carbon particles. Thus, they observed a similar effect of layer formation, but with switched polarity.

When CaCO_3 particles are coated with more oleic acid (more than one monolayer) the first layer of oleic acid still combines with CaCO_3 surface. We suppose that a portion of the carboxyl groups of oleic acid molecules, which are not in the first layer, will be exposed on the particle surface in analogy to the formation of lipid bilayers, e.g. cells. The particle surface then becomes more hydrophilic and in terms of Kelvin/FHH theory the interaction of water with the OA surface becomes stronger, A_{FHH} increases and likely also the interaction between the higher water layers (B_{FHH} decreases). From this point of view water adsorption should become similar to thin malonic acid layers. In addition, when droplets form, oleic acid will transfer to the surface of the droplets and lower the surface tension of the solution (the surface tension of oleic acid is 0.033 J m^{-2} , which is much lower than that of pure water of 0.072 J m^{-2}). Thus, the activation of OA coated particles is probably a complex interaction between formation of specific hydrophobic layers and more hydrophilic multilayers, surface tension and for the largest coatings amount size effects. As shown in Figure S2, SS_{crit} for OA is lower than for thin malonic acid coatings, probably because of the surface tension effect, but higher than for thick MA coatings, because of the missing solute effect.

We will the discussion above implement in parts in the manuscript. This passages are highlighted in yellow in the revised manuscript.

C2. Focusing on the coating device temperature in the results section is a bit confusing and I am not convinced about the reproducibility of the experiment, given

that the experimental cases are identified mainly by the temperature of the coating device. Focusing more on presenting the mass of organics coated on the particles would improve the paper significantly. Does the coating thickness depend on the original particle size? Can this give more information towards understanding the observations?

Response:

First of all we would like to clarify that we did not mean that coating thickness depends only on temperature. Our intention was to use the coating temperature to classify our experiments, because the organic mass itself has some uncertainty, related to limitations of the measurements method. It means that we are convinced that for a given particle size (distribution) and fixed experimental conditions (flows, residence time etc.) will indeed lead to reproducible amounts of coatings for a given temperature.

In Table 1 (revised) in our manuscript we showed the organic mass per particle data. We will focus on the organic mass and organic volume fraction in the revision of our manuscript. Due to the Kelvin Effect, the amount of organic acid coating depends somewhat on the particle size of the core. In our study, we selected CaCO₃ particles at a diameter of 101.8nm and detailed discussion focus on the impact of coating thickness on the CCN activity of 101.8nm CaCO₃ particles. However, as shown in Figures polydisperse particles with a distribution of particle size and coatings behave similar.

C3. In the motivation of the chosen substances: is oleic acid really a good choice for a surface-active compound, considering its low solubility?

Response:

Yes, we think that the two acids are good choices as the water solubility of the two organic acids is complementary; it is high for malonic acid while it is very low for oleic acid, and we speculated in our planning that oleic acid would form kind of self-assembled layers. Surface active compounds do not need to be water soluble. Moreover, oleic acid is observed in the atmosphere.

C4. On line 179, the residence time in the flow tube is given. However in a laminar flow, the residence time varies with the position, i.e. whether the air passes at the center or near the walls. Is this effect considered and may it influence the results?

Response:

The flow tube was supposed to act as delay tube. The residence time of 23.7 s for the particles in the flow tube is the average residence time. This compares to the average residence time of only about 5.8 s for the particles in the coating device (including the water cooler). Thus average residence time in the flow tube is about 4 times of that in the coating device. 1.) In the way we sampled aerosol from the flow tube, the aerosol contains flow both from the center and near the walls. 2.) increasing of residence time (by 23.7 s) had no significant impact on CCN activity at all conditions, thus fact that particles travelling in center and particles travelling near the wall was not important.

C5. Lines 180 to 185: At first reading it sounds as if the relative humidities given are at 80 °C. However, in the case of 47% RH, the air would then be strongly supersaturated at 25 °C. Please clarify the temperature at which the RH is given. Also, if 47% RH refers to 25 °C, the RH at 80 °C will still be very low, just a few percent. How does this influence the experiments?

Response:

We thank the referee for the comment as our description maybe indeed misleading. RH experiments were performed at 60°C(MA) and 80°C(OA) coating temperature. The N₂ stream was passed through a bubbling device filled with Milli-Q water to saturate the N₂ stream and RH was measured to be >90% at T =25 °C (room temperature). The RH of the aerosol flow before entering the coating device is measured to be <10% at T =25 °C. The RH of the mixed stream should be about 50% at 25 °C, since the flow rate of the N₂ stream and the aerosol flow is the same. This corresponds to water vapor pressure of 1500 Pa. So, within the coating device at 60°C the RH will be >7% (MA experiment) and at 80°C >3% (OA experiment), still about an order of magnitude higher than the RH, when the stream is not humidified. In fact it will be a somewhat higher as the gas-phase may not reach the bath temperature which primarily served to warm up the coating agent and control its vapor pressure.

During passing through the cooler, RH increases to 47% at 25°C at the exit of the cooler.

We clarified this in the manuscript.

C6. In lines 228 to 231 proportionalities between AMS signals and organic particle mass and volume are described. Are they observations or assumptions? Also, determination of the amount of organic coating: If I read the table 1 correctly, and make some calculation, the change in diameter and the change in organic mass, do not agree. Is this correct? Why is that?

Response:

Yes, AMS determined mass and observed volume increase should be linearly related. This is the working hypothesis. There are apparent deviations from strict linearity, mainly because of limitations in determining the volume increase through coating, as the formed layers are thin, and growth is smaller than the bin width of the SMPS. The size resolution of the SMPS was set to maximum of 64 channels per decade.

AMS is obviously able to detect the smallest coating amounts, as described in the manuscript, but standard relative ionization efficiency (RIE = 1.4) for organics, which can be well applied to atmospheric systems, fails in our case as it underestimates the volume observed by SMPS for the thickest coating by more than a factor of two (applying the macroscopic densities). It is well known that application of average RIE for organics often fails for specific single compounds.

Therefore it seemed to us, a reasonable way out could be the procedure which we applied and described in the experimental section. We assume the particles with the thickest coating are spherical, coatings are bulk like, and can be measured by SMPS with sufficient accuracy. Then we calibrated the largest m/z observed by AMS as marker for the thickest coating, and apply the marker calibration to the thinner coatings. As can be seen from the STDEV the reproducibility is quite good but there are systematic errors. The bin width “uncertainty” in the range of diameters from 101.8 to 120.9 nm is 3.9 and 4.3 nm, respectively. At coating thicknesses of about 5 - 20 nm this introduces uncertainties of 32 to 12% already. If one recalculates the

expected diameter for the coated particle from core + coating volume

$$D_{coat} = \sqrt[3]{D_{core} \cdot \frac{6}{\pi} \cdot \frac{m_{org}}{\rho_{org}}}$$

the derived diameters D_{coat} fall in the bin-width of the channel noted in Table 1 (old) as mode diameter. As a consequence within these uncertainties the relation between SMPS volume and AMS mass agree. (These uncertainties of the coating mass was the reason why we use the operational coating temperature to classify our experiments).

We will show the relation between AMS data and SMPS data in Figure S1 in the supplement. See response to next comment.

C7. Line 234 to 235. Have you tried to account for mode shift within the bin, by fitting a function to the distribution?

Response:

Thanks for the suggestion. We now fitted the maxima of the SMPS number distribution by a lognormal function (considering 5 to 9 neighbor bins centered around the mode), and took the maximum of the fits as mode diameter. This led indeed to changes. The most significant changes were that for the thickest coating the fitted maxima shifted from 121.9 to 121 nm and from 121.9 to 124.3 nm for MA and OA respectively. This led to different calibration factors and thus to different coating amounts for the thinner coatings. The effects were -5% and +11% for OA and MA, respectively. By interpolating the mode position the linearity between SMPS volume and AMS also improved as indicated in Figure S3. In the Figure S3 also the mass range over the bin width is given as x error bars. (The error bars are different for MA and OA as the density ρ_{org} entered the calculation.) One can see that mass calculated with nominal mode position (old Table 1) is centered over the bin width bars. One can also recognize how much the mass calculated from the interpolated mode diameters

(Table 1(revised)) were shifted inside the bin width bar.

We will use the revised data in the revised manuscript. See previous comment.

C8. Line 293: You say “and our kappa value is somewhat higher but still in this range”. Isn’t it just in the range?

Response:

Yes, it is just in the range. We will correct in the manuscript and will mention that larger kappas for wet generated CaCO₃ has been found before.

C9. Line 298: You say “The increased kappa value of 0.0008”. Shouldn’t it be “The increase in kappa value of 0.0008”?

Response:

Yes, it should be “The increase in kappa value of 0.0008”. We will correct in the manuscript.

C10. Line 323: What do you mean by a “significant amount” of coating? Is a coating of less than 2 nm insignificant? In all aspects?

Response:

We will reformulate that section.

C11. Line 323-325: Unclear expression. Please specify that the sizing according to mobility diameter is referred to (if that is the case) and specify the temperature limit, instead of saying “a certain value”.

Response:

We will reformulate that section.

C12. Line 371: Why does the activated fraction level off at 83%? Did you make an intercalibration between numbers in the CCNC and CPC for other compounds?

Response:

The activation efficiency (i.e., the activated fraction when aerosol particles are completely activated) was 83% for our CCN instrument, determined using 150 nm (NH₄)₂SO₄ particles at SS=0.85%. In Figure 4 and Figure 6 in our manuscript, reaching the plateau of about 83% means that the aerosol particles were completely activated. Activation efficiency around 80% are typical compare the study of Abbatt et al. (2005). We prefer not to correct for better looks.

C13. In section 3.2 there is a lot of repetition, I think. Please see if the text can be made more efficient.

Response:

We will try to make the text more efficient and avoid repetition.

C14. Line 413, the sentence starting with “This suggestion is supported by very low CCN activity of pure oleic acid....” Is this based on some calculations? Please describe. Line 421 to 423: But the low surface tension does not seem to help the pure oleic acid particles to activate, according to your measurements as well as Kumar et al. (2003) and Broekhuizen et al. (2004). Also, the first “of” on line 422 should be removed.

Response:

Our CCN activity measurements show that oleic acid particles up to 333 nm do not activate at 0.87% SS, thus pure oleic acid particles have very low CCN activity ($\kappa < 0.0005$). The research of Kumar et al. (2003) and Broekhuizen et al. (2004) also showed pure oleic acid particles have very low CCN activity. In pure oleic acid particles micelle like structures are formed, with the hydrophilic ends (the carboxyl groups) of the oleic acid molecules tend to combine together by hydrogen bonds and the hydrophobic tail (the hydrocarbon chains) are exposed at the outside (Iwahashi et al., 2000; Garland et al., 2008). The arrangement of oleic acid molecules in pure oleic

acid particles should be similar to that in pure oleic acid liquid. This can increase the hydrophobicity of the particle surface and hinder the uptake of water. Even low surface tension cannot help the pure oleic acid particles to activate. And oleic acid is highly insoluble in water.

We will remove the first “of” on line 422.

C15. Figure 6: The fitted curves for 30-60 °C do not seem to follow the data very well. Why? Have you accounted for doubly charged particles? In my opinion there is a tendency to a two step-function, the first step reaching to CCN/CN of 0.15-0.2.

Response:

We can deduct the presence of doubly charged particles in the CN measurement, but we cannot deduct the activated doubly charged particles from CCN. One method for solving this problem is provided by Sullivan et al. (2009). In their paper they fitted the data from the “multiply-charged plateau” to the “completely-activated plateau” when the data had a clear “multiply-charged plateau”. But in our data, we don’t have a clear “multiply-charged plateau”, so we fitted from the beginning to the “completely-activated plateau”. This will lead to a systematic underestimate of the SS_{crit} . The underestimate is the largest when the malonic acid mass is the smallest (30 °C coating temperature), and we underestimate SS_{crit} by only about 0.02% (difference between fitting from the first point and fitting from the third point (multiply-charged plateau)). When the malonic acid mass is larger, the underestimate will be smaller. At the largest two malonic acid mass, the underestimate can be neglected.

We will also make that clearer in the revision in our manuscript.

References

Abbatt, J. P. D., Broekhuizen, K., Kumal, P. P., Cloud condensation nucleus activity of internally mixed ammonium sulfate/organic acid aerosol particles. *Atmos. Environ.* 2005, 39 (26), 4767-4778.

AIOMFAC model, <http://www.aiomfac.caltech.edu>

Broekhuizen, K. E., Thornberry, T., Kumar, P. P., and Abbatt, J. P. D., Formation of cloud condensation nuclei by oxidative processing: Unsaturated fatty acids, *J. Geophys. Res.-Atmos.*, 109, D24206, 10.1029/2004jd005298, 2004.

Dalirian, M., Ylisirniö, A., Buchholz, A., Schlesinger, D., Ström, J., Virtanen, A., and Riipinen, I.: Cloud droplet activation of black carbon particles coated with organic compounds of varying solubility, *Atmos. Chem. Phys. Discuss.*, 2017, 1-25, 10.5194/acp-2017-1084, 2017.

Garland, E. R.; Rosen, E. P.; Clarke, L. I.; Baer, T., Structure of submonolayer oleic acid coverages on inorganic aerosol particles: evidence of island formation. *Phys. Chem. Chem. Phys.* 2008, 10 (21), 3156-3161.

Iwahashi, M.; Kasahara, Y.; Matsuzawa, H.; Yagi, K.; Nomura, K.; Terauchi, H.; Ozaki, Y.; Suzuki, M., Self-diffusion, dynamical molecular conformation, and liquid structures of n-saturated and unsaturated fatty acids. *J. Phys. Chem. B* 2000, 104 (26), 6186-6194.

Koehler, H., The nucleus in and the growth of hygroscopic droplets. *Trans. Faraday Soc.* 1936, 32 (2), 1152-1161.

Kumar, P. P., Broekhuizen, K., and Abbatt, J. P. D., Organic acids as cloud condensation nuclei: Laboratory studies of highly soluble and insoluble species, *Atmos. Chem. Phys.*, 3, 509-520, 2003.

Kumar, P., Nenes, A., and Sokolik, I. N.: Importance of adsorption for CCN activity and hygroscopic properties of mineral dust aerosol, *Geophys. Res. Lett.*, 36, 10.1029/2009gl040827, 2009.

Linke W. F., Seidell A., *Solubilities: Inorganic and metal-organic compounds*, a compilation of solubility data from the periodical literature. Amer. Chem. Soc., 1958.

Neagle, W., Rochester, C. H., Infrared study of the adsorption of water and ammonia on calcium carbonate. *Journal of the Chemical Society, Faraday Transactions* 1990,

86 (1), 181-183.

Petters, M. D., Kreidenweis, S. M., A single parameter representation of hygroscopic growth and cloud condensation nucleus activity. *Atmos. Chem. Phys.* 2007, 7 (8), 1961-1971.

Ruehl, C. R., Davies, J. F., and Wilson, K. R.: An interfacial mechanism for cloud droplet formation on organic aerosols, *Science*, 351, 1447-1450, 10.1126/science.aad4889, 2016.

Seinfeld, J. H., Pandis, S. N., *Atmospheric Chemistry and Physics-From Air Pollution to Climate Change*, Second edition, Published by John Wiley & Sons, Inc., Hoboken, New Jersey, 773-776, 2006.

Sorjamaa, R., and Laaksonen, A.: The effect of H₂O adsorption on cloud drop activation of insoluble particles: a theoretical framework, *Atmos. Chem. Phys.*, 7, 6175-6180, 10.5194/acp-7-6175-2007, 2007.

Stipp, S. L. S., Toward a conceptual model of the calcite surface: hydration, hydrolysis, and surface potential. *Geochimica et Cosmochimica Acta* 1999, 63 (19-20), 3121.

Stipp, S. L., Hochella Jr, M. F., Structure and bonding environments at the calcite surface as observed with X-ray photoelectron spectroscopy (XPS) and low energy electron diffraction (LEED). *Geochimica et Cosmochimica Acta* 1991, 55 (6), 1723-1736.

Sullivan, R. C., Moore, M. J. K., Petters, M. D., Kreidenweis, S. M., Roberts, G. C., and Prather, K. A., Effect of chemical mixing state on the hygroscopicity and cloud nucleation properties of calcium mineral dust particles, *Atmos. Chem. Phys.*, 9, 3303-3316, 10.5194/acp-9-3303-2009, 2009.

Tang, M. J., Cziczo, D. J., and Grassian, V. H.: Interactions of Water with Mineral Dust Aerosol: Water Adsorption, Hygroscopicity, Cloud Condensation, and Ice Nucleation, *Chemical Reviews*, 116, 4205-4259, 10.1021/acs.chemrev.5b00529, 2016.

Zhao, D. F., Buchholz, A., Mentel, T. F., Müller, K. P., Borchardt, J., Kiendler-Scharr, A., Spindler, C., Tillmann, R., Trimborn, A., Zhu, T., and Wahner, A., Novel method of generation of $\text{Ca}(\text{HCO}_3)_2$ and CaCO_3 aerosols and first determination of hygroscopic and cloud condensation nuclei activation properties, *Atmos. Chem. Phys.*, 10, 8601-8616, 10.5194/acp-10-8601-2010, 2010.

Zuend, A., Marcolli, C., Booth, A. M., Lienhard, D. M., Soonsin, V., Krieger, U. K., Topping, D. O., McFiggans, G., Peter, T., and Seinfeld, J. H.: New and extended parameterization of the thermodynamic model AIOMFAC: calculation of activity coefficients for organic-inorganic mixtures containing carboxyl, hydroxyl, carbonyl, ether, ester, alkenyl, alkyl, and aromatic functional groups, *Atmospheric Chemistry and Physics*, 11, 9155-9206, 10.5194/acp-11-9155-2011, 2011.

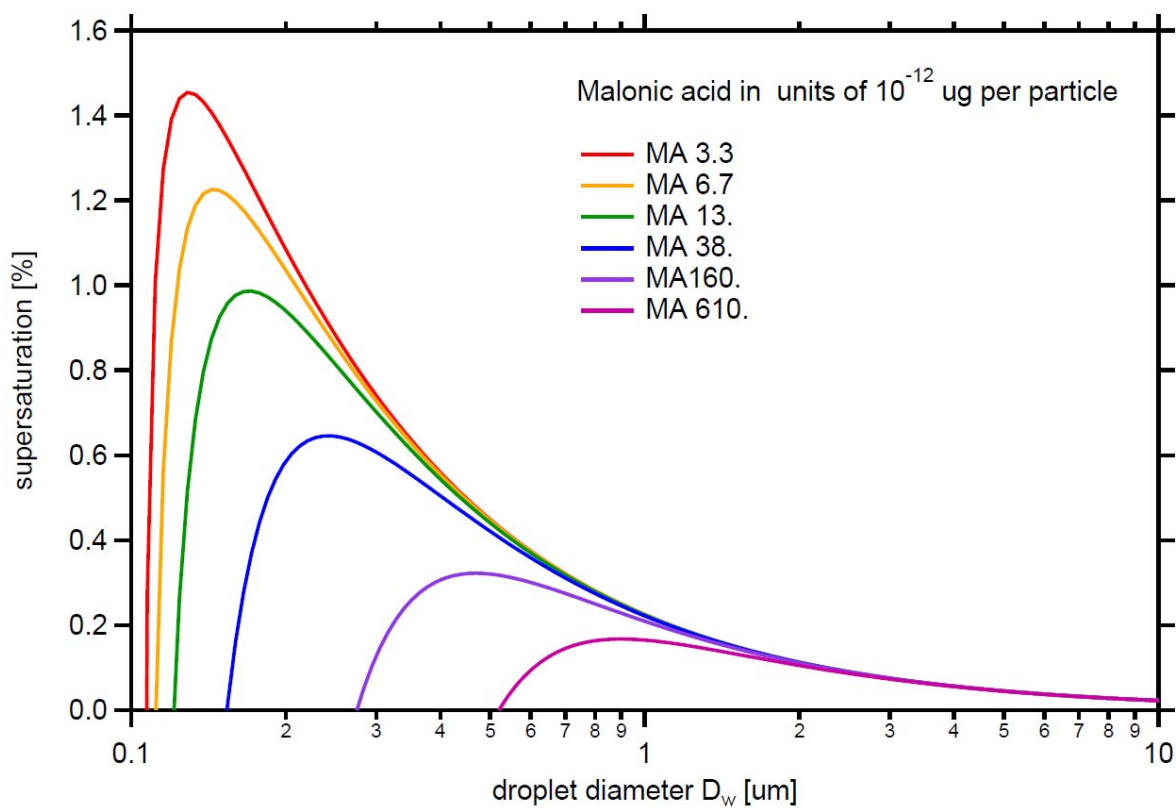


Figure S1. Variation of the equilibrium supersaturation over aqueous solution drops containing CaCO_3 and different mass of malonic acid at 293 K, assuming CaCO_3 is insoluble and doesn't react with malonic acid and the solution is dilute (water activity coefficient is close to 1). The diameter of insoluble CaCO_3 is 101.8 nm. Malonic acid mass per particle is 3.3, 6.7, 13, 38, 160, and 610 ($\times 10^{-12}$ μg , different color curves in the figure).

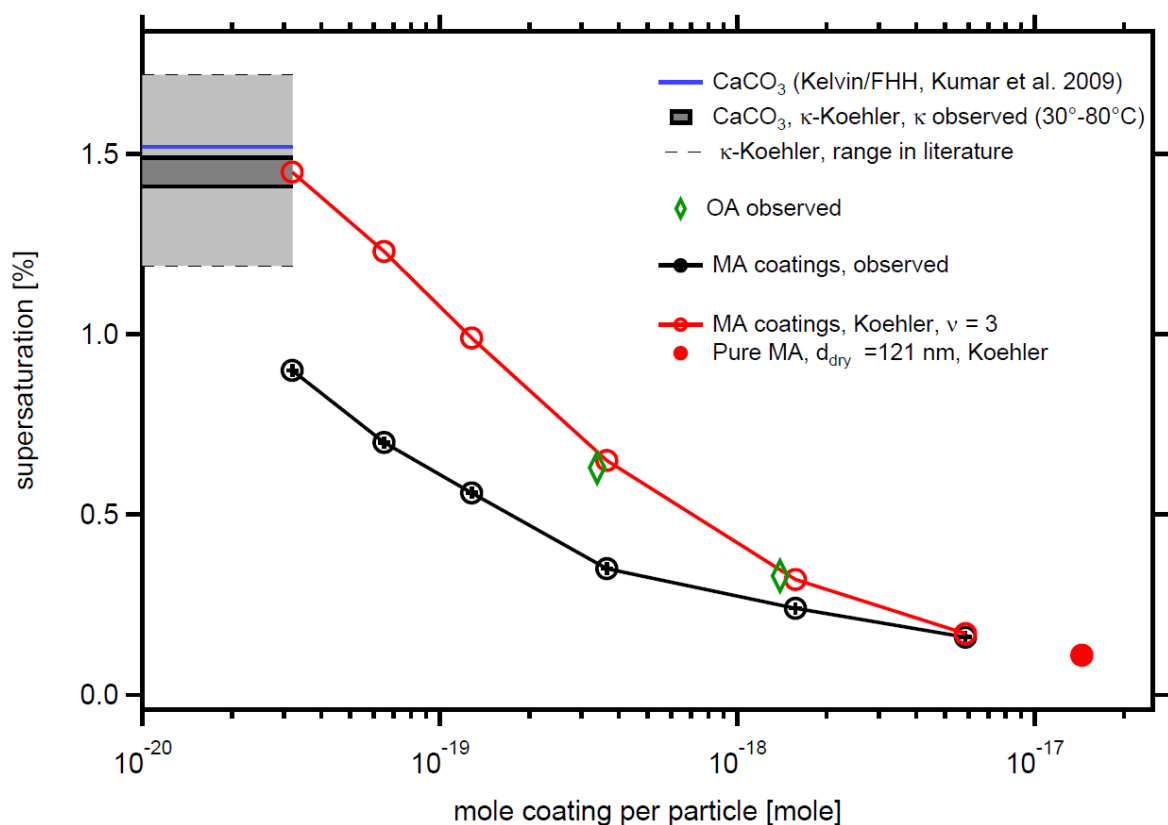


Figure S2: Comparison of SS_{crit} predicted by Koehler and Koehler/FHH theory with observations. The red circles are predictions by the Köhler theory for aqueous MA solutions assuming full dissociation, the black points present the observation. The red filled circle represents the Koehler prediction of SS_{crit} for 121.0 nm particles made of pure malonic acid. The horizontal lines give reference values for the bare $CaCO_3$ particles as calculated from our observed κ (black) and predicted by Koehler/FFH theory (blue). Light grey area between the thin dashed black lines indicates the range of SS_{crit} for 101.9 nm particles calculated from the range of κ in literature for wet generated $CaCO_3$ particles. Green diamonds show observed SS_{crit} for the two thickest OA coatings.

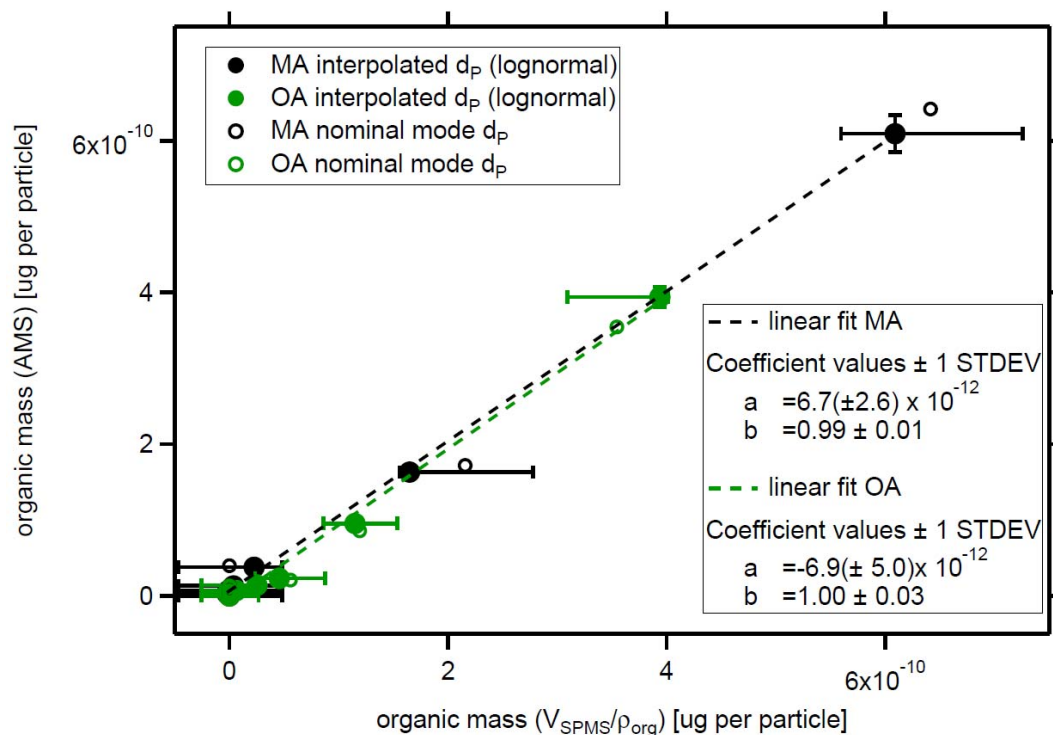


Figure S3: Linear relation between organic mass of the coating (AMS) and the organic coating mass calculated from the SMPS measurements for oleic acid coatings (green) and maleic acid coatings (black). For full circles the organic mass was calculated from the interpolated mode diameters (new). For interpolation we fitted a lognormal function in the range of the nominal mode diameter (considering 5-7 bins). The open circles are the data from the manuscript, where the nominal mode diameters were used to calculate the organic mass expected from SMPS measurements. Error bars in y give the reproducibility of the AMS measurement, error bars in x indicate the mass range (volume range) spanned by the SMPS bin width for the respective nominal mode diameter that entered the mass calculation. Note that the highest values must be the same as they were used to calibrate AMS organic mass vs SMPS volume.

Table S1. Theory and experimental SS_{crit} and κ values of $CaCO_3$ particles with different mass of MA coating.

Dry diam. (nm)	MA per particle ($\times 10^{-12}$ μg)	Theory SS_{crit} (%)	Experimental SS_{crit} (%)	Theory κ	Experimental κ
102.0	3.3 \pm 0.3	1.44	0.90	0.0024	0.0123 \pm 0.0005
102.1	6.8 \pm 1.2	1.20	0.70	0.0053	0.0231 \pm 0.0008
102.2	13 \pm 1.8	0.97	0.56	0.0107	0.0380 \pm 0.0012
102.7	38 \pm 1.6	0.63	0.35	0.0315	0.1056 \pm 0.0023
107.8	160 \pm 8.1	0.31	0.24	0.1110	0.1813 \pm 0.0031
121.0	610 \pm 24	0.16	0.16	0.3001	0.3001 \pm 0.0062

Table 2. Properties of investigated compounds.

Name	Formula	Molecular weight (g mol ⁻¹)	Density (g cm ⁻³)	Solubility (g/100 g water, at 298K)	Surface tension (dyn/cm)
Calcite	CaCO ₃	100.1	2.71	0.00058	- ^a
Malonic acid	C ₃ H ₄ O ₄	104.1	1.62	62	69 ^b
Oleic acid	C ₁₈ H ₃₄ O ₂	282.5	0.89	Very low	33 ^c

Values are taken from: Handbook of Chemistry and Physics, the 82nd Edition; Handbook of aqueous solubility data, Samuel H. Yalkowsky and Yan He, 2003; Chumpitaz et al., 1999; Hyvarinen et al., 2006.

a: no data

b: Surface tension of 0.01 mole fraction malonic acid aqueous solution at 298K

c: Surface tension of pure oleic acid at 293K

Chumpitaz, L. D. A., Coutinho, L. F., and Meirelles, A. J. A.: Surface tension of fatty acids and triglycerides, *J. Am. Oil Chem. Soc.*, 76, 379-382, 10.1007/s11746-999-0245-6, 1999.

Hyvarinen, A. R.; Lihavainen, H.; Gaman, A.; Vairila, L.; Ojala, H.; Kulmala, M.; Viisanen, Y., Surface tensions and densities of oxalic, malonic, succinic, maleic, malic, and cis-pinonic acids. *Journal of Chemical and Engineering Data* 2006, 51 (1), 255-260.

Cloud Condensation Nuclei Activity of CaCO₃ Particles with Oleic Acid and Malonic Acid Coatings

Mingjin Wang^{1,2}, Tong Zhu^{1*}, Defeng Zhao², Florian Rubach^{2,3}, Andreas Wahner², Astrid Kiendler-Scharr², and Thomas F. Mentel^{2*}

A figure for illustration of the responses is given in an extra file

C1: Overall the paper is nicely illustrated but it contains some repetitive text blocs, especially in the result section, that could be avoided in order to ease the reading of this manuscript (and reinforcing also its content).

Response:

We thank the referee for the positive comment. We will optimize the text of our manuscript to avoid repetition and to make the text more efficient and easier to read.

C2: While the argument of a bilayer of oleic acid does make sense, I'm still puzzled by the fact that the CCN properties are apparently higher for a coated particle compared to a pure oleic acid particle. I would have simply assumed that once thick enough, the water probing the surface does not see the core CaCO₃ particle (over the time scale of these experiments). In this situation, the pure oleic acid particle would exhibit a kind of upper limit for water adsorption and droplet activation. Maybe the authors could comment more on that, and maybe add the pure oleic acid data on their figures (this would ease the comparison with both systems).

Response:

Our CCN activity measurement showed that pure oleic acid particles up to 333 nm did not activate at 0.87% SS; this sets an upper limit for CCN activity of oleic acid particles ($\kappa < 0.0005$), in agreement with Kumar et al. (2003) and Broekhuizen et al. (2004). In liquid state oleic acid (OA) forms micelle like structures, the hydrophilic

ends (the carboxyl groups) of oleic acid molecules tend to combine together by hydrogen bonds and the hydrophobic tails (the hydrocarbon chains) are exposed at the outside (Iwahashi et al., 2000; Garland et al., 2008). The arrangement of oleic acid molecules in pure oleic acid particles should be similar. Hydrophobic tails facing outwards can explain the hydrophobicity of the particle surface and the hindrance of the uptake of water, making the CCN activity of pure oleic acid particles very low. Dalirian et al. (2017) studied OA coatings on black carbon (BC). They also found *no* activation of pure OA, but droplet activation for OA coated BC particles at SS_{crit} lower than that of BC and pure OA. Their particles were larger than ours, though, but also more heavily coated, i.e. more OA like. So, better droplet activation than for pure OA seems to be possible in coated systems.

We assume that $\text{Ca}(\text{OH})(\text{HCO}_3)$ structures act as hydrophilic sites on the surface of CaCO_3 (Kuriyavar et al., 2000; Stipp, 1999; Stipp and Hochella, 1991; Neagle and Rochester, 1990). Garland et al. (2008) suggested that OA at sub-monolayer coverage form self-associated islands rather than uniformly covering the surfaces, and OA molecules were oriented vertically on both hydrophobic and hydrophilic surfaces with the hydrocarbon chains of oleic acid molecules facing away from the surface. This is in support of our working hypothesis: the formation of a hydrophobic surface film.

When CaCO_3 particles are coated with only a small amount of oleic acid (less than one monolayer), the hydrophilic ends (the carboxyl groups) of oleic acid molecules will combine with the hydrophilic sites ($-\text{OH}$ and $-\text{HCO}_3$ groups) on CaCO_3 surface by hydrogen bonds. We conclude that all hygroscopic sites on the CaCO_3 surface are covered somewhere between 50°C and 60°C coating temperature, i.e. between $14 \cdot 10^{-12}$ and $23 \cdot 10^{-12}$ μg OA mass per particle, as here the trend turns and droplet activation increase again. This would place the monolayer coverage above 3%, organic volume fraction. According to the measurements and calculations of the length of oleic acid molecule, the thickness of oleic acid sub-monolayer on solid surfaces, and the thickness of deuterated oleic acid monolayers at the air-water interface (Garland et al., 2008; King et al., 2009; Iwahashi et al., 2000), we determined 2.3 nm as the likely thickness of oleic acid monolayer on CaCO_3 particles, accordingly a monolayer would be achieved at about 12-13% organic volume fraction. As a consequence the formation of the “hydrophilic bilayer” starts at sub-monolayer

coverage in accordance with island formation observed by Garland et al. (2008).

For CaCO_3 particles coated with more OA (thicker than one monolayer, at 70 and 80 °C coating temperatures), OA in the first layer still combines with the CaCO_3 surface by hydrogen bonds. We suppose that a portion of the carboxyl groups of oleic acid molecules, which are not in the first layer, will be exposed to the particle surface, in analogy to the formation of lipid bilayers, e.g. in cells, though the structure of this part of oleic acid is not known. The particle surface then becomes more hydrophilic. Activation of wettable, insoluble material can be described by the Kelvin term and a water absorption term, e.g. Frenkel Halsey Hill isotherm (Sorjamaa and Laaksonen, 2007, Kumar et al. 2009).

When carboxylic groups of OA are exposed at the surface, the interaction of water with the OA layer becomes stronger. In terms of the Kelvin/FHH approach, the surface water interaction becomes stronger and A_{FHH} increases and likely also the interaction between the higher water layers (B_{FHH} decreases). From this point of view water adsorption by the “OA bilayer” should become similar to thin malonic acid layers. In addition, when droplets form, oleic acid will transfer to the surface of the droplets and lower the surface tension of the solution (the surface tension of oleic acid is 0.033 J m^{-2} , which is much lower than that of pure water of 0.072 J m^{-2}). Thus, the activation of OA coated particles is probably a complex interaction between formation of specific hydrophobic layers and more hydrophilic multilayers, surface tension effects and for the largest coating amounts, simple size effects. As shown in Figure S1, SS_{crit} for OA is lower than for thin malonic acid coatings, probably because of the surface tension effect, but higher than for thick MA coatings, because of the missing solute effect.

We will implement parts of this discussion in the manuscript, highlighted in yellow.

C3: If my reading is correct, the CaCO_3 particles with a thick coating do exhibit better CCN properties than the pure oleic acid particles (if my reading is incorrect, this would highlight that an in-depth editing would be beneficial for the reader). How can you explain such a fact? Is the CaCO_3 surface leading to some kind of ordering of

the adsorbed organic acid (which might not be observed in the pure homogeneous organic particle) leading effectively to the above mentioned bilayer structure?

Response:

Your reading is correct. Note, the oleic acid coatings achieved at 70° or 80°C coating temperature are still thin. The largest coating thickness is about 10 nm at an organic volume fraction of 44%, which corresponds to about 4 monolayers of oleic acid (assuming the thickness of oleic acid monolayer on CaCO₃ particles is about 2.3 nm). To our knowledge, no previous study has investigated the structure of oleic acid coating on particle or solid surface thicker than one monolayer.

In our understanding the arrangement of oleic acid molecules in the thin coatings will be influenced by the CaCO₃ core (the polar, hydrophilic sides) and can thus be different from the arrangement of oleic acid molecules in pure oleic acid particles. Water can probably adsorb at the carboxylic groups facing outward (“bilayer” type structure) and diffuse through the thin oleic acid coatings. It may form an adsorbed water phase near the CaCO₃ surface. This could push the oleic acid out to act as surfactant which lowers the Kelvin term. Such a process should also happen in pure oleic acid particles. Because of the presence of CaCO₃ core the SS to achieve is lower than for pure OA.

We will explicitly refer to the lower κ of pure oleic acid in relation to higher κ observed for the oleic acid coated CaCO₃.

C4: Is the temperature in the coating device leading to some kind of ordering (for instance, by increase surface mobility before an ordering when cooling down)? Also, oleic acid has only a moderate thermal stability as it decomposes at higher temperature (typically at temperature at a factor 2 higher than those used here), potentially via an epoxide pathway in presence of air (and enhanced by light or metallic traces). Could traces of oxidized products nevertheless affect the composition of the coating at 80 °C already? If so, then this effect should increase with time. Did the authors observed any variation with time of kappa at 80 °C? Did the authors tried

to have thicker coatings at lower temperature by changing the gas flow conditions in their coating device?

Response:

We agree with the referee that the temperature in the coating device can increase the surface mobility of OA molecules, which would help to optimize the layering arrangement (ordering) of adsorbed oleic acid molecules on CaCO₃ surface.

We can exclude oxidation of OA since we used high-purity N₂ (Linde LiPur 6.0, purity 99.9999%, Linde AG, Munich, Germany) and we did not have much light in our system because both the coating device and the flow tube were covered with light tight materials (black polyurethane foam). Metallic traces might exist in our system, though, as we used some stainless steel tubes in our system.

The only way in which we modified the time between coating process and particle detection was provided by a flow tube to increase the average residence time from 5.8 to 23.7 s. Longer residence time (by 23.7 s) had no significant impact on CCN activity for both oleic acid coated particles and malonic acid coated particles at both dry and 47% RH conditions, probably because the coating process was already completed in the coating device and no further reactions occurred in the flow tube.

At the beginning of our experimental study, we modified the gas flow condition in the coating device in order to choose an appropriate gas flow condition. But we only measured the particle size when we changed the gas flow condition. After finding the appropriate gas flow conditions, we fixed the gas flow condition and did not change it anymore.

C5: Line 238. This sentence is unclear.

Response:

This sentence should be: In the discussion we also use the coating mass per particle to give a rationale, which is easier to imagine, to the finding and classification.

C6: Line 249: where a polydisperse

Response:

This sentence should be: In cases where a polydisperse aerosol was coated ...

C7: Line 296: remained at

Response:

This sentence should be: The κ value remained at 0.0028 ± 0.0001 at 60 °C and increased to 0.0036 ± 0.0001 at 80 °C.

And we also made the revision in our manuscript according to your comments.

References

Broekhuizen, K. E., Thornberry, T., Kumar, P. P., and Abbatt, J. P. D., Formation of cloud condensation nuclei by oxidative processing: Unsaturated fatty acids, *J. Geophys. Res.-Atmos.*, 109, D24206, 10.1029/2004jd005298, 2004.

Dalirian, M., Ylisirniö, A., Buchholz, A., Schlesinger, D., Ström, J., Virtanen, A., and Riipinen, I.: Cloud droplet activation of black carbon particles coated with organic compounds of varying solubility, *Atmos. Chem. Phys. Discuss.*, 2017, 1-25, 10.5194/acp-2017-1084, 2017.

Garland, E. R.; Rosen, E. P.; Clarke, L. I.; Baer, T., Structure of submonolayer oleic acid coverages on inorganic aerosol particles: evidence of island formation. *Phys. Chem. Chem. Phys.* 2008, 10 (21), 3156-3161.

Iwahashi, M.; Kasahara, Y.; Matsuzawa, H.; Yagi, K.; Nomura, K.; Terauchi, H.; Ozaki, Y.; Suzuki, M., Self-diffusion, dynamical molecular conformation, and liquid structures of n-saturated and unsaturated fatty acids. *J. Phys. Chem. B* 2000, 104 (26), 6186-6194.

King, M. D.; Rennie, A. R.; Thompson, K. C.; Fisher, F. N.; Dong, C. C.; Thomas, R. K.; Pfrang, C.; Hughes, A. V., Oxidation of oleic acid at the air-water interface and its

potential effects on cloud critical supersaturations. *Phys. Chem. Chem. Phys.* 2009, 11 (35), 7699-7707.

Koehler, H., The nucleus in and the growth of hygroscopic droplets. *Trans. Faraday Soc.* 1936, 32 (2), 1152-1161.

Kumar, P. P., Broekhuizen, K., and Abbatt, J. P. D., Organic acids as cloud condensation nuclei: Laboratory studies of highly soluble and insoluble species, *Atmos. Chem. Phys.*, 3, 509-520, 2003.

Kumar, P., Nenes, A., and Sokolik, I. N.: Importance of adsorption for CCN activity and hygroscopic properties of mineral dust aerosol, *Geophys. Res. Lett.*, 36, 10.1029/2009gl040827, 2009.

Sorjamaa, R., and Laaksonen, A.: The effect of H₂O adsorption on cloud drop activation of insoluble particles: a theoretical framework, *Atmos. Chem. Phys.*, 7, 6175-6180, 10.5194/acp-7-6175-2007, 2007.

Kuriyavar, S. I., Vetrivel, R., Hegde, S. G., Ramaswamy, A. V., Chakrabarty, D., Mahapatra, S. Insights into the formation of hydroxyl ions in calcium carbonate: temperature dependent FTIR and molecular modelling studies. *Journal of Materials Chemistry*, 2000, 10 (8): 1835-1840.

Neagle, W., Rochester, C. H., Infrared study of the adsorption of water and ammonia on calcium carbonate. *Journal of the Chemical Society, Faraday Transactions* 1990, 86 (1), 181-183.

Stipp, S. L. S., Toward a conceptual model of the calcite surface: hydration, hydrolysis, and surface potential. *Geochimica et Cosmochimica Acta* 1999, 63 (19-20), 3121.

Stipp, S. L., Hochella Jr, M. F., Structure and bonding environments at the calcite surface as observed with X-ray photoelectron spectroscopy (XPS) and low energy electron diffraction (LEED). *Geochimica et Cosmochimica Acta* 1991, 55 (6), 1723-1736.

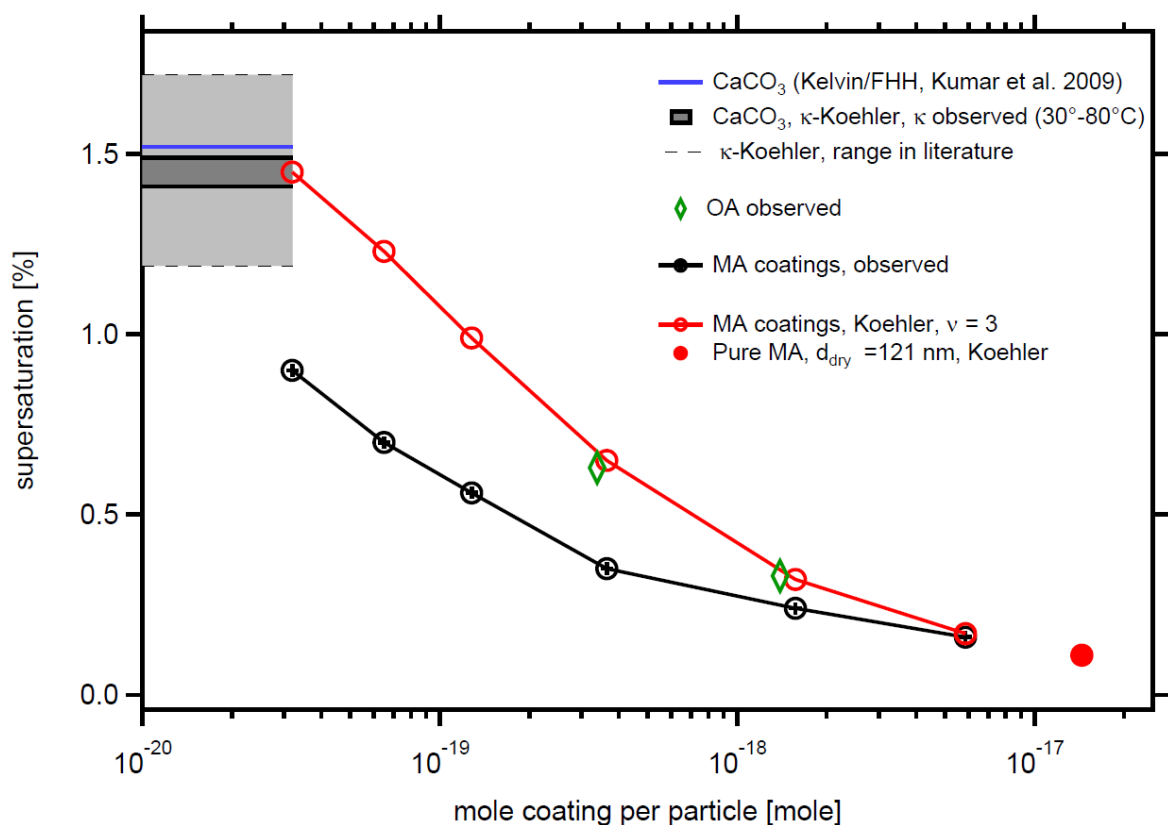


Figure S1: Comparison of SS_{crit} predicted by Koehler and Koehler/FHH theory with observations. The red circles are predictions by the Köhler theory for aqueous MA solutions assuming full dissociation, the black points present the observation. The red filled circle represents the Koehler prediction of SS_{crit} for 121.0 nm particles made of pure malonic acid. The horizontal lines give reference values for the bare $CaCO_3$ particles as calculated from our observed κ (black) and predicted by Koehler/FFH theory (blue). Light grey area between the thin dashed black lines indicates the range of SS_{crit} for 101.9 nm particles calculated from the range of κ in literature for wet generated $CaCO_3$ particles. Green diamonds show observed SS_{crit} for the two thickest OA coatings.

1 **Cloud Condensation Nuclei Activity of CaCO₃ Particles**
2 **with Oleic Acid and Malonic Acid Coatings**

3 **Mingjin Wang^{1,2}, Tong Zhu^{1*}, Defeng Zhao², Florian Rubach^{2,3}, Andreas**
4 **Wahner², Astrid Kiendler-Scharr², and Thomas F. Mentel^{2*}**

5 ¹BIC-ESAT and SKL-ESPCI, College of Environmental Sciences and Engineering,
6 Peking University, Beijing 100871, China.

7 ²Institut für Energie- and Klimaforschung (IEK-8), Forschungszentrum Jülich GmbH,
8 52425 Jülich, Germany.

9 ³Klimageochemie, Max Planck Institut für Chemie, 55128 Mainz, Germany

10

11 * To whom correspondence should be addressed: tzhu@pku.edu.cn;
12 t.mentel@fz-juelich.de

13

14 **Abstract.**

15 Condensation of carboxylic acids on mineral particles will lead to coatings, and
16 impact on the particles' potential to act as cloud condensation nuclei (CCN). To
17 determine how the CCN activity of mineral particles is impacted by carboxylic acid
18 coatings, the CCN activity of CaCO₃ particles and CaCO₃ particles with oleic acid
19 and malonic acid coatings were compared in this study. The results revealed that small

20 amounts of oleic acid coating (volume fraction (vf) \leq 4.3%) decreased the CCN
21 activity of CaCO₃ particles, while more oleic acid coating (vf \geq 16%) increased the
22 CCN activity of CaCO₃ particles. This phenomenon has not been reported before. On
23 the other hand, the CCN activity of CaCO₃ particles coated with malonic acid
24 increased with the thickness of the malonic acid coating (vf = 0.4 - 40%). Even
25 smallest amounts of malonic acid coating (vf = 0.4%) significantly enhanced the CCN
26 activity of CaCO₃ particles from $\kappa = 0.0028 \pm 0.0001$ to $\kappa = 0.0123 \pm 0.0005$. This
27 supports that a small amount of water-soluble organic acid coating may significantly
28 enhance the CCN activity of mineral particles. The presence of water vapor during the
29 coating process with malonic acid additionally increased the CCN activity of the
30 coated CaCO₃ particles, probably because more CaCO₃ reacts with malonic acid if
31 sufficient water is available.
32

33 **1 Introduction**

34 Atmospheric aerosols serve as cloud condensation nuclei and change the radiative
35 properties (cloud albedo effect) and lifetime (cloud lifetime effect) of clouds, thus
36 affecting the Earth's climate indirectly (Liu and Wang, 2010; Gantt et al., 2012;
37 Penner et al., 2004; Haywood and Boucher, 2000). Mineral aerosol is one of the most
38 abundant components of the atmospheric aerosol. It is estimated that 1500-2600 Tg of
39 mineral aerosol particles with radii between 0.1 and 8 μm are emitted annually into
40 the atmosphere on a global scale (Cakmur et al., 2006). Mineral aerosol particles are
41 mainly composed of substances that are slightly soluble or insoluble in water. Cloud
42 condensation nuclei (CCN) activity measurements show that the hygroscopicity
43 parameter κ (Petters and Kreidenweis, 2007) varies between 0.001 and 0.08 for
44 mineral aerosols, including CaCO_3 aerosol, clay aerosols and mineral dust aerosols
45 generated in the laboratory or sampled from various locations worldwide (Garimella
46 et al., 2014; Yamashita et al., 2011; Zhao et al., 2010; Koehler et al., 2009; Sullivan et
47 al., 2010; Herich et al., 2009). The low κ indicates that the CCN activity of mineral
48 aerosol is much lower than the CCN activity of water soluble salts like $(\text{NH}_4)_2\text{SO}_4$ (κ
49 = 0.61) and NaCl ($\kappa = 1.28$), which are also common in atmospheric aerosols (Petters
50 and Kreidenweis, 2007). Tang et al. (2016) reviewed recently the interaction of
51 mineral dust particles with water.

52 Mineral aerosol particles can be coated by organic vapors during their residence and
53 transport in the atmosphere. Many individual particle measurements have shown that
54 mineral components and organic matter can coexist in the same individual aerosol

55 particle in the real atmosphere (Falkovich et al., 2004; Falkovich et al., 2001; Russell
56 et al., 2002; Li and Shao, 2010). Carboxylic acids ($R(C=O)OH$) are abundant species
57 among the organic matter that coexists with mineral particles. Russell et al. (2002)
58 found that carbonyls ($R(C=O)R$), alkanes, and $R(C=O)OH$ are present in individual
59 mineral (and sea salt) aerosol particles, with enhanced concentration of $R(C=O)OH$.
60 They also found that Ca^{2+} , CO_3^{2-} , $R(C=O)OH$ and $R(C=O)R$ coexisted in some
61 individual mineral aerosol particles with a strong correlation between CO_3^{2-} and
62 $R(C=O)OH$. These particles could be formed by $CaCO_3$ particles (partly) coated with
63 organic film. Falkovich et al. (2004) also found that organic and inorganic
64 components coexisted in individual mineral aerosol particles with the organic
65 component consisting of various short-chain (C_1 - C_{10}) mono- and dicarboxylic acids
66 (MCA and DCA). The concentration of short-chain carboxylic acids in mineral
67 aerosol particles increased with the increase of the ambient relative humidity. A
68 possible explanation for such observations could be that when more water is
69 condensed onto mineral particles at higher ambient relative humidity, the adsorbed
70 carboxylic acids are ionized in the aqueous environment and react with mineral
71 particles forming organic acid salts. Of the major components of mineral aerosol
72 particles (clay, calcite ($CaCO_3$), quartz, mica, feldspar, etc.), only $CaCO_3$ with
73 alkaline character can react with carboxylic acids in this way. Thus $CaCO_3$ may play a
74 key role in the uptake of carboxylic acids by mineral aerosol particles.

75 Carboxylic acid coatings on mineral aerosol particles change their chemical
76 composition and thus may have an impact on their CCN activity. Many previous
77 studies have investigated the CCN activity of pure mineral aerosol (Garimella et al.,
78 2014; Yamashita et al., 2011; Zhao et al., 2010; Koehler et al., 2009; Sullivan et al.,
79 2010; Herich et al., 2009) and pure carboxylic acid aerosol (Kumar et al., 2003; Hori

80 et al., 2003; Cruz and Pandis, 1997; Hartz et al., 2006), but only a few studies have
81 investigated the CCN activity of mineral aerosol particles with carboxylic acid
82 coatings (Tang et al., 2015; Hatch et al., 2008; Gierlus et al., 2012).

83 In this study we used malonic acid and oleic acid as coating materials and CaCO_3
84 particles as cores, and investigated the CCN activity of the coated CaCO_3 particles.
85 Herein we varied the coating thickness and the relative humidity during the coating
86 process. Malonic acid is a representative of the class of dicarboxylic acids and oleic
87 acid is an example of surfactant like compounds. Dicarboxylic acids are ubiquitous in
88 the atmosphere (Kawamura et al., 1996; Kawamura and Ikushima, 1993; Ho et al.,
89 2007; Mkoma and Kawamura, 2013; Kawamura and Bikkina, 2016) and formed by
90 photochemical reactions and ozonolysis (Chebbi and Carlier 1996; Kawamura and
91 Bikkina, 2016; Kawamura et al., 1996; Khare et al. 1999; Mellouki et al., 2015). It has
92 been reported that dicarboxylic acids ($\text{C}_2\text{-C}_{10}$) account for 0.06-1.1% of the total
93 aerosol mass, with higher values in the summer, and 1.8% of the total aerosol carbon
94 (TC) in urban aerosol, in which oxalic acid, malonic acid, and succinic acid are the
95 most abundant species (Kawamura et al., 1996; Kawamura and Ikushima, 1993; Ho et
96 al., 2007; Mkoma and Kawamura, 2013). Oleic acid, which is emitted into the
97 atmosphere by the cooking of meat, wood burning, and automobile source (Schauer et
98 al., 1999; Rogge et al., 1998; Rogge et al., 1993), is present in atmospheric aerosols of
99 urban, rural, and forest areas (Cheng et al., 2004; Ho et al., 2010). The water
100 solubility of the two organic acids is complementary; it is high for malonic acid while
101 it is very low for oleic acid. Coatings of malonic acid and oleic acid could thus have
102 different effects on CCN activity of mineral particles.

103

104

105 **2 Experimental**

106 As general procedure, CaCO₃ aerosol was generated according to Zhao et al. (2010),
107 and then poly- or monodisperse CaCO₃ aerosol particles were coated by malonic or
108 oleic acid in a coating device. A flow tube was optionally applied to extend the
109 residence time. The particle size, chemical composition, and CCN activity of the
110 CaCO₃ particles were measured before and after coating. Figure 1 shows the
111 schematic of the experimental set up.

112 **2.1 Generation of CaCO₃ aerosol**

113 CaCO₃ aerosol was generated by spraying a saturated Ca(HCO₃)₂ solution. A sample
114 of CaCO₃ powder (2 g, pro analysis, ≥99%, Merck, Darmstadt, Germany) was
115 suspended in 1-L Milli-Q water (18.2 MΩcm, TOC <5 ppb). Then about 1.5 L min⁻¹
116 CO₂ (purity ≥99.995%, Praxair Industriegase GmbH & Co. KG, Magdeburg,
117 Germany) was bubbled into the suspension at room temperature for 3 h, while the
118 suspension was stirred using a magnetic stirrer. During bubbling, CO₂ reacted with
119 CaCO₃ to produce Ca(HCO₃)₂. After bubbling, the suspension was allowed to settle
120 for 10 min, the supernatant clear Ca(HCO₃)₂ solution was decanted and used for
121 spraying by a constant output atomizer (Model 3076, TSI, Shoreview, MN, USA)
122 using 1.75 L min⁻¹ high-purity N₂ (Linde LiPur 6.0, purity 99.9999%, Linde AG,
123 Munich, Germany).

124

125 The major portion (0.9 L min^{-1}) of the aerosol flow generated by spraying was dried
126 in a diffusion drier filled with silica gel. The relative humidity was below 10% after
127 drying. The remainder of the aerosol flow was drawn off by a pump and discarded.
128 The dry aerosol was passed through a tube furnace (Model RS 120/1000/12,
129 Nabertherm GmbH, Lilienthal, Germany) set at $300 \text{ }^\circ\text{C}$. The residence time of the
130 aerosol in the furnace was 5.2 s. Zhao et al. (2010) described this method for
131 generating CaCO_3 aerosol in detail. At room temperature dry $\text{Ca}(\text{HCO}_3)_2$ is
132 thermodynamically unstable and decays into CaCO_3 , CO_2 , and H_2O (Keiser and
133 Leavitt, 1908). With this method the aerosol still contained some $\text{Ca}(\text{HCO}_3)_2$ after
134 drying, but after heating at $300 \text{ }^\circ\text{C}$ it was completely converted into CaCO_3 (Zhao et
135 al., 2010). The CaCO_3 aerosol generated was either first size selected by a Differential
136 Mobility Analyzer (DMA, TSI 3081) with a neutralizer on the inlet or entered the
137 coating device directly as poly-disperse aerosol.

138 Figure 2 (upper panel) shows the total number concentration and mean size of the
139 bare CaCO_3 aerosol particles generated at different spraying time, which were
140 measured with the SMPS described below. The diameter size stabilized after about 50
141 min in the range 49.8-55.5 nm. Over the 232 min spraying time, the total number
142 concentration varied in the range 1.8×10^6 – $4.5 \times 10^6 \text{ cm}^{-3}$. The total number
143 concentration decreased by about 1/3 in the initial 70 min. The decrease became
144 slower after 70 min and the total number concentration tended to stabilize after 155
145 min. After 70 min the total number concentration varied in a smaller range of
146 1.8×10^6 – $2.9 \times 10^6 \text{ cm}^{-3}$, therefore, the measurements in this study typically started after

147 70 min spraying. The typical size distribution of the CaCO₃ aerosol particles after 70
148 min spraying is shown in Fig. 2 (lower panel). The CaCO₃ particles showed a single
149 mode distribution with a mode diameter at 32.2 nm. The number concentration was
150 more than 100 cm⁻³ for particles between 9.82 and 346 nm.

151 **2.2 Organic acid coating**

152 The coating device (Fig. 1, right hand side) used in this study was designed by Roselli
153 (2006), and showed good reproducibility, controllability, and stability. The glass
154 apparatus consisted of a small storage bulb (100 ml) holding the organic coating
155 substances which was directly connected to a mixing cell (about 35 ml). The storage
156 bulb and mixing cell were fully immersed in a flow-through water heater connected to
157 a thermostatic bath (F25, Julabo GmbH, Seelbach, Germany). The temperature range
158 of the thermostatic bath used in this study was 30-80 °C. An extra N₂ stream could be
159 passed through the storage bulb in order to enhance the organic vapors flowing into
160 the mixing cell. The outflow of the coating device was connected to a Liebig type
161 water cooler. The water cooler was controlled by another thermostatic bath (F25,
162 Julabo GmbH, Seelbach, Germany) operated at 25 °C throughout all of the
163 experiments.

164 The bottom of the storage bulb was filled with either 5.0 g malonic acid powder
165 (assay ≥98%(T), Fluka Chemika, Sigma-Aldrich, St Louis, MO, USA) or 10.0 ml
166 oleic acid (chemical purity (GC) 99.5%, Alfa Aesar, Ward Hill, MA, USA). A flow of
167 0.9 L min⁻¹ high purity N₂ was used to carry the organic acid vapor up into the mixing
168 cell. The flow of 0.9 L min⁻¹ CaCO₃ aerosol was passed through the mixing cell and
169 mixed with the 0.9 L min⁻¹ N₂ flow carrying the organic acid vapor. The mixed flow

170 then entered the water cooler. The organic acid vapor was condensed on CaCO₃
171 aerosol particles in both the mixing cell and the water cooler. The residence time of
172 the aerosol in the coating device including the cooler was about 6 seconds Three
173 identical coating devices, with the same heating and cooling thermostatic bath, were
174 used: one for malonic acid coating, one for oleic acid coating, and a blank one without
175 organic acid for assessing the impact caused by heating the CaCO₃ aerosol in the
176 coating device without organic acid (Roselli, 2006).

177 The aerosol could enter the measuring instruments directly, or after passing through a
178 flow tube to increase its residence time. The flow tube was made of a straight circular
179 glass tube with a 2.5 cm internal diameter. The aerosol flow in the flow tube was
180 laminar flow. The residence time of the aerosol in the flow tube was 23.7 s.

181 For the coating process we mixed flows of 0.9 L min⁻¹ of dry N₂ and of aerosol dried
182 to <10% relative humidity (RH) at room temperature (RT). As a consequence RH at
183 the outlet of the coating device was <5% at RT. To investigate the impact of water on
184 the coating process and CCN activity, organic coating at a higher relative humidity
185 was also performed. For that a bubbling device filled with Milli-Q water was utilized
186 to saturate the N₂ stream with water vapor before it entered the storage bulb (RH>90%
187 at RT). After mixing with the aerosol stream at RH ≈10%, the water concentration in
188 the mixing cell corresponded to RH ≈ 50% at RT or a partial pressure of ≈1500 Pa.
189 The relative humidity of the aerosol at the outlet of the coating device at RT was
190 indeed ~47% when humidification was applied. For the partial water vapor pressure
191 of 1500 Pa we calculated RH >7% at 60°C (for MA), and RH >3% at 80°C (for OA)
192 which is about an order of magnitude higher than RH in the dry cases. In fact RH will
193 be somewhat higher as the gas-phase may not reach the bath temperature which

194 primarily serves to warm up the coating agent and control its vapor pressure.

195 **2.3 Size and chemical composition measurements**

196 The number size distribution of the aerosol particles was measured using a Scanning
197 Mobility Particle Sizer (SMPS, TSI 3080 Electrostatic Classifier with TSI 3081 DMA,
198 TSI 3786 UWCPC). The sample flow was set to 0.6 L min^{-1} and the sheath flow was
199 set to 6.0 L min^{-1} . The size range measured was 9.82-414.2 nm with a size resolution
200 of 64 channels per decade and the time resolution was 3 min for a complete scan.
201 Despite the maximum resolution of the SMPS the size bin width was still substantial
202 compared to the observed growth by coating. We therefore derived the diameter of the
203 coated (and the respective bare CaCO_3 particles) by interpolating in between the size
204 bins. For that we considered 5-9 size bins around the size bin of nominal mode and
205 fitted a lognormal distribution to these data. The fitted mode positions are listed in
206 Table 1. The error bars in x direction in Figure S1 in the supplement, show the shifts
207 of the fitted mode position relative to the nominal size bin.

208 The chemical composition and the vacuum aerodynamic diameter of the aerosol
209 particles were measured using a High-Resolution Time-of-Flight Aerosol Mass
210 Spectrometer (HR-ToF-AMS, Aerodyne Research Inc., Billerica, MA, USA (DeCarlo
211 et al., 2006)). The aerosol particles were vaporized at $600 \text{ }^\circ\text{C}$ and ionized by electron
212 impact ionization at 70 eV, i.e. we focused on the measurements of the organic
213 coatings and sacrificed a direct CaCO_3 determination by AMS (compare Zhao et al.
214 2010). The AMS was routinely operated in V-mode in two alternating modes: 1 min
215 MS mode to measure the chemical composition and 2 min PToF mode. Only MS
216 mode data were analyzed. AMS measurements and SMPS measurements were
217 synchronous and both were repeated at least four times for each sample. Size

218 information for bare CaCO₃ was taken from SMPS data in the blank coating device.

219 We used specific marker m/z to derive the amount of organic coating. For pure oleic
220 acid the signal at $m/z41$ (C₃H₅⁺) was reported to be the strongest signal in the mass
221 spectrum measured by Q-AMS at EI energy of 70 eV and vaporizer temperature of
222 600 °C (Sage et al., 2009). The signal at $m/z41$ was also strongest for oleic acid
223 coatings in our HR mass spectra. In order to get a high signal to noise ratio we choose
224 the signal at $m/z41$ in the MS mode of the AMS measurement as a marker for oleic
225 acid in the coated CaCO₃ particles. There was no significant signal at $m/z41$ for the
226 uncoated CaCO₃ particles. The average background signal at $m/z41$ per single aerosol
227 particle corresponded to $2.4 \pm 0.79 \cdot 10^{-12}$ µg for bare CaCO₃. The average value
228 presented the baseline of the mass spectra and the standard deviation was derived
229 from the noise of the mass spectra at $m/z41$. Similarly, the signal at $m/z42$ (C₂H₂O⁺)
230 was one of the strongest signals in the mass spectrum of pure malonic particles
231 measured by Q-AMS with EI energy of 70 eV and vaporizer temperature of 600 °C
232 (Takegawa et al., 2007). That signal was also observed for malonic acid coatings in
233 our HR mass spectra and used as marker for malonic acid coatings. The average
234 background signal per aerosol particle at $m/z42$ for bare CaCO₃ particles was
235 $1.4 \pm 0.42 \cdot 10^{-12}$ µg. The average value represented the baseline of the mass spectra at
236 $m/z42$ and the standard deviation was derived from the noise in the mass spectra.

237 The coating amount for both organic compounds was derived as follows. The
238 observed signal at the respective marker m/z was corrected for the background signal
239 from bare CaCO₃ and then scaled to the volume increase (per particle) calculated
240 from the shift of the particle diameter D_p for the largest coating amount achieved at 80
241 °C coating temperature. Because of the relative large bin width compared to the

242 growth by coating we used the D_p 's, interpolated between the nominal size bins of the
243 SMPS (see above). This assumed spherical core shell morphology, based on Zhao et
244 al. (2011) where we showed that the CaCO_3 particles generated by our spray drying
245 method are spherical. The relation between AMS derived organic mass (baseline
246 corrected marker signals at $m/z41$ or $m/z42$ per particle) and SMPS derived organic
247 mass ($\pi/6 \cdot (D_p)^3 / \rho_{\text{org}}$) is linear within the limits of the method (see Figure S1 in the
248 supplement). For discussion we will refer to the AMS results, as we are able to detect
249 amounts of organic coatings as small as few time 10^{-12} ug per particle with the AMS,
250 while these could be not be detected by the SPMS.

251 **2.4 CCN activity measurement**

252 The aerosol was dried to RH <3% by another diffusion drier before the CCN activity
253 was measured. To determine the CCN activity of the aerosol, the number
254 concentration of the cloud condensation nuclei (CCN) of the aerosol was measured
255 with a continuous flow CCN counter (CCNC, DMT-100, Droplet Measurement
256 Technologies, Boulder, CO, USA). The total number concentration (CN) of the
257 aerosol particles was synchronously measured using an ultrafine water-based
258 condensation particle counter (UWCPC, TSI 3786, cf. Zhao et al., 2010). The ratio of
259 CCN to CN (CCN/CN) is called the activated fraction (a_f). In cases where
260 poly-disperse aerosol was coated, the coated aerosol particles were size selected by
261 scanning a DMA between 10.6 and 478.3 nm , and the CCN and CN concentrations
262 were determined for each size bin while the super-saturation (SS) kept constant
263 (known as 'Scanning Mobility CCN Analysis (SMCA)', Moore et al., 2010). The
264 activated fraction was calculated after the CCN and CN concentrations were corrected
265 for the multiple charged particles.

266 The activated fraction as a function of the particle size was fitted with a cumulative
267 Gaussian distribution function (Rose et al., 2008). The turning point of the function is
268 the critical dry diameter (D_{crit} or D_{50}) at the set SS. The activation efficiency (i.e., the
269 activated fraction when aerosol particles are completely activated) was 83% for the
270 CCN instrument, determined using 150 nm $(\text{NH}_4)_2\text{SO}_4$ particles at $\text{SS}=0.85\%$.
271 Besides CaCO_3 and coated CaCO_3 particles, the CCN activity of malonic acid
272 particles, oleic acid particles, and mixed particles of CaCO_3 and malonic acid was
273 also measured. The oleic acid particles were generated by heating 10.0 ml oleic acid
274 to 97 °C in the storage bulb and then cooling the vapor to 2 °C in the water cooler in a
275 clean coating device. 1.75 L min^{-1} high-purity N_2 was used as carrying gas and went
276 into the storage bulb through '1 N_2 in' entrance in Fig. 1; the '3 Aerosol in' entrance in
277 Fig. 1 was closed. This way, pure oleic acid particles with diameters up to 333 nm
278 were generated. Mixed CaCO_3 /malonic acid particles were generated by spraying the
279 supernatant clear solutions which were prepared by settling suspensions containing
280 CaCO_3 and malonic acid in molar ratios of about 1:1 and 3:1. The suspensions were
281 prepared with 0.020 g malonic acid and 0.021 g CaCO_3 and 0.025 g malonic acid and
282 0.076 g CaCO_3 in 1000 ml Milli-Q water, respectively. The suspensions were allowed
283 to stand for 24h.

284 For aerosols where monodisperse aerosol particles with a dry diameter D_p were
285 coated, the CCN concentration was measured at different SS and the CN
286 concentration was measured synchronously. Similarly, the activated fraction as a
287 function of SS was fitted with a cumulative Gaussian distribution function. The
288 turning point of the function is the critical supersaturation (SS_{crit}) and the
289 corresponding to the dry diameter D_p is also called the critical diameter, D_{crit} . The
290 hygroscopicity parameter κ (Petters and Kreidenweis, 2007) was then calculated from

291 the $D_p(D_{crit})$ - SS_{crit} or $SS(SS_{crit})$ - D_{crit} data set. The SS settings of the CCN counter were
292 calibrated weekly using $(NH_4)_2SO_4$ aerosol based on the theoretic values in the
293 literature (summarized by Rose et al., 2008).

294 **3 Results and discussion**

295 **3.1 CCN activity of $CaCO_3$ aerosol**

296 Before the coating experiments we determined the CCN activity of the bare $CaCO_3$
297 aerosol particles. It was measured by the scanning method (SMCA) using
298 poly-disperse $CaCO_3$ aerosol particles. The value of the hygroscopicity parameter κ of
299 the $CaCO_3$ aerosol was 0.0028 ± 0.0001 derived by the least-square-fitting of D_{crit} as a
300 function of SS (SS_{crit}). This κ value is quite small, indicating that the CCN activity of
301 the $CaCO_3$ aerosol is low. Our κ is well within the range of κ 's of 0.0011 ± 0.0004 to
302 0.0070 ± 0.0017 found in previous studies for wet generated $CaCO_3$ particles (Zhao et
303 al., 2010; Sullivan et al., 2009; Gierlus et al., 2012, Tang et al., 2016), but larger than
304 κ for dry generated $CaCO_3$ aerosols (0.008-0.0018, Sullivan et al., 2009).

305 The CCN activity for $CaCO_3$ aerosol passed through the blank coating device and
306 exposed to temperatures of 60 °C and 80 °C was determined using the same method.
307 The κ value remained 0.0028 ± 0.0001 up to 60 °C and increased to 0.0036 ± 0.0001
308 at 80 °C. The increased κ value of 0.0008 at 80 °C was lower than the differences of
309 reported κ values for $CaCO_3$ aerosol in various studies, and much lower than the
310 changes of κ values measured in this study when the $CaCO_3$ aerosol particles were
311 coated by malonic or oleic acid. So the effect of heating the $CaCO_3$ aerosol during the

312 coating process on the CCN activity of the CaCO₃ aerosol was neglected. The D_{crit} at
 313 different supersaturations (SS_{crit}) for the CaCO₃ aerosol and for the CaCO₃ aerosol
 314 passed through a blank coating device at heating temperatures of 60 °C and 80 °C are
 315 shown in Fig. 5 (red, yellow and green circles).

316 As the solubility of CaCO₃ in water is very low, droplet activation of CaCO₃ (and
 317 other mineral dust components) is often described by a water adsorption approach,
 318 wherein the solute term B in the Köhler equation (Köhler 1936, Seinfeld and Pandis,
 319 2006, see eq. (S1-S3) in the supplement) is replaced by a water adsorption term. The
 320 equations (1) and (2) show application of the Frenkel Halsey Hill adsorption isotherm
 321 (FHH) as proposed by Sorjamaa and Laaksonen (2007) and Kumar et al. (2009):

$$322 \quad B = -A_{\text{FHH}} \cdot \theta^{-B_{\text{FHH}}} \quad (1)$$

323 Therein the water coverage θ by (Sorjamaa and Laaksonen, 2007) is given as:

$$324 \quad \theta = \frac{D_w - d_u}{2 \cdot 2.75 \cdot 10^{-4}} \quad [\text{um}] \quad (2)$$

325 and D_w and d_u are the diameter of the wet particles and the insoluble core. We applied
 326 the FHH parameter for CaCO₃ (AFHH=0.25 and BFHH=1.19, Kumar et al. 2009) and
 327 derived a critical supersaturation of 1.52% for CaCO₃ particles with d_u = 101.9 nm
 328 (Figure 7, blue line). In comparison κ -Köhler theory predicts SS_{crit}=1.49% for
 329 $\kappa=0.0028$. Such an SS_{crit}=1.49% would also be achieved by 8.5·10⁻²⁰ mole solute per
 330 particle (Figure 7, black line). Figure 7 also shows the SS_{crit} for the bare CaCO₃
 331 particles processed at 80°C coating temperature and the range of SS_{crit} for 101.9nm

332 particles calculated from the range of κ 's given in the literature (Tang et al., 2016 and
333 references therein) for wet generated CaCO₃ particles.

334 We conclude that the surface of our CaCO₃ particles is a little more wettable than the
335 dry generated particles studied by Kumar et al. (2009). We presume formation of
336 Ca(OH)(HCO₃) structures on the surface during the spray-drying generation process
337 as commonly observed whenever the CaCO₃ surface has been exposed to gaseous
338 water or liquid water (Stipp, 1999; Stipp and Hochella, 1991; Neagle and Rochester,
339 1990). In case of soluble components causing the lower SS_{crit} their amount must be of
340 the order of $1 \cdot 10^{-19}$ mole per particles.

341 **3.2 CCN activity of CaCO₃ particles with oleic acid coating**

342 For the coating with oleic acid, we selected monodisperse CaCO₃ aerosol particles of
343 101.8 nm diameter using the DMA, and measured the size and chemical composition
344 of the particles before (uncoated) and after (coated) coating with oleic acid. The
345 results are listed in the upper part of Table 1.

346 The mode diameters of number size distribution for the uncoated CaCO₃ particles at
347 30-80 °C remained in the 101.8 nm size bin, identical to that selected by the DMA.
348 Interpolation in between the size bins as described in the experimental section led to
349 an average dry diameters of bare CaCO₃ of $d_u = 101.9$ nm. The mode diameters of the
350 CaCO₃ particles after coating with oleic acid in the range of 30-50 °C stayed in the
351 pre-selected size bin at 101.8 nm, which means that the layers were too thin to

352 effectively grow the particles to the next size bin; the mode diameters increased
353 distinctively in the temperature range of 60-80 °C (Fig. 3, upper panel). However, the
354 bin-interpolated diameters D_p which are shown in Table 1 increased monotonically
355 over the whole temperature range.

356 The values of $m/z41$ [μg per particle] originating from the oleic acid coating for the
357 coated CaCO_3 particles at 30-80 °C were at all temperatures significantly larger than
358 for the bare CaCO_3 particles, and increased with the increasing coating temperature
359 ($3.7 \cdot 10^{-12}$ - $390 \cdot 10^{-12}$ μg per particle, compare Table 1 and Fig. 3, bottom panel, red
360 circles). The AMS detected increase at $m/z41$ showed that the CaCO_3 particles already
361 contained small amounts of oleic acid after coating with oleic acid at temperatures
362 below 60 °C although the D_p shifted less than a size bin.

363 The organic volume fraction (vf) in the aerosol particles, $V_{\text{OA}}/V_{\text{par}}$ [%], was calculated.
364 Herein $V_{\text{par}} = (V_{\text{OA}} + V_{\text{CaCO}_3})$, V_{OA} is the oleic acid volume derived by AMS and
365 V_{CaCO_3} the volume of the bare CaCO_3 before coating (101.9 nm). $V_{\text{OA}}/V_{\text{par}}$ for the
366 uncoated CaCO_3 particles is by definition zero. The vf for the coated CaCO_3 particles
367 at 30-80 °C increased with the increase in the coating temperature from 0.8% at 30 °C
368 to 44% at 80 °C (Fig. 3, bottom panel, red crosses and Table 1). The CaCO_3 particles
369 were indeed coated with a significant amount of oleic acid and the amount of oleic
370 acid coating increased with the increase in the coating temperature. The experiments
371 were repeated at least four times. The according standard deviations for the oleic acid
372 mass per particle in Table 1 demonstrate that the reproducibility of the experiments

373 was good and the performance of the coating device was stable.

374 The activated fractions at different SS for monodisperse CaCO₃ particles with d_u =
375 101.9 nm before and after oleic acid coating at 30-80 °C are shown in Fig. 4. The top
376 panel in Fig. 4 shows the results at 30-60 °C with up to $23 \pm 1.2 \cdot 10^{-12}$ ug of coating
377 material deposited on the CaCO₃ particles (vf = 4.3%). At the lowest SS of 0.17% and
378 0.35%, the activated fractions were very low and independent of the presence of the
379 coating material within the errors. When the SS increased to 0.52%, 0.70%, and
380 0.87%, the activated fractions for the coated CaCO₃ particles were *lower* than those
381 for the uncoated particles. Notably the activated fractions for the coated CaCO₃
382 particles *decreased* with the increase in the coating material in the range of vf
383 0.8-2.7%. The activated fractions for the CaCO₃ particles with different amounts of
384 coating spread with larger SS applied. However this trend reversed at the coating
385 temperature of 60 °C and an oleic acid vf of 4.3%, and the activated fractions at vf =
386 4.3% became higher than those at 2.7% at the three largest SS. In summary, we found
387 that the CCN activity of the coated CaCO₃ particles with vf of OA in a range 0.8-4.3%
388 was lower than that of the uncoated CaCO₃ particles. The CCN activity of the coated
389 CaCO₃ particles decreased with the increasing vf in between 0.8-2.7%, i.e. the CCN
390 activity became lower when more coating material deposited on the CaCO₃ particles.
391 This trend turned somewhere at a vf somewhere between 2.7 and 4.3%. As the D_p also
392 increased at 60 °C we cannot differentiate if the increase in the activated fractions is
393 due to increasing size or because of increasing wettability.

394 The activated fractions of CaCO₃ particles after coating with oleic acid with vf of 16%
395 and 44% (coating temperatures of 70 and 80 °C , respectively) were considerably
396 higher than that before coating, as shown in Fig. 4 (bottom panel). The increased
397 activated fractions resulted from both the increase in particle size (Fig. 3) and the
398 increase of the OA volume fraction of particles. At vf of 16% and 44%, the activated
399 fractions of the CaCO₃ particles after coating increased with the increase of SS and
400 reached complete activation. (Note, because the activation efficiency is 83%, the
401 activated fractions appear at values less than 100% at the points of full activation.)
402 For vf of 16% and 44% SS_{crit} was determined by Gaussian fitting of the activated
403 fraction as a function of SS. The particle dry diameter D_p which is D_{crit} in these cases
404 is given as in Table 1. The hygroscopicity parameter κ was determined from D_p (D_{crit})
405 and the corresponding SS_{crit}. The κ values of the CaCO₃ particles coated with vf of
406 oleic acid of 16% and 44% were 0.0237 ± 0.0006 and 0.0673 ± 0.0016, respectively.
407 The respective κ values for the CaCO₃ particles with a diameter of 101.9 nm without
408 coating and after coating with oleic acid at 30-60 °C (oleic acid vf ≤4.1%) could not
409 be determined by this method because these particles could not be fully activated at
410 the highest SS reachable by the CCN counter. Therefore we give as upper limit κ =
411 0.0028 ± 0.0001 for the uncoated CaCO₃ particles determined by scanning the size of
412 the poly-disperse CaCO₃ aerosol particles as described above (see Fig. 5).

413 So we conclude that for vf of oleic acid of 0.8-2.7% the CCN activity of CaCO₃
414 particles after coating is lower than that of uncoated CaCO₃ particles and decreases
415 with the fraction of oleic acid. The trend turns at a vf between 2.7 and 4.3%. CCN

416 activity was higher than that of the bare CaCO₃ particles at vf of oleic acid of 16%
417 (70°C) and 44% (80°C) with CCN activity $\kappa = 0.0237 \pm 0.0006$ and $\kappa = 0.0673 \pm$
418 0.0016), respectively. The enhanced and reduced CCN activity of CaCO₃ particles
419 coated with oleic acid at 80 °C and 60 °C, respectively, was also evident from the
420 CCN activity measurement using *poly-disperse* aerosols (Fig. 5).

421 A possible explanation for our observation can be based on the amphiphilic character
422 of oleic acid, namely that one end of the oleic acid molecule is hydrophobic (the
423 hydrocarbon chain), while the other is hydrophilic (the carboxyl group).

424 We refer to Ca(OH)(HCO₃) structures at the surface which offer polar surface sites to
425 bind the hydrophilic ends (the carboxyl groups) of the oleic acid molecules. The
426 hydrophobic ends of oleic acid molecules (the hydrocarbon chains) are then exposed
427 on the particle surface hence increase the hydrophobicity of the particle surface. Such
428 a formation of a hydrophobic layer should be occurring until all polar sites are
429 occupied or monolayer coverage - maybe in form of a self-assembled layer - is
430 reached. This can hinder the uptake of water. Activation of CaCO₃ particles can be
431 described by the Kelvin term and a water absorption term, e.g. Frenkel Halsey Hill
432 isotherm (Sorjamaa and Laaksonen, 2007, Kumar et al. 2009). In terms of
433 Kelvin/FHH theory the hydrophobic OA coating will lower A_{FHH} and/or likely
434 increase B_{FHH} . (The formation of a monolayer of OA on black carbon particles with
435 the polar groups pointing outwards was postulated by Dalirian et al. (2017), which
436 lead to increased activation of the black carbon particles. Thus, they observed a

437 similar effect of layer formation, but with switched polarity.)

438 Garland et al. (2008) suggested that OA at sub-monolayer coverage form
439 self-associated islands rather than uniformly covering the surfaces, and OA molecules
440 are oriented vertically, with polar heads facing to the surface. This is in support of our
441 working hypothesis: the formation of a hydrophobic surface film. We conclude that
442 all hygroscopic sides on the CaCO₃ surface are covered at OA vf somewhere between
443 2.7% and 4.3%, as here the trend turns and droplet activation starts to increase again.
444 This would place the monolayer coverage above 3%, organic volume fraction.
445 According to the measurements and calculations of the length of oleic acid molecule,
446 the thickness of oleic acid sub-monolayer on solid surfaces, and the thickness of
447 deuterated oleic acid monolayers at the air-water interface (Garland et al., 2008; King
448 et al., 2009; Iwahashi et al., 2000), we estimate 2.3 nm as the likely thickness of oleic
449 acid monolayer on CaCO₃ particles, accordingly a monolayer would be achieved at
450 about 12-13% organic volume fraction. As a consequence the re-increase of
451 hygroscopicity starts at sub-monolayer coverage and we propose that a fraction of
452 oleic acid binds to already adsorbed oleic acid tail by tail such that carboxylic groups
453 are facing outwards.

454 For CaCO₃ particles coated with more than an OA monolayer (vf = 16% and 44% at
455 70 and 80 °C coating temperatures), OA in the first layer should still combine with the
456 CaCO₃ surface, the heads pointing downwards. We suppose that now a portion of the
457 carboxyl groups of the oleic acid molecules, which are not in the first layer, will be

458 exposed to the particle surface, in analogy to the formation of lipid bilayers, e.g. in
459 cells, though the structure of this part of oleic acid is not known. The particle surface
460 then becomes more hydrophilic.

461 When carboxylic groups of OA are exposed at the surface, the interaction of water
462 with the OA layer becomes stronger, and the surface becomes wettable. In terms of
463 the Kelvin/FHH approach, the surface water interaction becomes stronger and A_{FHH}
464 increases and likely also the interaction between the higher water layers (B_{FHH}
465 decreases). From this point of view water adsorption by the “OA bilayer” should
466 become similar to thin malonic acid layers (compare next section). In addition, when
467 droplets form, oleic acid will transfer to the surface of the droplets and lower the
468 surface tension of the solution (the surface tension of oleic acid is 0.033 J m^{-2} , which
469 is much lower than that of pure water of 0.072 J m^{-2}). Thus, the activation of OA
470 coated particles is probably a complex interaction between formation of a specific
471 hydrophobic layers and more hydrophilic multilayers, surface tension effects and for
472 the largest coating amounts, simple size effects. As shown in Figure 7, SS_{crit} for OA is
473 lower than for thin malonic acid coatings, probably because of the surface tension
474 effect, but higher than for thick MA coatings, because of the missing solute effect.

475 The CCN activity of all oleic coated particles is higher than the CCN activity of pure
476 oleic acid. Our CCN activity measurement showed that pure oleic acid particles up to
477 333 nm did not activate at 0.87% SS; this sets an upper limit for CCN activity of oleic
478 acid particles ($\kappa < 0.0005$), in agreement with Kumar et al. (2003) and Broekhuizen et

479 al. (2004). In liquid state oleic acid (OA) forms micelle like structures, the hydrophilic
480 ends (the carboxyl groups) of oleic acid molecules tend to combine together by
481 hydrogen bonds and the hydrophobic tails (the hydrocarbon chains) are exposed at the
482 outside (Iwahashi et al., 2000; Garland et al., 2008). The arrangement of oleic acid
483 molecules in pure oleic acid particles should be similar. Hydrophobic tails facing
484 outwards can explain the hydrophobicity of the particle surface and the hindrance of
485 the uptake of water, making the CCN activity of pure oleic acid particles very low.
486 For sub-monolayer coatings of OA of v_f 0.8 - 2.7% the CCN activity seem to
487 approach that of pure OA. However, the arrangement of oleic acid molecules in these
488 thin coatings will be influenced by the CaCO_3 core with its polar, hydrophilic sides
489 differing from pure oleic acid particles and can thus be less hydrophobic

490 Even at the largest coating with an organic volume fraction of 44%, the coating
491 thickness is about 10 nm, which corresponds to about only 4 monolayers of oleic acid
492 (assuming the thickness of oleic acid monolayer on CaCO_3 particles is about 2.3 nm).
493 And the arrangement of oleic acid molecules will still be likely influenced by the
494 CaCO_3 core. Water can probably adsorb at the carboxylic groups facing outward
495 ("bilayer" type structure) and diffuse through the thin oleic acid coatings. It may form
496 an adsorbed water phase near the CaCO_3 surface. This could push the oleic acid out to
497 act as surfactant which lowers the Kelvin term. Such processes should also happen in
498 pure oleic acid particles. Because of the presence of CaCO_3 core the SS to achieve
499 this is lower than for pure OA.

500 The phenomenon described above is reported for the first time in the studies on the
501 CCN activity of multicomponent aerosols. This phenomenon also shows a limitation
502 of the otherwise very useful mixing rule (Petters and Kreidenweis, 2007) for
503 multicomponent aerosols with specific morphologies.

504 In Fig. 5 we additionally show the influence of water vapor on CCN activity of
505 CaCO_3 particles coated with oleic acid for the highest coating temperature (80 °C)
506 and thus largest oleic acid amount. Herein we determined D_{crit} at different
507 super-saturations (SS_{crit}) for *poly-disperse* CaCO_3 aerosol particles (by SMCA). The
508 experiments were performed at RH 0.3% and at RH 3% at the coating temperature of
509 80 °C on cooling to room temperature the RH increased to 47%. The presence of
510 more water vapor (1500 Pa) in the coating process increased κ somewhat and
511 enhanced the CCN activity. This is of importance since often RH will larger than 0.3%
512 if coating appears in the atmosphere. This will be discussed further in context of
513 malonic acid coatings at enhanced water vapor.

514 **3.3 CCN activity of CaCO_3 particles with malonic acid coating**

515 For the study with malonic acid coatings, the CaCO_3 particles were also size selected
516 with a diameter of 101.8 nm. The size D_p and chemical composition of CaCO_3 aerosol
517 particles are listed in Table 1 before and after coating with malonic acid (MA) at
518 temperatures in a range of 30-80 °C. The mode diameter did not shift after coating in a
519 temperature range of 30-60 °C, but it increased for coatings at 70 and 80 °C with
520 increasing coating temperature. The size bin interpolated particle diameter D_p of the

521 MA coated particles increased monotonically with the coating temperature. The
522 average of the interpolated diameter of bare CaCO₃ particles in the temperature range
523 30°C-80°C was $d_u = 101.9$ nm.

524 Values of the malonic acid marker $m/z42$ per particle were significantly larger for
525 CaCO₃ particles after coating at 30-80 °C and the MA mass increased from $3.3 \cdot 10^{-12}$
526 to $610 \cdot 10^{-12}$ ug per particle with the coating temperature (Table 1, Figure 3, bottom
527 panel). The organic volume fraction vf of malonic acid ($V_{MA}/(V_{MA}+V_{CaCO_3})[\%]$) was
528 calculated as in the case of the oleic acid and ranged from 0.4 to 40%. As for oleic
529 acid the malonic acid experiments were repeated at least four times and the
530 reproducibility and stability were good (see standard deviations in Table 1).

531 The activated fractions at different SS for 101.9 nm CaCO₃ particles before and after
532 coating with malonic acid at 30-80 °C are shown in Fig. 6. SS_{crit} was determined by
533 fitting a single cumulative gauss function to the data and the κ value was calculated
534 from the $D_p(D_{crit})$ and the corresponding SS_{crit} . The results are listed in Table 1. In this
535 procedure we had to neglect the contribution of double charged particles as the step in
536 the CN/CCN vs SS data in Fig.6 is not sufficiently expressed to separate a plateau for
537 multiply charged particles (e.g. Sullivan et al. 2009). The exception is the MA coating
538 with $vf = 0.04\%$. For this case we compared a sigmoid fitting both from the beginning
539 (the first point) and from the multiply-charged plateau (the third point) to the
540 “completely-activated plateau” (Figure S3, supplement). We yield $SS_{crit} =$
541 $0.887 \pm 0.005\%$ for fitting from the beginning and $SS_{crit} = 0.900 \pm 0.013\%$ for fitting

542 from the multiply-charged plateau, a difference of 0.013%. The underestimate in SS_{crit}
543 is the largest (0.013%) when the MA mass is the smallest ($vf = 0.04\%$) and the
544 underestimate will be reduced with increasing vf of MA. At the largest two MA vf it
545 can be neglected. We have to concede a systematic error in SS_{crit} , but it is distinctively
546 less than 0.02%

547 The κ values of the $CaCO_3$ particles after coating with malonic acid at 30-80 °C were
548 higher than the κ value of the uncoated $CaCO_3$ particles ($\kappa = 0.0028 \pm 0.0001$), and
549 increased with the increasing coating MA mass per particle and increasing MA vf .
550 The CCN activity of the $CaCO_3$ particles increased monotonically after coating with
551 increasing malonic acid mass. This result differs from that of oleic acid which is not
552 surprising since malonic acid is easily soluble in water.

553 The κ value for the $CaCO_3$ particles after coating with a mass of malonic acid as small
554 as $3.3 \cdot 10^{-12}$ ug per particle and vf of MA of only 0.4% was 0.0123 ± 0.0005 thus
555 considerably larger than the κ value for the uncoated $CaCO_3$ particles ($\kappa = 0.0028 \pm$
556 0.0001). This suggests that already a small amount of malonic acid can significantly
557 enhance the CCN activity of $CaCO_3$ particles. Such phenomenon, that traces of water
558 soluble substances can strongly affect droplet activation has been reported before
559 (Bilde and Svenningsson, 2004).

560 We applied Koehler theory to $CaCO_3$ particles coated with malonic acid assuming
561 that the malonic acid coating will fully dissolve in water when droplets form (see
562 supplement eq. (S1-S3). Increasing MA solute decreases the activity of water in

563 solution, and lowers the critical supersaturation SS_{crit} for droplet activation.

564 The resulting Koehler curves, i.e. equilibrium supersaturation (SS) over the solution
565 droplet as a function of the wet diameter D_w , are shown in Figure S2. Therein the
566 maximum of each SS curve is the critical supersaturation (theory SS_{crit}). In Table S1
567 and Figure 7 we compare the SS_{crit} predicted by the Köhler approach (red) with the
568 observed SS_{crit} (black). Koehler theory overpredicts SS_{crit} for thin coatings
569 substantially, meaning it underestimates the hygroscopicity of the thinly coated
570 particles. But with increasing coating Koehler theory approaches the observed SS_{crit}
571 and SS_{crit} for a particle of 121 nm diameter composed of pure malonic acid is the
572 limiting case (red circle).

573 From the Koehler results we derived the water content of the particles at SS_{crit} and we
574 calculated molality and mass fraction of the solute in the solution at the point of
575 activation. The molality at minimum and maximum malonic acid load of $3.3 \cdot 10^{-12}$
576 $\mu\text{g}/\text{particle}$ and $610 \cdot 10^{-12}$ $\mu\text{g}/\text{particle}$ were $0.006 \text{ mol kg}^{-1}$ and $0.0015 \text{ mol kg}^{-1}$,
577 respectively. We used these values in the AIOMFAC model (Zuend et al. 2011) to
578 calculate the deviation from ideality for the solution at point of activation for a flat
579 solution. The both solutions are highly non-ideal with respect to the MA ($a_x = 0.4$),
580 wherein MA was treated as solute with reference state infinite dilution (mole fraction
581 $x_{solute} \rightarrow 0$). However this did not affect much the activity coefficient of water, which
582 is essentially 1, water treated as solvent with reference state pure liquid (mole fraction
583 $x_{water} = 1$). Moreover, in this concentration range, the surface tension of aqueous

584 malonic acid solutions is about 0.070 J m^{-2} , thus the nearly same as for water (Table
585 S2 in the supplement). One should expect that Koehler theory would predict SS quite
586 well under such conditions.

587 To bring Köhler theory in agreement with the observation for the thinnest coating,
588 *more* solute entities would be required. Thus, disagreement cannot be caused by an ill
589 determined van't Hoff factor as we used already maximum $\nu = 3$ and reducing ν will
590 increase the deviation. Note, that recent observations point to the importance of the
591 surface effect by organic surface films over the solute effect for water soluble
592 inorganics in presence of organics, including malonic acid (Ruehl et al., 2016). A
593 lower surface tension will bring Koehler prediction and observation punctually in
594 better agreement and still allow for smaller van't Hoff factors. As an example, a
595 surface tension of 55% of σ_w and a van't Hoff factor of one will bring SS_{crit} predicted
596 by Koehler theory and observation in agreement for the thinnest coating. However, a
597 surface tension 55% of σ_w will cause disagreement for the thickest coating, because
598 the solute term gains in importance. Probably, the findings for the mixed solutions of
599 malonic acid and water soluble ammonium sulfate are not directly transferable to our
600 systems with insoluble inorganic core, where we expect dilute aqueous solutions of
601 0.006 mol/kg of malonic acid at the activation point. At such concentrations malonic
602 acid does not reduce σ_w , moreover in the study of Ruehl et al. (2016) malonic acid
603 was one of the more Koehler κ behaving organics.

604 In Figure 7 we show the prediction of $SS_{crit}=1.52\%$ for activating CaCO_3 by the

605 Kelvin/FHH theory with the CaCO_3 parameters taken from Kumar et al. (2009). SS_{crit}
606 for our bare CaCO_3 particles is 1.49% and the lower SS_{crit} should be due to a more
607 adsorptive surface, e.g. the presence of $\text{Ca(OH)(HCO}_3\text{)}$ structures. According to
608 classical Koehler theory the equivalent of $8.5 \cdot 10^{-20}$ moles of dissolvable entities
609 would be needed to explain a κ of 0.0028 and SS_{crit} of 1.49%, which is only about $\frac{1}{4}$
610 of the moles MA in the thinnest MA coating. Therefore, whatever makes our CaCO_3
611 particles wettable is not sufficient to explain the low SS_{crit} of 0.9 % at the thinnest MA
612 coating - in terms of Koehler theory.

613 We estimate monolayer coverage by MA at 2-3% vf; this would be achieved in
614 between MA mass loads of $13 \cdot 10^{-12}$ - $38 \cdot 10^{-12}$ ug per particle. Thus a sub-monolayer
615 coating of $3.3 \cdot 10^{-12}$ ug MA per particle caused a drop of SS_{crit} from 1.49 to 0.9 and
616 increased κ from 0.0028 to 0.012. Therefore we conclude that CaCO_3/MA coatings
617 show a non-Koehler behavior at thin coatings, but approach Koehler behavior with
618 increasing MA load.

619 This means there must be specific interactions between MA and the CaCO_3 surface
620 which eases water adsorption and CCN activation. We refer to the $\text{Ca(OH)(HCO}_3\text{)}$
621 structures that likely exist on the particle surface. When CaCO_3 particles are coated by
622 malonic acid (or oleic acid) the hydrophilic sides can serve as polar surface active
623 sites for accommodation of the acids. In case of MA there is no long hydrophobic
624 organic chain, but a second carboxylic group which still could support the adsorption
625 of water films.

626 In terms of Kelvin/FHH theory one could explain the observed low SS_{crit} for thin MA
627 coatings by net stronger interaction with water (higher A_{FHH}) and/or stronger
628 interaction between the adsorbed water layers (lower B_{FHH}) compared to bare $CaCO_3$.
629 If coatings become thicker the Koehler solute effect starts increasingly to contribute
630 and eventually controls the CCN activation. Our data are not sufficient to determine
631 A_{FHH} and B_{FHH} . (The only system in the literature which comes close - in a far sense -
632 is CaOxalate Monohydrate, with $A_{FHH} = 0.57$ and $B_{FHH} = 0.88$ (Kumar et al., 2009).
633 Plug in these FHH parameters will lead to $SS_{crit} = 0.53\%$ commensurable with our
634 observed value of 0.56% for $13 \cdot 10^{-12}$ ug MA coating which represents an organic
635 volume fraction of 1.6% , thus is close to monolayer.)

636 The D_{crit} at different super-saturations (SS_{crit}) for *poly-disperse* $CaCO_3$ aerosol
637 particles before and after coating with malonic acid are shown in Fig. 8. Our
638 observation of $\kappa = 0.25 \pm 0.04$ for pure malonic is consistent with the κ derived from
639 the data of Kumar et al. (2003) ($\kappa = 0.20-0.25$) and Prenni et al. (2001) ($\kappa = 0.24$), but
640 significantly lower than the κ derived from the data of Giebl et al. (2002) ($\kappa =$
641 $0.41-1.04$). The behavior of poly-disperse coated aerosol was similar to the result
642 obtained from the monodisperse $CaCO_3$ aerosol particles.

643 In Fig. 8 we added results for coating in presence of enhanced water vapor (1500 Pa)
644 and aerosols generated by spraying mixtures of malonic acid and $CaCO_3$. At the
645 coating temperature of $60^\circ C$, when the RH increased from 0.7% to 7% and eventually
646 to 47% at room temperature, the CCN activity of the coated $CaCO_3$ particles

647 increased substantially (compare “dry” (blue triangles) and “wet” (lilac triangles) in
648 Fig. 8). The effect is more distinct than for the oleic acid coating shown in Fig. 5, and
649 κ increases by about an order of magnitude. At a wet conditions, the reaction between
650 CaCO_3 and malonic acid maybe more efficient and formation of calcium malonate
651 will reduce d_u , i.e. the diameter of the insoluble core and according to eq, (S1) this
652 may be the reason for the higher CCN activity at the higher RH. The hypothesis of
653 malonate formation is supported by the CCN activity of “calcium malonate” aerosols,
654 generated by spraying solutions containing CaCO_3 and malonic acid with molar ratios
655 of about 1:1 and 3:1. Here the CCN activity is similar to that arising in the coating
656 process in presence of water vapor. The change of the Ca/malonate ratio from 3:1 to
657 1:1 had no large effects. But taking the data of pure malonic acid particles also into
658 account there is a trend to lower κ with increasing Ca in the initial solution.

659 The increasing of residence time (by 23.7 s) had no significant impact on CCN
660 activity for both oleic acid coating and malonic acid coating at both dry and enhanced
661 water vapor conditions, probably because the coating process was already completed
662 in the coating device and no further reactions occurred in the flow tube.

663 Our findings may be important for aging processes of mineral particles in the
664 atmosphere. The dependence of CCN activity of the coated particles on RH during the
665 coating process will help to enhance the increase of the CCN activity by the coating
666 process as water will be abundant in many instances. The effect probably will be
667 relatively small for oleic acid and similar organics, which are hardly water soluble,

668 but strong for malonic acid and similar organic acids, which are highly water soluble.

669 **4 Conclusions**

670 The CCN activity of CaCO₃ particles with oleic acid and malonic acid coatings was
671 investigated in this study. The results show that oleic acid coating and malonic acid
672 coating have different impacts on the CCN activity of CaCO₃ particles. This can be
673 attributed to the amphiphilic property of oleic acid in contrast to the high water
674 solubility of malonic acid. Small amounts of oleic acid coating ($vf \leq 4.3\%$) decreased
675 the CCN activity of the CaCO₃ particles, while more oleic acid coating ($vf \geq 16\%$)
676 increased it. This phenomenon was reported here for the first time, and attributed to
677 stepwise passivating the active sites of CaCO₃ by oleic acid. Once all active sites are
678 occupied we suggest the formation of a lipid like bilayer with the carboxylic groups
679 facing outwards.

680 On the other hand, malonic acid coating (0.4-40%) increased the CCN activity of
681 CaCO₃ particles regardless of the amount of the coating. The CCN activity of CaCO₃
682 particles with malonic acid coating increased with the amount of the coating. Even a
683 small amount of malonic acid coating ($vf = 0.4\%$) significantly enhanced the CCN
684 activity of CaCO₃ particles from $\kappa = 0.0028 \pm 0.0001$ to $\kappa = 0.0123 \pm 0.0005$.
685 Increasing the relative humidity during the coating increased the CCN activity of the
686 CaCO₃ particles with malonic acid coating, probably because more CaCO₃ reacted
687 with malonic acid to soluble CaMalonate. This process will help to increase the CCN
688 activity.

689 Although malonic acid is well soluble in water, SS_{crit} for MA coated particles was
690 overpredicted by Köhler theory. Our results indicate that thin MA coatings provide a
691 wettable particle surface, which favors adsorption of water. For thicker coatings the
692 coated particles approached Köhler behavior, because of increasing importance of the
693 solute effect.

694 Mineral aerosol is one of the most abundant components of the atmospheric aerosol,
695 but its low water solubility limits its CCN activity. This study showed that
696 water-soluble organic acid coating might significantly enhance the CCN activity of
697 mineral aerosol particles. This could lead to mineral aerosol playing a more important
698 role in cloud formation.

699

700 **Acknowledgments**

701 This study was supported by Forschungszentrum Jülich, the National Natural Science
702 Foundation Committee of China (41421064, 21190051, 41121004), and the China
703 Scholarship Council.

704

705

706 **References**

- 707 AIOMFAC model, <http://www.aiomfac.caltech.edu>
- 708 Broekhuizen, K. E., Thornberry, T., Kumar, P. P., and Abbatt, J. P. D.: Formation of cloud
709 condensation nuclei by oxidative processing: Unsaturated fatty acids, *J. Geophys.*
710 *Res.-Atmos.*, 109, D24206, 10.1029/2004jd005298, 2004.
- 711 Cakmur, R. V., Miller, R. L., Perlwitz, J., Geogdzhayev, I. V., Ginoux, P., Koch, D., Kohfeld,
712 K. E., Tegen, I., and Zender, C. S.: Constraining the magnitude of the global dust cycle by
713 minimizing the difference between a model and observations, *J. Geophys. Res.-Atmos.*, 111,
714 D06207, 10.1029/2005jd005791, 2006.
- 715 Charbouillot, T., Gorini, S., Vuyard, G., Parazols, M., Brigante, M., Deguillaume, L., Delort,
716 A. M., and Mailhot, G.: Mechanism of carboxylic acid photooxidation in atmospheric
717 aqueous phase: Formation, fate and reactivity, *Atmos. Environ.*, 56, 1-8,
718 10.1016/j.atmosenv.2012.03.079, 2012.
- 719 Chebbi, A. and P. Carlier (1996). "Carboxylic acids in the troposphere, occurrence, sources,
720 and sinks: A review." *Atmospheric Environment* 30(24): 4233-4249.
- 721 Cheng, Y., Li, S. M., Leithead, A., Brickell, P. C., and Leitch, W. R.: Characterizations of
722 cis-pinonic acid and n-fatty acids on fine aerosols in the Lower Fraser Valley during Pacific
723 2001 Air Quality Study, *Atmos. Environ.*, 38, 5789-5800, 10.1016/j.atmosenv.2004.01.051,
724 2004.
- 725 Chumpitaz, L. D. A., Coutinho, L. F., and Meirelles, A. J. A.: Surface tension of fatty acids
726 and triglycerides, *J. Am. Oil Chem. Soc.*, 76, 379-382, 10.1007/s11746-999-0245-6, 1999.
- 727 Cruz, C. N., and Pandis, S. N.: A study of the ability of pure secondary organic aerosol to act
728 as cloud condensation nuclei, *Atmos. Environ.*, 31, 2205-2214,
729 10.1016/s1352-2310(97)00054-x, 1997.
- 730 Dalirian, M., Ylisirniö, A., Buchholz, A., Schlesinger, D., Ström, J., Virtanen, A., and
731 Riipinen, I.: Cloud droplet activation of black carbon particles coated with organic
732 compounds of varying solubility, *Atmos. Chem. Phys. Discuss.*, 2017, 1-25,
733 10.5194/acp-2017-1084, 2017.
- 734 DeCarlo, P. F., Kimmel, J. R., Trimborn, A., Northway, M. J., Jayne, J. T., Aiken, A. C.,
735 Gonin, M., Fuhrer, K., Horvath, T., Docherty, K. S., Worsnop, D. R., and Jimenez, J. L.:
736 Field-deployable, high-resolution, time-of-flight aerosol mass spectrometer, *Anal. Chem.*, 78,
737 8281-8289, 10.1021/ac061249n, 2006.
- 738 Falkovich, A. H., Ganor, E., Levin, Z., Formenti, P., and Rudich, Y.: Chemical and
739 mineralogical analysis of individual mineral dust particles, *J. Geophys. Res.-Atmos.*, 106,
740 18029-18036, 10.1029/2000jd900430, 2001.
- 741 Falkovich, A. H., Schkolnik, G., Ganor, E., and Rudich, Y.: Adsorption of organic
742 compounds pertinent to urban environments onto mineral dust particles, *J. Geophys.*
743 *Res.-Atmos.*, 109, D02208, 10.1029/2003jd003919, 2004.

744 Gantt, B., Xu, J., Meskhidze, N., Zhang, Y., Nenes, A., Ghan, S. J., Liu, X., Easter, R., and
745 Zaveri, R.: Global distribution and climate forcing of marine organic aerosol - Part 2: Effects
746 on cloud properties and radiative forcing, *Atmos. Chem. Phys.*, 12, 6555-6563,
747 10.5194/acp-12-6555-2012, 2012.

748 Garimella, S., Huang, Y. W., Seewald, J. S., and Cziczo, D. J.: Cloud condensation nucleus
749 activity comparison of dry- and wet-generated mineral dust aerosol: the significance of
750 soluble material, *Atmos. Chem. Phys.*, 14, 6003-6019, 10.5194/acp-14-6003-2014, 2014.

751 Garland, E. R., Rosen, E. P., Clarke, L. I., and Baer, T.: Structure of submonolayer oleic acid
752 coverages on inorganic aerosol particles: evidence of island formation, *Phys. Chem. Chem.
753 Phys.*, 10, 3156-3161, 10.1039/b718013f, 2008.

754 Giebl, H., Berner, A., Reischl, G., Puxbaum, H., Kasper-Giebl, A., and Hitzemberger, R.:
755 CCN activation of oxalic and malonic acid test aerosols with the University of Vienna cloud
756 condensation nuclei counter, *J. Aerosol Sci.*, 33, 1623-1634, Pii s0021-8502(02)00115-5,
757 10.1016/s0021-8502(02)00115-5, 2002.

758 Gierlus, K. M., Laskina, O., Abernathy, T. L., and Grassian, V. H.: Laboratory study of the
759 effect of oxalic acid on the cloud condensation nuclei activity of mineral dust aerosol, *Atmos.
760 Environ.*, 46, 125-130, 10.1016/j.atmosenv.2011.10.027, 2012.

761 Hartz, K. E. H., Tischuk, J. E., Chan, M. N., Chan, C. K., Donahue, N. M., and Pandis, S. N.:
762 Cloud condensation nuclei activation of limited solubility organic aerosol, *Atmos. Environ.*,
763 40, 605-617, 10.1016/j.atmosenv.2005.09.076, 2006.

764 Hatch, C. D., Gierlus, K. M., Schuttlefield, J. D., and Grassian, V. H.: Water adsorption and
765 cloud condensation nuclei activity of calcite and calcite coated with model humic and fulvic
766 acids, *Atmos. Environ.*, 42, 5672-5684, 10.1016/j.atmosenv.2008.03.005, 2008.

767 Haywood, J., and Boucher, O.: Estimates of the direct and indirect radiative forcing due to
768 tropospheric aerosols: A review, *Reviews of Geophysics*, 38, 513-543,
769 10.1029/1999rg000078, 2000.

770 Herich, H., Tritscher, T., Wiacek, A., Gysel, M., Weingartner, E., Lohmann, U.,
771 Baltensperger, U., and Cziczo, D. J.: Water uptake of clay and desert dust aerosol particles at
772 sub- and supersaturated water vapor conditions, *Phys. Chem. Chem. Phys.*, 11, 7804-7809,
773 10.1039/b901585j, 2009.

774 Ho, K. F., Cao, J. J., Lee, S. C., Kawamura, K., Zhang, R. J., Chow, J. C., and Watson, J. G.:
775 Dicarboxylic acids, ketocarboxylic acids, and dicarbonyls in the urban atmosphere of China,
776 *J. Geophys. Res.-Atmos.*, 112, D22s27, 10.1029/2006jd008011, 2007.

777 Ho, K. F., Lee, S. C., Ho, S. S. H., Kawamura, K., Tachibana, E., Cheng, Y., and Zhu, T.:
778 Dicarboxylic acids, ketocarboxylic acids, alpha-dicarbonyls, fatty acids, and benzoic acid in
779 urban aerosols collected during the 2006 Campaign of Air Quality Research in Beijing
780 (CAREBeijing-2006), *J. Geophys. Res.-Atmos.*, 115, D19312, 10.1029/2009jd013304, 2010.

781 Hori, M., Ohta, S., Murao, N., and Yamagata, S.: Activation capability of water soluble
782 organic substances as CCN, *J. Aerosol Sci.*, 34, 419-448, 10.1016/s0021-8502(02)00190-8,

783 2003.

784 Iwahashi, M., Kasahara, Y., Matsuzawa, H., Yagi, K., Nomura, K., Terauchi, H., Ozaki, Y.,
785 and Suzuki, M.: Self-diffusion, dynamical molecular conformation, and liquid structures of
786 n-saturated and unsaturated fatty acids, *J. Phys. Chem. B*, 104, 6186-6194,
787 10.1021/jp000610l, 2000.

788 Kawamura, K., and Ikushima, K.: Seasonal-changes in the distribution of dicarboxylic-acids
789 in the urban atmosphere, *Environ. Sci. Technol.*, 27, 2227-2235, 10.1021/es00047a033, 1993.

790 Kawamura, K., Kasukabe, H., and Barrie, L. A.: Source and reaction pathways of
791 dicarboxylic acids, ketoacids and dicarbonyls in arctic aerosols: One year of observations,
792 *Atmos. Environ.*, 30, 1709-1722, 10.1016/1352-2310(95)00395-9, 1996.

793 Kawamura, K., and Bikkina, S.: A review of dicarboxylic acids and related compounds in
794 atmospheric aerosols: Molecular distributions, sources and transformation, *Atmospheric*
795 *Research*, 170, 140-160, 10.1016/j.atmosres.2015.11.018, 2016.

796 Keiser, E. H., and Leavitt, S.: On the preparation and the composition of the acid carbonates
797 of calcium and barium, *J. Am. Chem. Soc.*, 30, 1711-1714, 10.1021/ja01953a008, 1908.

798 Khare, P., et al. (1999). "Atmospheric formic and acetic acids: An overview." *Reviews of*
799 *Geophysics* 37(2): 227-248.

800 King, M. D., Rennie, A. R., Thompson, K. C., Fisher, F. N., Dong, C. C., Thomas, R. K.,
801 Pfrang, C., and Hughes, A. V.: Oxidation of oleic acid at the air-water interface and its
802 potential effects on cloud critical supersaturations, *Phys. Chem. Chem. Phys.*, 11, 7699-7707,
803 10.1039/b906517b, 2009.

804 Koehler, H.: The nucleus in and the growth of hygroscopic droplets, *Trans. Faraday Soc.*, 32,
805 1152-1161, 10.1039/tf9363201152, 1936.

806 Koehler, K. A., Kreidenweis, S. M., DeMott, P. J., Petters, M. D., Prenni, A. J., and Carrico,
807 C. M.: Hygroscopicity and cloud droplet activation of mineral dust aerosol, *Geophys. Res.*
808 *Lett.*, 36, L08805, 10.1029/2009gl037348, 2009. Kumar, P. P., Broekhuizen, K., and Abbatt,
809 J. P. D.: Organic acids as cloud condensation nuclei: Laboratory studies of highly soluble and
810 insoluble species, *Atmos. Chem. Phys.*, 3, 509-520, 2003.

811 Kumar, P. P., Broekhuizen, K., and Abbatt, J. P. D.: Organic acids as cloud condensation
812 nuclei: Laboratory studies of highly soluble and insoluble species, *Atmos. Chem. Phys.*, 3,
813 509-520, 2003.

814 Kumar, P., Nenes, A., and Sokolik, I. N.: Importance of adsorption for CCN activity and
815 hygroscopic properties of mineral dust aerosol, *Geophys. Res. Lett.*, 36,
816 10.1029/2009gl040827, 2009.

817 Li, W. J., and Shao, L. Y.: Mixing and water-soluble characteristics of particulate organic
818 compounds in individual urban aerosol particles, *J. Geophys. Res.-Atmos.*, 115, D02301,
819 10.1029/2009jd012575, 2010.

820 Liu, X. H., and Wang, J. A.: How important is organic aerosol hygroscopicity to aerosol

821 indirect forcing?, *Environ. Res. Lett.*, 5, 044010, 10.1088/1748-9326/5/4/044010, 2010.

822 Mkoma, S. L., and Kawamura, K.: Molecular composition of dicarboxylic acids,
823 ketocarboxylic acids, alpha-dicarbonyls and fatty acids in atmospheric aerosols from
824 Tanzania, East Africa during wet and dry seasons, *Atmos. Chem. Phys.*, 13, 2235-2251,
825 10.5194/acp-13-2235-2013, 2013.

826 Moore, R. H., Nenes, A., and Medina, J.: Scanning Mobility CCN Analysis-A Method for
827 Fast Measurements of Size-Resolved CCN Distributions and Activation Kinetics, *Aerosol*
828 *Sci. Technol.*, 44, 861-871, 10.1080/02786826.2010.498715, 2010.

829 Neagle, W., and Rochester, C. H., Infrared study of the adsorption of water and ammonia on
830 calcium carbonate. *Journal of the Chemical Society, Faraday Transactions*, 86, 181-183,
831 1990.

832 Penner, J. E., Dong, X. Q., and Chen, Y.: Observational evidence of a change in radiative
833 forcing due to the indirect aerosol effect, *Nature*, 427, 231-234, 10.1038/nature02234, 2004.

834 Petters, M. D., and Kreidenweis, S. M.: A single parameter representation of hygroscopic
835 growth and cloud condensation nucleus activity, *Atmos. Chem. Phys.*, 7, 1961-1971, 2007.

836 Rogge, W. F., Hildemann, L. M., Mazurek, M. A., Cass, G. R., and Simoneit, B. R. T.:
837 Sources of fine organic aerosol .2. Noncatalyst and catalyst-equipped automobiles and
838 heavy-duty diesel trucks, *Environ. Sci. Technol.*, 27, 636-651, 10.1021/es00041a007, 1993.

839 Rogge, W. F., Hildemann, L. M., Mazurek, M. A., Cass, G. R., and Simoneit, B. R. T.:
840 Sources of fine organic aerosol. 9. Pine, oak and synthetic log combustion in residential
841 fireplaces, *Environ. Sci. Technol.*, 32, 13-22, 10.1021/es960930b, 1998.

842 Rose, D., Gunthe, S. S., Mikhailov, E., Frank, G. P., Dusek, U., Andreae, M. O., and Pöschl,
843 U.: Calibration and measurement uncertainties of a continuous-flow cloud condensation
844 nuclei counter (DMT-CCNC): CCN activation of ammonium sulfate and sodium chloride
845 aerosol particles in theory and experiment, *Atmos. Chem. Phys.*, 8, 1153-1179, 2008.

846 Rühl, C. R., Davies, J. F., and Wilson, K. R.: An interfacial mechanism for cloud droplet
847 formation on organic aerosols, *Science*, 351, 1447-1450, 10.1126/science.aad4889, 2016.

848 Russell, L. M., Maria, S. F., and Myneni, S. C. B.: Mapping organic coatings on atmospheric
849 particles, *Geophys. Res. Lett.*, 29, 1779, 10.1029/2002gl014874, 2002.

850 Sage, A. M., Weitkamp, E. A., Robinson, A. L., and Donahue, N. M.: Reactivity of oleic acid
851 in organic particles: changes in oxidant uptake and reaction stoichiometry with particle
852 oxidation, *Phys. Chem. Chem. Phys.*, 11, 7951-7962, 10.1039/b904285g, 2009.

853 Schauer, J. J., Kleeman, M. J., Cass, G. R., and Simoneit, B. R. T.: Measurement of emissions
854 from air pollution sources. 1. C-1 through C-29 organic compounds from meat charbroiling,
855 *Environ. Sci. Technol.*, 33, 1566-1577, 10.1021/es980076j, 1999.

856 Sorjamaa, R., and Laaksonen, A.: The effect of H₂O adsorption on cloud drop
857 activation of insoluble particles: a theoretical framework, *Atmos. Chem. Phys.*, 7, 6175-6180,
858 10.5194/acp-7-6175-2007, 2007.

859 Stipp, S. L. S.: Toward a conceptual model of the calcite surface: hydration, hydrolysis, and
860 surface potential. *Geochimica et Cosmochimica Acta*, 63, 3121-3131, 1999.

861 Stipp, S. L., Hochella Jr, M. F.: Structure and bonding environments at the calcite surface as
862 observed with X-ray photoelectron spectroscopy (XPS) and low energy electron diffraction
863 (LEED). *Geochimica et Cosmochimica Acta*, 55, 1723-1736, 1991.

864 Sullivan, R. C., Moore, M. J. K., Petters, M. D., Kreidenweis, S. M., Roberts, G. C., and
865 Prather, K. A.: Effect of chemical mixing state on the hygroscopicity and cloud nucleation
866 properties of calcium mineral dust particles, *Atmos. Chem. Phys.*, 9, 3303-3316,
867 10.5194/acp-9-3303-2009, 2009.

868 Sullivan, R. C., Moore, M. J. K., Petters, M. D., Kreidenweis, S. M., Qafoku, O., Laskin, A.,
869 Roberts, G. C., and Prather, K. A.: Impact of Particle Generation Method on the Apparent
870 Hygroscopicity of Insoluble Mineral Particles, *Aerosol Sci. Technol.*, 44, 830-846,
871 10.1080/02786826.2010.497514, 2010.

872 Takegawa, N., Miyakawa, T., Kawamura, K., and Kondo, Y.: Contribution of selected
873 dicarboxylic and omega-oxocarboxylic acids in ambient aerosol to the m/z 44 signal of an
874 aerodyne aerosol mass spectrometer, *Aerosol Sci. Technol.*, 41, 418-437,
875 10.1080/02786820701203215, 2007.

876 Tang, M. J., Cziczo, D. J., and Grassian, V. H.: Interactions of Water with Mineral Dust
877 Aerosol: Water Adsorption, Hygroscopicity, Cloud Condensation, and Ice Nucleation,
878 *Chemical Reviews*, 116, 4205-4259, 10.1021/acs.chemrev.5b00529, 2016.

879 Tang, M. J., Whitehead, J., Davidson, N. M., Pope, F. D., Alfarra, M. R., McFiggans, G., and
880 Kalberer, M.: Cloud condensation nucleation activities of calcium carbonate and its
881 atmospheric ageing products, *Phys. Chem. Chem. Phys.*, 17, 32194-32203,
882 10.1039/c5cp03795f, 2015.

883 Yamashita, K., Murakami, M., Hashimoto, A., and Tajiri, T.: CCN Ability of Asian Mineral
884 Dust Particles and Their Effects on Cloud Droplet Formation, *Journal of the Meteorological
885 Society of Japan*, 89, 581-587, 10.2151/jmsj.2011-512, 2011.

886 Zhao, D. F., Buchholz, A., Mentel, T. F., Muller, K. P., Borchardt, J., Kiendler-Scharr, A.,
887 Spindler, C., Tillmann, R., Trimborn, A., Zhu, T., and Wahner, A.: Novel method of
888 generation of Ca(HCO₃)₂ and CaCO₃ aerosols and first determination of hygroscopic
889 and cloud condensation nuclei activation properties, *Atmos. Chem. Phys.*, 10, 8601-8616,
890 10.5194/acp-10-8601-2010, 2010.

891 Zuend, A., Marcolli, C., Booth, A. M., Lienhard, D. M., Soonsin, V., Krieger, U. K., Topping,
892 D. O., McFiggans, G., Peter, T., and Seinfeld, J. H.: New and extended parameterization of
893 the thermodynamic model AIOMFAC: calculation of activity coefficients for
894 organic-inorganic mixtures containing carboxyl, hydroxyl, carbonyl, ether, ester, alkenyl,
895 alkyl, and aromatic functional groups, *Atmospheric Chemistry and Physics*, 11, 9155-9206,
896 10.5194/acp-11-9155-2011, 2011.

Table 1. Mode diameters, chemical compositions, and κ values of CaCO₃ aerosol particles (size selected by DMA at 101.8 nm) before (uncoated) and after coating with oleic (OA) or malonic acid (MA) at 30-80 °C.

	D_p [nm]	Organic mass per particle [10 ⁻¹² μg]	Mole organics per particle [10 ⁻²⁰ mole]	Org. volume fraction [%]	κ
Oleic acid					
Uncoated CaCO₃ 30-80 °C	101.9	(backgr. <i>m/z</i> 41: 2.7±0.9)	0	0.0	0.0028±0.0001
CaCO₃+Oleic acid 30 °C	102.1	3.7±1.9	1.3	0.8	
CaCO₃+Oleic acid 40 °C	102.5	7.0±2.8	2.5	1.4	
CaCO₃+Oleic acid 50 °C	103.7	14±3.7	5.1	2.7	
CaCO₃+Oleic acid 60 °C	104.9	23±1.2	8.3	4.3	
CaCO₃+Oleic acid 70 °C	109.2	96±3.7	34	16	0.0237±0.0006
CaCO₃+Oleic acid 80 °C	123.7	390±14	140	44	0.0673±0.0016
Malonic acid					
Uncoated CaCO₃ 30-80 °C	101.9	(backgr. <i>m/z</i> 42: 1.4±0.4)	0	0.0	0.0028±0.0001
CaCO₃+Malonic acid 30 °C	102.0	3.3±0.3	3.2	0.4	0.0123±0.0005
CaCO₃+Malonic acid 40 °C	102.1	6.8±1.2	6.5	0.8	0.0231±0.0008
CaCO₃+Malonic acid 50 °C	102.2	13±1.8	13	1.5	0.0380±0.0012
CaCO₃+Malonic acid 60 °C	102.7	38±1.6	36	4.1	0.1056±0.0023
CaCO₃+Malonic acid 70 °C	107.8	160±8.1	160	15	0.1813±0.0031
CaCO₃+Malonic acid 80 °C	121.0	610±24	590	40	0.3001±0.0062

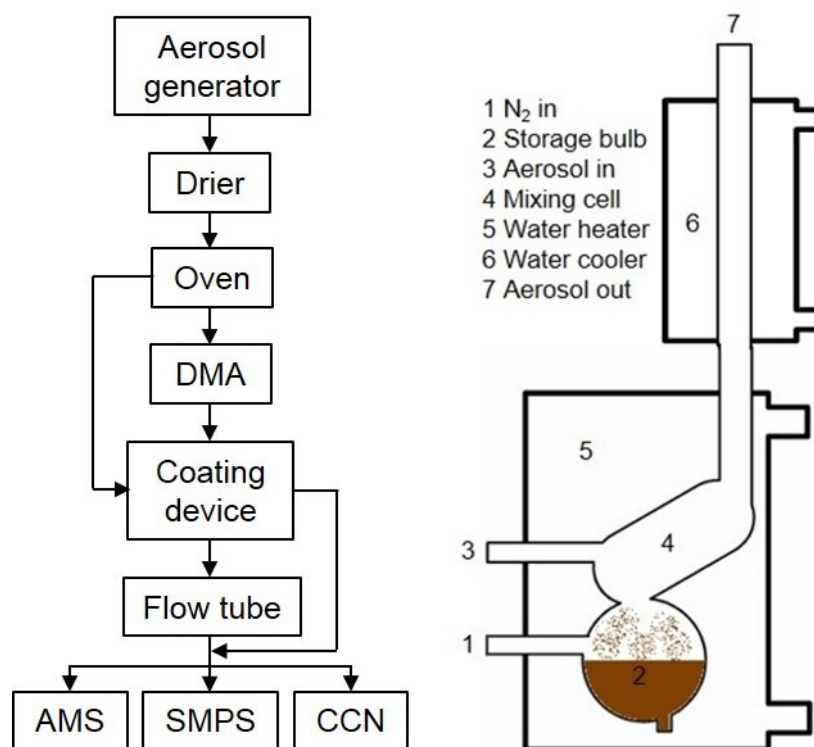


Figure 1. Schematics of the experimental set up (left side). CaCO_3 aerosol is generated by spray-drying of saturated $\text{Ca}(\text{HCO}_3)_2$ solutions and tempering the aerosol passing through an oven at 300°C . The *poly-disperse* CaCO_3 aerosol is either led directly to the coating device (right side, after Roselli, 2006) or led to a differential mobility Analyzer (DMA) for size selection first. Optional, a flow tube can be switched into the pass to enhance the reaction time of the coated particles. The stream of coated particles is finally split to the analytical instruments, namely aerosol mass spectrometer (AMS), scanning mobility particle sizer (SMPS) and CCN counter.

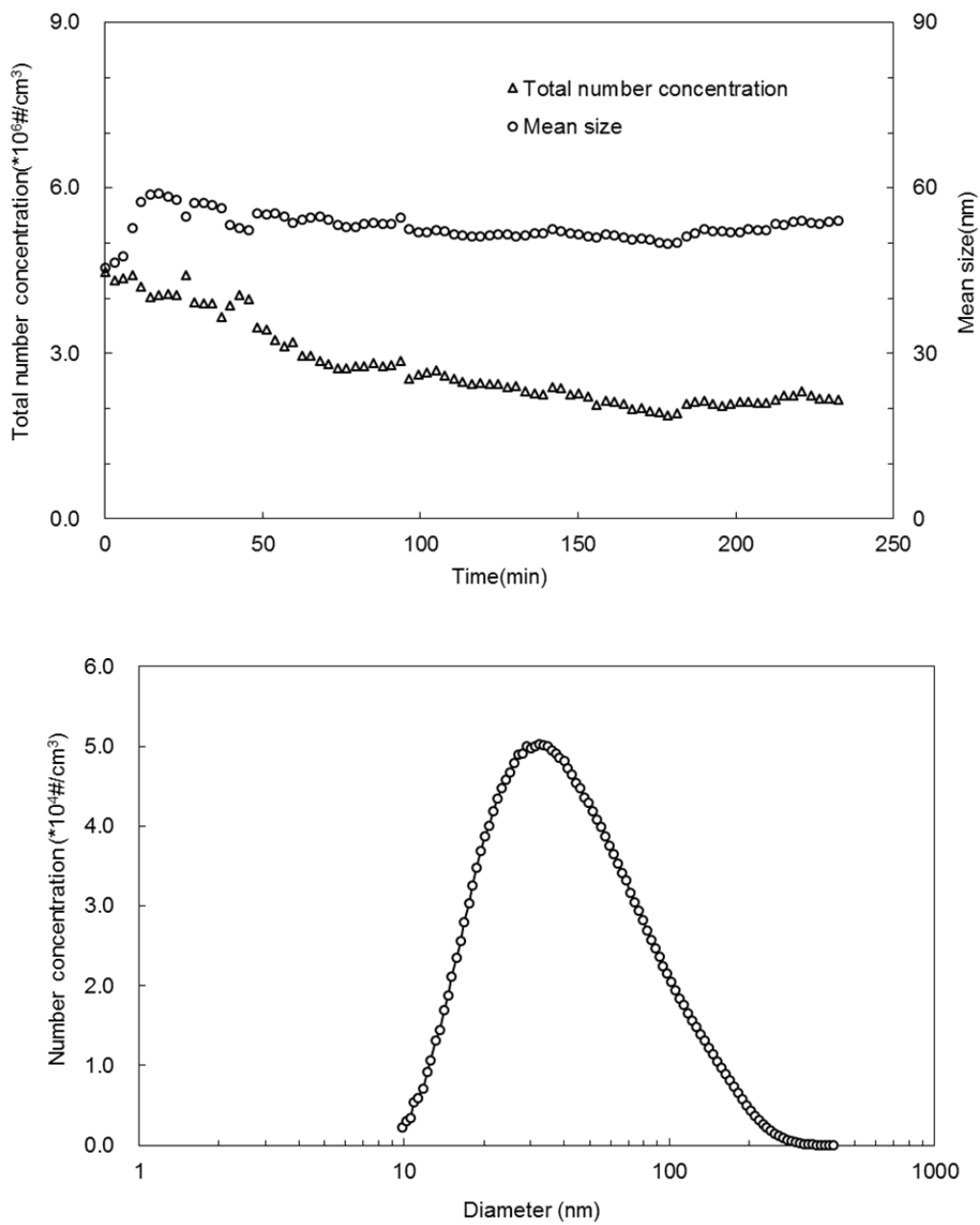


Figure 2. Total number concentration and mean diameter of CaCO₃ aerosol particles generated as a function of the spraying time (upper panel). Typical size distribution of the CaCO₃ aerosol after 70 min spraying (lower panel).

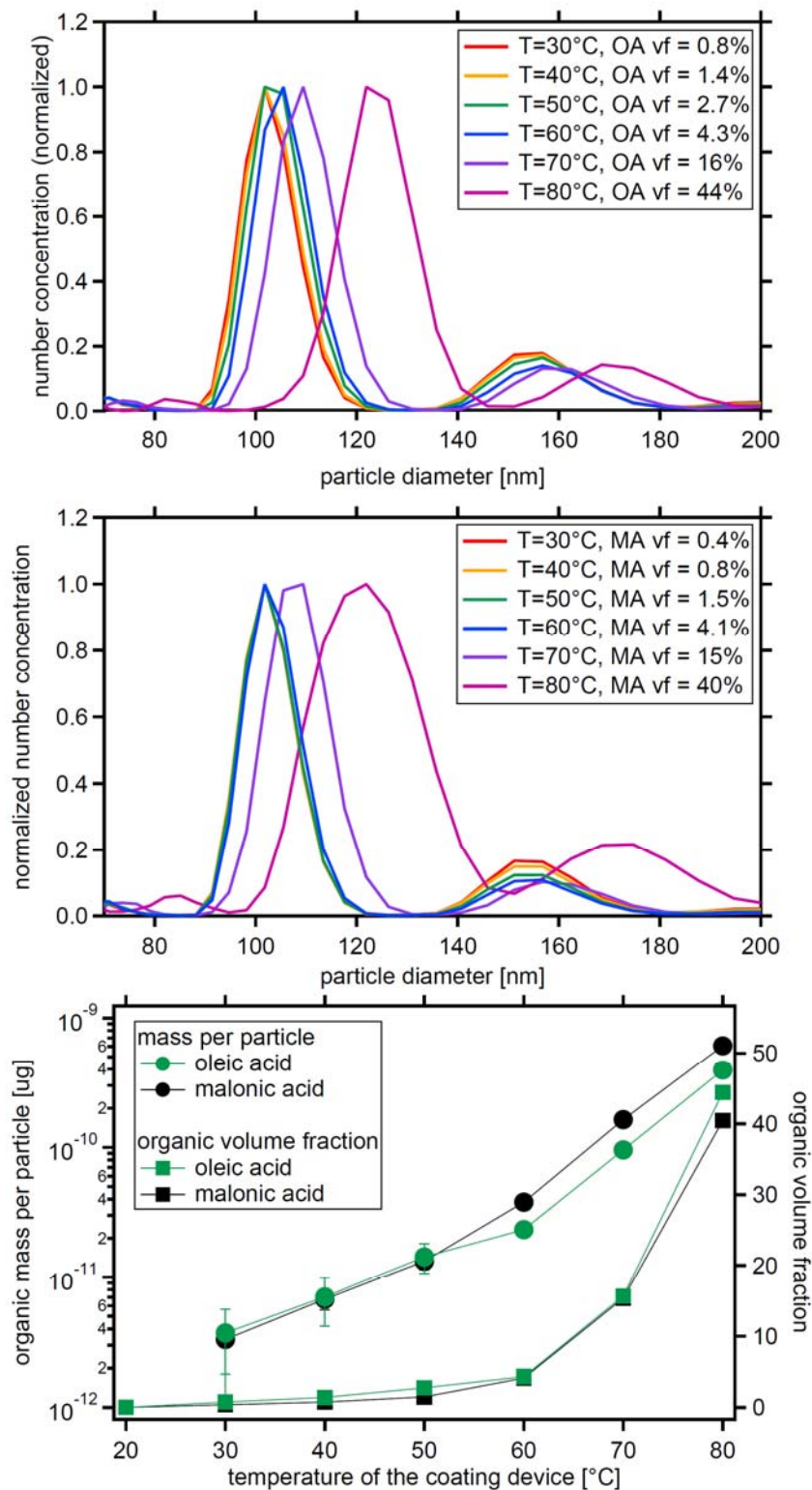


Figure 3. Size distribution of monodisperse CaCO_3 aerosol particles after coating with oleic acid (top panel) or malonic acid (middle panel). Coating amount and organic volume fraction for oleic and malonic acid as a function of the coating temperature for the same experiments (bottom panel, data in Table 1).

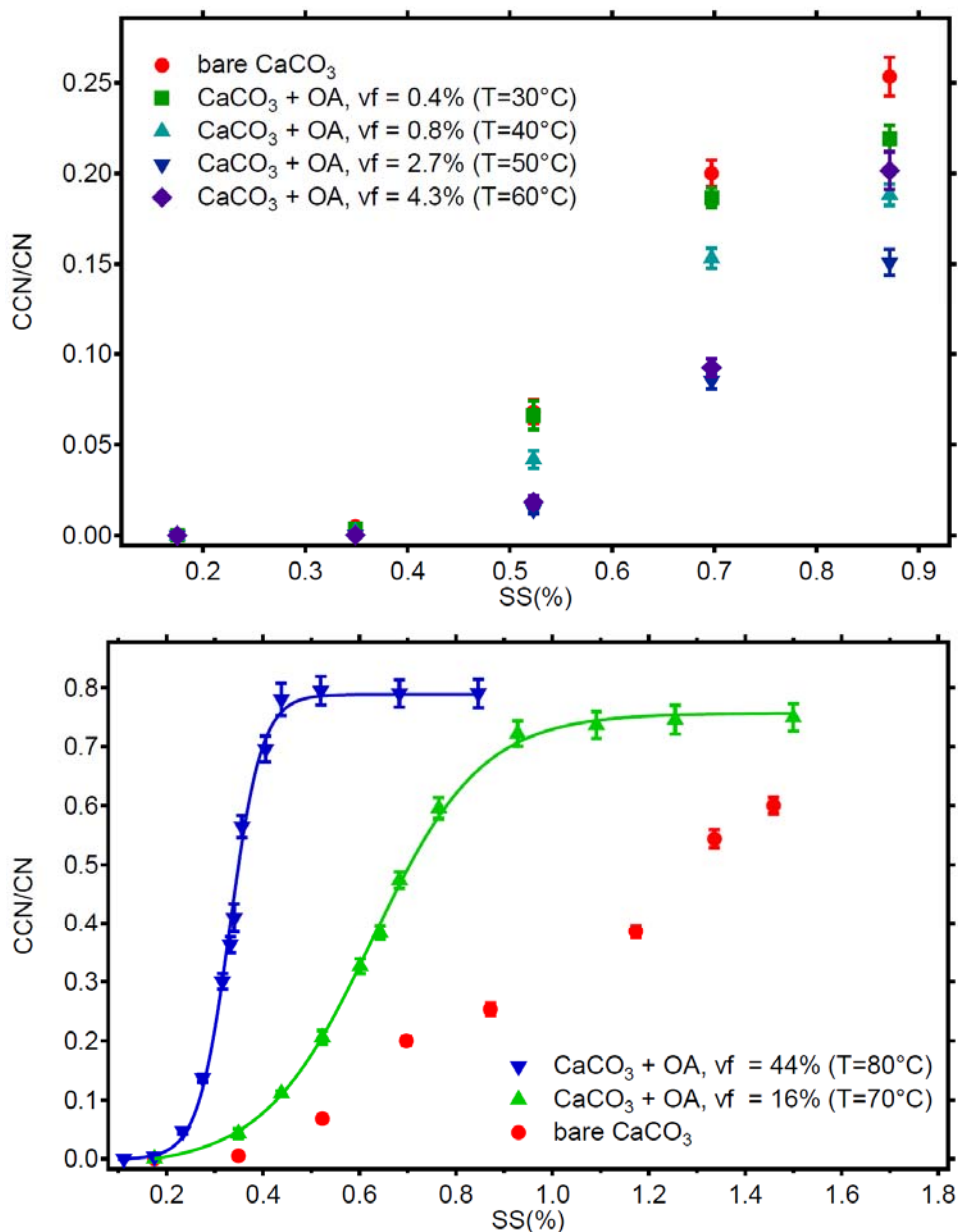


Figure 4. Activated fractions (CCN/CN) of *monodisperse* CaCO₃ aerosol particles (diameter $d_u = 101.9$ nm) at different supersaturations before and after oleic acid coating. With increasing coating temperatures of 30-50 °C the activated fraction decreases despite the increase of organic vf from 0.8% - 2.7%. At vf = 4.3% at 60°C this trend turns. Considering the invariant particle diameter at 30-50 °C, the increased particle diameter at 60 °C, and the reduced activated fraction simultaneously, the CCN activity of the coated CaCO₃ particles at 30-60 °C was lower than that of the uncoated CaCO₃ particles (top panel). At coating vf of 16% and 44% (T= 70-80 °C) the activated fractions, thus CCN activities, are higher than for bare CaCO₃ and increase with coating vf. In these two cases all particles are activated at the highest SS and SS_{crit} and κ can be determined from the turning point of the Gaussian fit (bottom panel, compare Table 1).

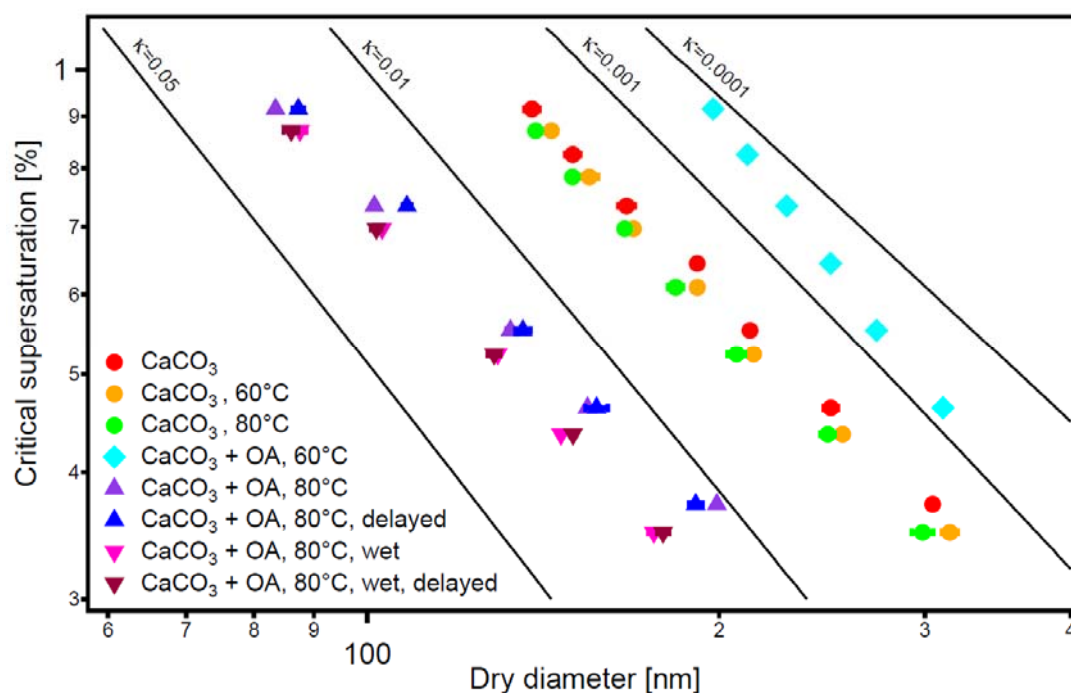


Figure 5. Critical dry diameters at different supersaturations (SS) of *poly-disperse* CaCO_3 aerosol before (circles) and after oleic acid coating. Experiments were performed at 60°C (turquoise diamond) and 80°C (triangles) coating temperatures. The flow tube experiments at 80°C were performed (indicated by ‘delayed’) at dry conditions (normal, blue triangles) and at enhanced water vapor (‘wet’, brown triangles). The effect of the temperature in the coating device on the CaCO_3 core is negligible (red, green, and orange circles). As for the monodisperse case in Figure 4, at 60°C coating temperature the particles are less CCN active than bare CaCO_3 while at 80°C the coated particle more CCN active. The presence of water vapor (1500 Pa) in the coating process enhances CCN activity. The increasing of residence time (23.7 s) of the coated aerosol in the flow tube had no significant effect on CCN activity in both experiments.

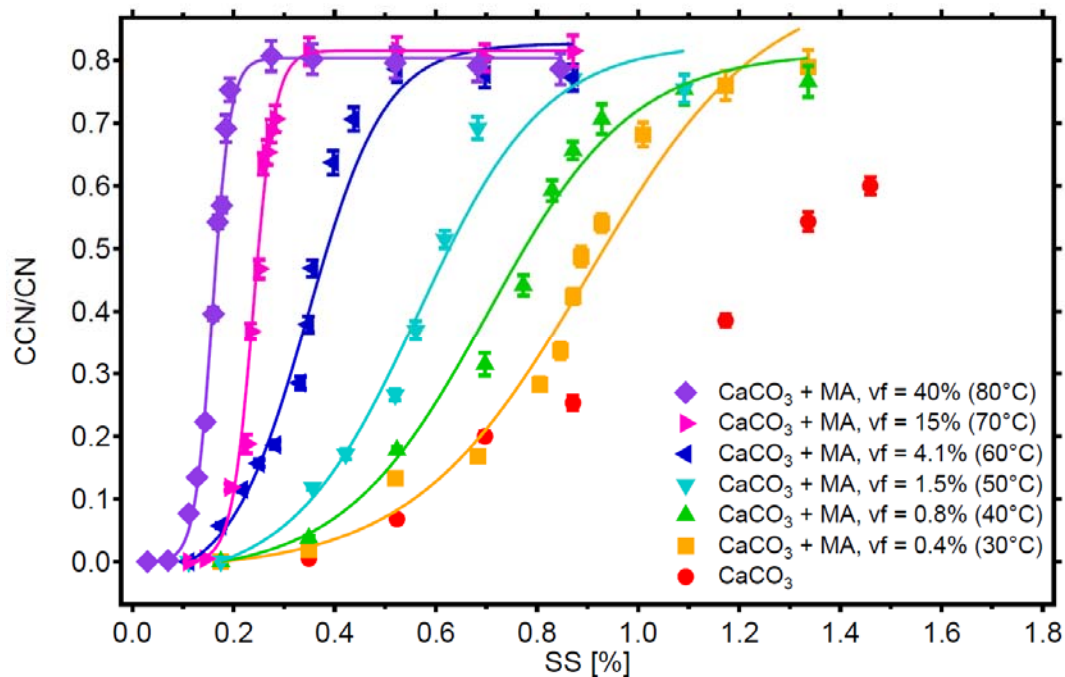


Figure 6. Activated fractions (CCN/CN) of *monodisperse* $CaCO_3$ aerosol particles (with $CaCO_3$ core, $d_u = 101.9$ nm) at different supersaturations before (red circles) and after malonic acid coating. With increasing coating, i.e. MA volume fraction vf the activated fraction, thus CCN activity, increase compared to bare $CaCO_3$ particles. All coated particles can be activated at sufficiently high SS and SS_{crit} and κ was determined (see Table 1).

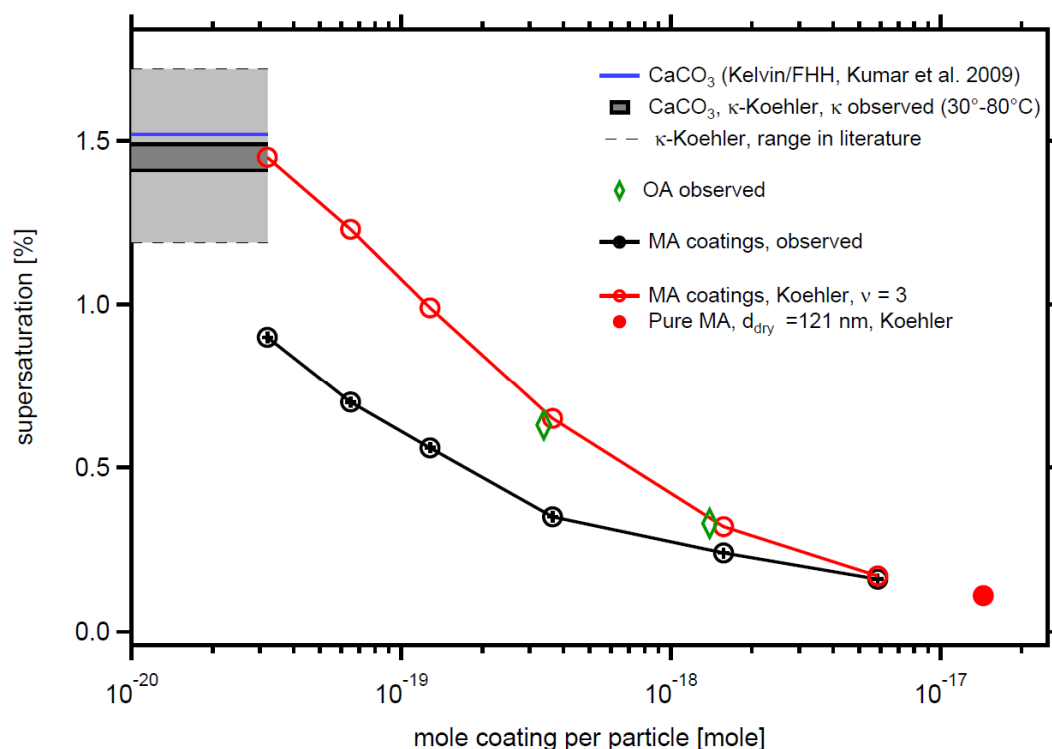


Figure 7: Comparison of SS_{crit} predicted by Koehler theory with observations. Koehler theory for aqueous MA solutions assuming full dissociation overpredicts SS_{crit} (red circles) compared to the observation (black circles). With increasing coating amount Koehler theory approaches the observation, with the limiting SS_{crit} for 121.0 nm particles made of pure malonic acid. For comparison we show observed SS_{crit} for the two thickest OA coatings (diamonds show). The horizontal lines indicate SS_{crit} of the bare $CaCO_3$ particles as calculated from our observed κ observed (black) and predicted by Kelvin/FFH theory (blue). Light grey area between the thin dashed grey lines shows the range of SS_{crit} for 101.9 nm particles calculated from the range of κ in literature for wet generated $CaCO_3$ particles (compare Tang et al. 2016).

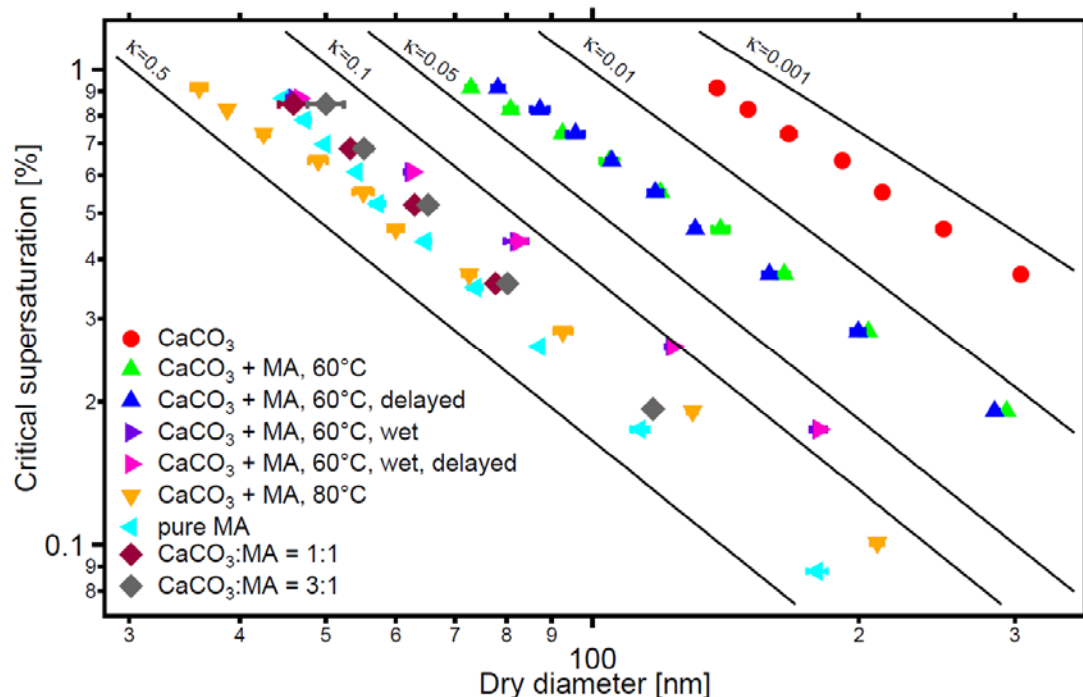


Figure 8. Critical dry diameters at different super-saturations (SS) of *poly-disperse* CaCO_3 aerosol before (circles) and after malonic acid coating (triangles). Experiments were performed at 60°C and 80°C coating temperatures. The results are similar to the monodisperse case in Figure 6. Critical dry diameters as a function of SS are also shown for malonic acid particles and particles that were generated by spraying mixed solution with molar ratios of CaCO_3 /malonic acid of 1:1 and 3:1. The CCN activity decreases with increasing CaCO_3 content. The flow tube experiments at 60 °C were performed (indicated by ‘delayed’) at dry condition (blue triangles) and in presence of 1500 Pa water vapor (magenta triangles). The presence of water in the coating process substantially enhanced κ and CCN activity. The increasing of residence time (23.7 s) of the coated aerosol in the flow tube had no significant effect on CCN activity in both experiments.

Supplement to

**Cloud Condensation Nuclei Activity of CaCO₃ Particles with
Oleic Acid and Malonic Acid Coatings**

**Mingjin Wang^{1,2}, Tong Zhu^{1*}, Defeng Zhao², Florian Rubach^{2,3}, Andreas Wahner²,
Astrid Kiendler-Scharr², and Thomas F. Mentel^{2*}**

¹BIC-ESAT and SKL-ESPCI, College of Environmental Sciences and Engineering, Peking University, Beijing 100871, China.

²Institut für Energie- and Klimaforschung (IEK-8), Forschungszentrum Jülich GmbH, 52425 Jülich, Germany.

³Klimageochemie, Max Planck Institut für Chemie, 55128 Mainz, Germany

* To whom correspondence should be addressed: tzhu@pku.edu.cn; t.mentel@fz-juelich.de

Experimental

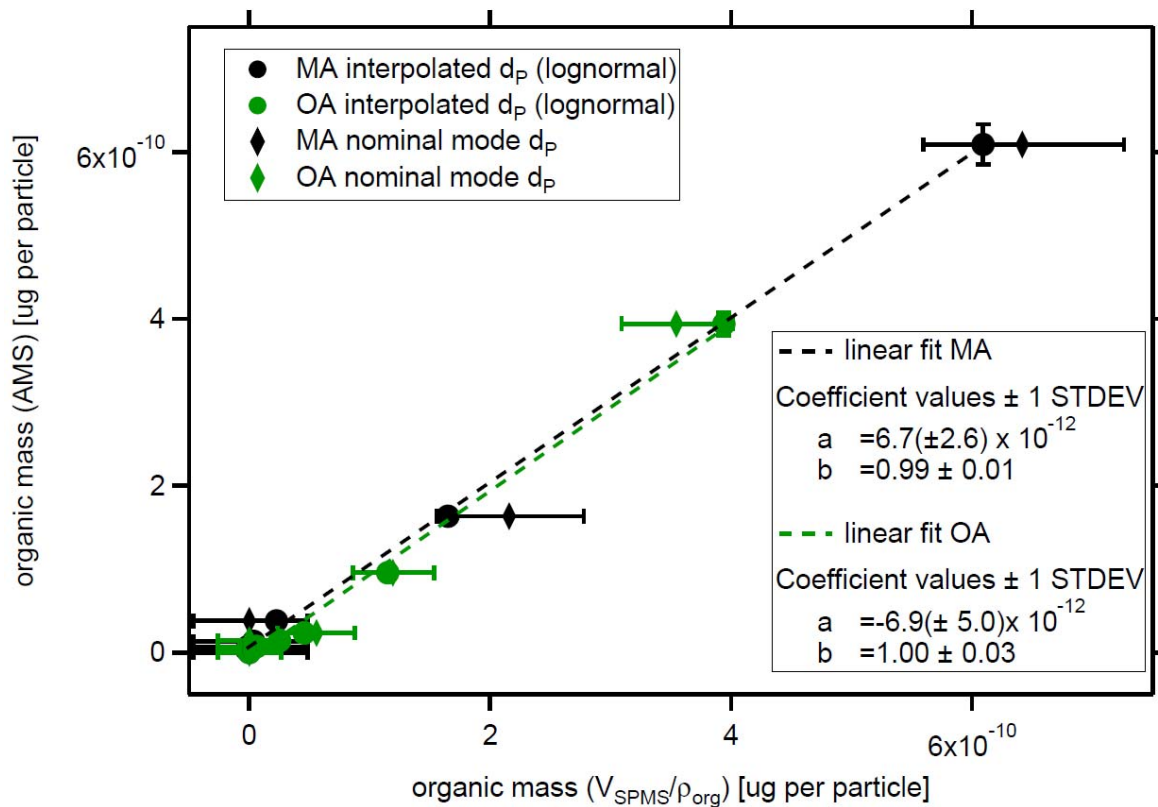


Figure S1: Linear relation between organic mass of the coating derived by AMS measurements and the organic coating mass calculated from the SMPS measurements for oleic acid coatings (green) and maleic acid coatings (black). For full circles the organic mass derived by SMPS was calculated from interpolated mode diameters given in Table 1. Error bars in y direction give the reproducibility of the AMS measurements; error bars in x direction indicate the mass span by considering the SMPS bin width for the respective nominal mode diameter. Note that the highest values must be the same as they were used to calibrate the marker m/z of AMS to the SMPS derived organic mass.

Koehler theory

We assume that at the critical supersaturation (SS_{crit}) the solution is ideal, i.e. water activity coefficient is close to 1, and the partial molar volume of water equals the molar volume of pure water M_w/ρ_w . Since the solubility of $CaCO_3$ in water is very low (0.00058 g/100 g water, at 298 K), while the solubility of malonic acid (MA) is quite high (62 g/100 g water at 298 K), we apply the linearized approach (e.g. Seinfeld and Pandis 2006), to predict the saturation ratio as a function of the mole solute on a insoluble core:

$$\ln\left(\frac{P_w(D_w)}{P^\circ}\right) = \frac{A}{D_p} - \frac{B}{(D_w^3 - d_u^3)} \quad (S1)$$

In this equation A represents the Kelvin effect while B contains the solute effect:

$$A = \frac{4M_w\sigma_w}{RT\rho_w} \cong \frac{0.66}{T} \quad (in \mu m) \quad (S2)$$

$$B = \frac{6n_s M_w}{\pi\rho_w} \cong 3.44 \times 10^{13} v \times n_s \quad (in \mu m^3) \quad (S3)$$

Herein $P_w(D_w)$ is the water vapor pressure over the droplet of diameter D_w ; P° is the water vapor pressure over a flat surface at the same T ; d_u is the diameter of insoluble particle fraction, in our case the $CaCO_3$ core; M_w is water molecular weight; σ_w is the air-water surface tension; ρ_w is the water density; T is in K; R is the universal gas constant; n_s is solute moles = m_s/M_s , with M_s as solute molecular weight. v is the dissociation degree, i.e. the number of ions resulting from the dissociation of one solute molecule.

We neglected the little dissolvable $CaCO_3$ and considered only malonic acid molecules for the dynamic growth. The insoluble $CaCO_3$ core was set to $d_u = 0.1019 \mu m$ as observed. We further assume that $CaCO_3$ doesn't react with malonic acid and that the surface tension of the solution at

activation is that of pure water. The dissociation constants $\text{p}K_{\text{A}1}$ and $\text{p}K_{\text{A}2}$ of MA are 2.8 and 5.7 in water, respectively. So MA will partly dissociate in water and in the limit of infinite dilute solutions the dissociation degree ν (van' Hoff factor) will be three for full dissociation. The moles of malonic acid coating n_s was taken from the AMS data in Table 1 and we applied $\nu = 3$.

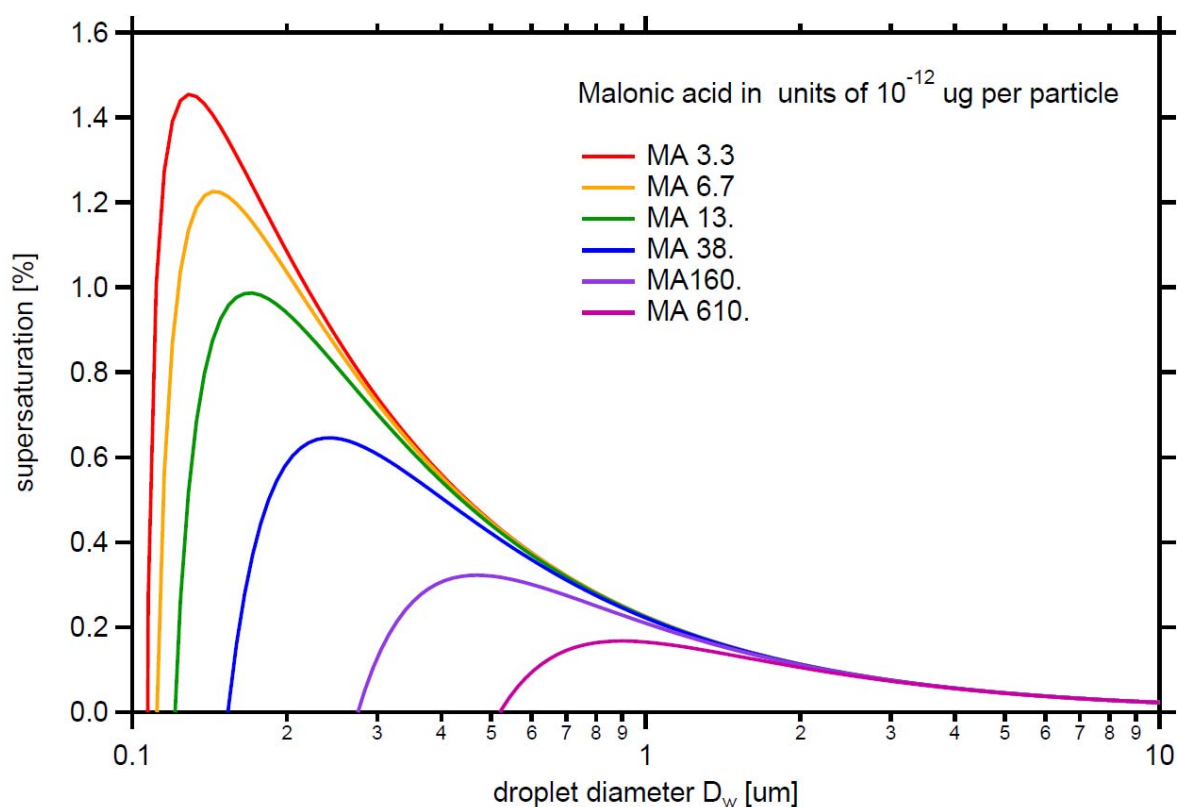


Figure S2. Variation of the equilibrium supersaturation over aqueous solution drops containing CaCO_3 and different mass of malonic acid at 293 K, assuming CaCO_3 is insoluble and doesn't react with malonic acid and the solution is dilute (water activity coefficient is close to 1). The diameter of insoluble CaCO_3 is 101.9 nm.

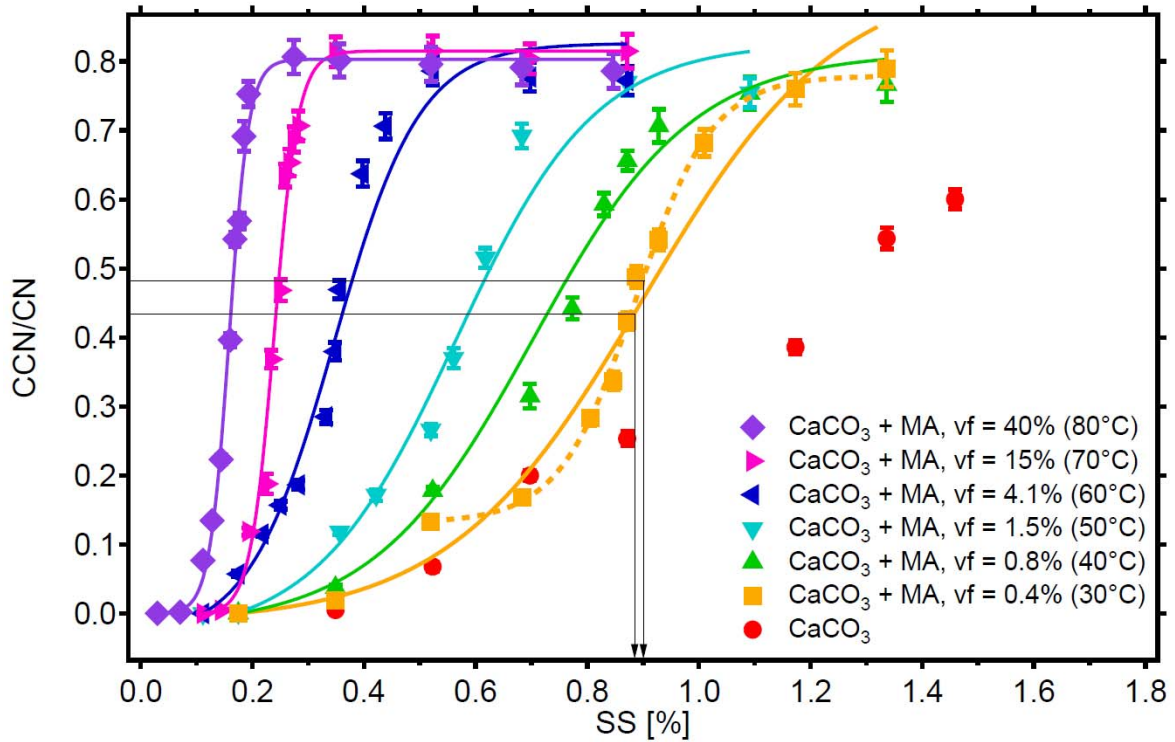


Figure S3: Systematic error introduced by neglecting the contribution of multiple charged particles in determining SS_{crit} by single sigmoidal fits. The multiple charge plateau is best recognizable for the MA coating with the smallest $vf=0.04\%$ (orange). The difference in SS_{crit} considering the plateau (0.900% dashed orange line) and neglecting it (0.887% solid orange line) is only 0.013%. The importance of the effect is largest for the smallest vf and disappears for the largest vf 's.

Table S1. Koehler theory and experimental SS_{crit} and κ values of $CaCO_3$ particles with different mass of MA coating.

Dry diam. (nm)	MA per particle ($\times 10^{-12}$ μg)	Theory SScrit (%)	Experimental SScrit (%)	Theory κ	Experimental κ
102.0	3.3 \pm 0.3	1.44	0.90	0.0024	0.0123 \pm 0.0005
102.1	6.8 \pm 1.2	1.20	0.70	0.0053	0.0231 \pm 0.0008
102.2	13 \pm 1.8	0.97	0.56	0.0107	0.0380 \pm 0.0012
102.7	38 \pm 1.6	0.63	0.35	0.0315	0.1056 \pm 0.0023
107.8	160 \pm 8.1	0.31	0.24	0.1110	0.1813 \pm 0.0031
121.0	610 \pm 24	0.16	0.16	0.3001	0.3001 \pm 0.0062

Table S2. Properties of investigated compounds.

Name	Formula	Molecular weight (g mol ⁻¹)	Density (g cm ⁻³)	Solubility (g/100 g water, at 298K)	Surface tension (dyn/cm)
Calcite	CaCO ₃	100.1	2.71	0.00058	- ^a
Malonic acid	C ₃ H ₄ O ₄	104.1	1.62	62	69 ^b
Oleic acid	C ₁₈ H ₃₄ O ₂	282.5	0.89	Very low	33 ^c

a: no data

b: Surface tension of 0.01 mole fraction malonic acid aqueous solution at 298K

c: Surface tension of pure oleic acid at 293K

Handbook of Chemistry and Physics, the 82nd Edition; Handbook of aqueous solubility data, Samuel H. Yalkowsky and Yan He, 2003; Chumpitaz et al., 1999; Hyvarinen et al., 2006.

Chumpitaz, L. D. A., Coutinho, L. F., and Meirelles, A. J. A.: Surface tension of fatty acids and triglycerides, J. Am. Oil Chem. Soc., 76, 379-382, 10.1007/s11746-999-0245-6, 1999.

Hyvarinen, A. R.; Lihavainen, H.; Gaman, A.; Vairila, L.; Ojala, H.; Kulmala, M.; Viisanen, Y., Surface tensions and densities of oxalic, malonic, succinic, maleic, malic, and cis-pinonic acids. Journal of Chemical and Engineering Data 2006, 51 (1), 255-260.

Cloud Condensation Nuclei Activity of CaCO₃ Particles with Oleic Acid and Malonic Acid Coatings

Mingjin Wang^{1,2}, Tong Zhu^{1*}, Defeng Zhao², Florian Rubach^{2,3}, Andreas Wahner², Astrid Kiendler-Scharr², and Thomas F. Mentel^{2*}

A figure for illustration of the responses is given in an extra file

C1: Overall the paper is nicely illustrated but it contains some repetitive text blocs, especially in the result section, that could be avoided in order to ease the reading of this manuscript (and reinforcing also its content).

Response:

We thank the referee for the positive comment. We will optimize the text of our manuscript to avoid repetition and to make the text more efficient and easier to read.

C2: While the argument of a bilayer of oleic acid does make sense, I'm still puzzled by the fact that the CCN properties are apparently higher for a coated particle compared to a pure oleic acid particle. I would have simply assumed that once thick enough, the water probing the surface does not see the core CaCO₃ particle (over the time scale of these experiments). In this situation, the pure oleic acid particle would exhibit a kind of upper limit for water adsorption and droplet activation. Maybe the authors could comment more on that, and maybe add the pure oleic acid data on their figures (this would ease the comparison with both systems).

Response:

Our CCN activity measurement showed that pure oleic acid particles up to 333 nm did not activate at 0.87% SS; this sets an upper limit for CCN activity of oleic acid particles ($\kappa < 0.0005$), in agreement with Kumar et al. (2003) and Broekhuizen et al. (2004). In liquid state oleic acid (OA) forms micelle like structures, the hydrophilic

ends (the carboxyl groups) of oleic acid molecules tend to combine together by hydrogen bonds and the hydrophobic tails (the hydrocarbon chains) are exposed at the outside (Iwahashi et al., 2000; Garland et al., 2008). The arrangement of oleic acid molecules in pure oleic acid particles should be similar. Hydrophobic tails facing outwards can explain the hydrophobicity of the particle surface and the hindrance of the uptake of water, making the CCN activity of pure oleic acid particles very low. Dalirian et al. (2017) studied OA coatings on black carbon (BC). They also found *no* activation of pure OA, but droplet activation for OA coated BC particles at SS_{crit} lower than that of BC and pure OA. Their particles were larger than ours, though, but also more heavily coated, i.e. more OA like. So, better droplet activation than for pure OA seems to be possible in coated systems.

We assume that $\text{Ca}(\text{OH})(\text{HCO}_3)$ structures act as hydrophilic sites on the surface of CaCO_3 (Kuriyavar et al., 2000; Stipp, 1999; Stipp and Hochella, 1991; Neagle and Rochester, 1990). Garland et al. (2008) suggested that OA at sub-monolayer coverage form self-associated islands rather than uniformly covering the surfaces, and OA molecules were oriented vertically on both hydrophobic and hydrophilic surfaces with the hydrocarbon chains of oleic acid molecules facing away from the surface. This is in support of our working hypothesis: the formation of a hydrophobic surface film.

When CaCO_3 particles are coated with only a small amount of oleic acid (less than one monolayer), the hydrophilic ends (the carboxyl groups) of oleic acid molecules will combine with the hydrophilic sites ($-\text{OH}$ and $-\text{HCO}_3$ groups) on CaCO_3 surface by hydrogen bonds. We conclude that all hygroscopic sites on the CaCO_3 surface are covered somewhere between 50°C and 60°C coating temperature, i.e. between $14 \cdot 10^{-12}$ and $23 \cdot 10^{-12}$ μg OA mass per particle, as here the trend turns and droplet activation increase again. This would place the monolayer coverage above 3%, organic volume fraction. According to the measurements and calculations of the length of oleic acid molecule, the thickness of oleic acid sub-monolayer on solid surfaces, and the thickness of deuterated oleic acid monolayers at the air-water interface (Garland et al., 2008; King et al., 2009; Iwahashi et al., 2000), we determined 2.3 nm as the likely thickness of oleic acid monolayer on CaCO_3 particles, accordingly a monolayer would be achieved at about 12-13% organic volume fraction. As a consequence the formation of the “hydrophilic bilayer” starts at sub-monolayer

coverage in accordance with island formation observed by Garland et al. (2008).

For CaCO_3 particles coated with more OA (thicker than one monolayer, at 70 and 80 °C coating temperatures), OA in the first layer still combines with the CaCO_3 surface by hydrogen bonds. We suppose that a portion of the carboxyl groups of oleic acid molecules, which are not in the first layer, will be exposed to the particle surface, in analogy to the formation of lipid bilayers, e.g. in cells, though the structure of this part of oleic acid is not known. The particle surface then becomes more hydrophilic. Activation of wettable, insoluble material can be described by the Kelvin term and a water absorption term, e.g. Frenkel Halsey Hill isotherm (Sorjamaa and Laaksonen, 2007, Kumar et al. 2009).

When carboxylic groups of OA are exposed at the surface, the interaction of water with the OA layer becomes stronger. In terms of the Kelvin/FHH approach, the surface water interaction becomes stronger and A_{FHH} increases and likely also the interaction between the higher water layers (B_{FHH} decreases). From this point of view water adsorption by the “OA bilayer” should become similar to thin malonic acid layers. In addition, when droplets form, oleic acid will transfer to the surface of the droplets and lower the surface tension of the solution (the surface tension of oleic acid is 0.033 J m^{-2} , which is much lower than that of pure water of 0.072 J m^{-2}). Thus, the activation of OA coated particles is probably a complex interaction between formation of specific hydrophobic layers and more hydrophilic multilayers, surface tension effects and for the largest coating amounts, simple size effects. As shown in Figure S1, SS_{crit} for OA is lower than for thin malonic acid coatings, probably because of the surface tension effect, but higher than for thick MA coatings, because of the missing solute effect.

We will implement parts of this discussion in the manuscript, highlighted in yellow.

C3: If my reading is correct, the CaCO_3 particles with a thick coating do exhibit better CCN properties than the pure oleic acid particles (if my reading is incorrect, this would highlight that an in-depth editing would be beneficial for the reader). How can you explain such a fact? Is the CaCO_3 surface leading to some kind of ordering of

the adsorbed organic acid (which might not be observed in the pure homogeneous organic particle) leading effectively to the above mentioned bilayer structure?

Response:

Your reading is correct. Note, the oleic acid coatings achieved at 70° or 80°C coating temperature are still thin. The largest coating thickness is about 10 nm at an organic volume fraction of 44%, which corresponds to about 4 monolayers of oleic acid (assuming the thickness of oleic acid monolayer on CaCO₃ particles is about 2.3 nm). To our knowledge, no previous study has investigated the structure of oleic acid coating on particle or solid surface thicker than one monolayer.

In our understanding the arrangement of oleic acid molecules in the thin coatings will be influenced by the CaCO₃ core (the polar, hydrophilic sides) and can thus be different from the arrangement of oleic acid molecules in pure oleic acid particles. Water can probably adsorb at the carboxylic groups facing outward (“bilayer” type structure) and diffuse through the thin oleic acid coatings. It may form an adsorbed water phase near the CaCO₃ surface. This could push the oleic acid out to act as surfactant which lowers the Kelvin term. Such a process should also happen in pure oleic acid particles. Because of the presence of CaCO₃ core the SS to achieve is lower than for pure OA.

We will explicitly refer to the lower κ of pure oleic acid in relation to higher κ observed for the oleic acid coated CaCO₃.

C4: Is the temperature in the coating device leading to some kind of ordering (for instance, by increase surface mobility before an ordering when cooling down)? Also, oleic acid has only a moderate thermal stability as it decomposes at higher temperature (typically at temperature at a factor 2 higher than those used here), potentially via an epoxide pathway in presence of air (and enhanced by light or metallic traces). Could traces of oxidized products nevertheless affect the composition of the coating at 80 °C already? If so, then this effect should increase with time. Did the authors observed any variation with time of kappa at 80 °C? Did the authors tried

to have thicker coatings at lower temperature by changing the gas flow conditions in their coating device?

Response:

We agree with the referee that the temperature in the coating device can increase the surface mobility of OA molecules, which would help to optimize the layering arrangement (ordering) of adsorbed oleic acid molecules on CaCO₃ surface.

We can exclude oxidation of OA since we used high-purity N₂ (Linde LiPur 6.0, purity 99.9999%, Linde AG, Munich, Germany) and we did not have much light in our system because both the coating device and the flow tube were covered with light tight materials (black polyurethane foam). Metallic traces might exist in our system, though, as we used some stainless steel tubes in our system.

The only way in which we modified the time between coating process and particle detection was provided by a flow tube to increase the average residence time from 5.8 to 23.7 s. Longer residence time (by 23.7 s) had no significant impact on CCN activity for both oleic acid coated particles and malonic acid coated particles at both dry and 47% RH conditions, probably because the coating process was already completed in the coating device and no further reactions occurred in the flow tube.

At the beginning of our experimental study, we modified the gas flow condition in the coating device in order to choose an appropriate gas flow condition. But we only measured the particle size when we changed the gas flow condition. After finding the appropriate gas flow conditions, we fixed the gas flow condition and did not change it anymore.

C5: Line 238. This sentence is unclear.

Response:

This sentence should be: In the discussion we also use the coating mass per particle to give a rationale, which is easier to imagine, to the finding and classification.

C6: Line 249: where a polydisperse

Response:

This sentence should be: In cases where a polydisperse aerosol was coated ...

C7: Line 296: remained at

Response:

This sentence should be: The κ value remained at 0.0028 ± 0.0001 at 60 °C and increased to 0.0036 ± 0.0001 at 80 °C.

And we also made the revision in our manuscript according to your comments.

References

Broekhuizen, K. E., Thornberry, T., Kumar, P. P., and Abbatt, J. P. D., Formation of cloud condensation nuclei by oxidative processing: Unsaturated fatty acids, *J. Geophys. Res.-Atmos.*, 109, D24206, 10.1029/2004jd005298, 2004.

Dalirian, M., Ylisirniö, A., Buchholz, A., Schlesinger, D., Ström, J., Virtanen, A., and Riipinen, I.: Cloud droplet activation of black carbon particles coated with organic compounds of varying solubility, *Atmos. Chem. Phys. Discuss.*, 2017, 1-25, 10.5194/acp-2017-1084, 2017.

Garland, E. R.; Rosen, E. P.; Clarke, L. I.; Baer, T., Structure of submonolayer oleic acid coverages on inorganic aerosol particles: evidence of island formation. *Phys. Chem. Chem. Phys.* 2008, 10 (21), 3156-3161.

Iwahashi, M.; Kasahara, Y.; Matsuzawa, H.; Yagi, K.; Nomura, K.; Terauchi, H.; Ozaki, Y.; Suzuki, M., Self-diffusion, dynamical molecular conformation, and liquid structures of n-saturated and unsaturated fatty acids. *J. Phys. Chem. B* 2000, 104 (26), 6186-6194.

King, M. D.; Rennie, A. R.; Thompson, K. C.; Fisher, F. N.; Dong, C. C.; Thomas, R. K.; Pfrang, C.; Hughes, A. V., Oxidation of oleic acid at the air-water interface and its

potential effects on cloud critical supersaturations. *Phys. Chem. Chem. Phys.* 2009, 11 (35), 7699-7707.

Koehler, H., The nucleus in and the growth of hygroscopic droplets. *Trans. Faraday Soc.* 1936, 32 (2), 1152-1161.

Kumar, P. P., Broekhuizen, K., and Abbatt, J. P. D., Organic acids as cloud condensation nuclei: Laboratory studies of highly soluble and insoluble species, *Atmos. Chem. Phys.*, 3, 509-520, 2003.

Kumar, P., Nenes, A., and Sokolik, I. N.: Importance of adsorption for CCN activity and hygroscopic properties of mineral dust aerosol, *Geophys. Res. Lett.*, 36, 10.1029/2009gl040827, 2009.

Sorjamaa, R., and Laaksonen, A.: The effect of H₂O adsorption on cloud drop activation of insoluble particles: a theoretical framework, *Atmos. Chem. Phys.*, 7, 6175-6180, 10.5194/acp-7-6175-2007, 2007.

Kuriyavar, S. I., Vetrivel, R., Hegde, S. G., Ramaswamy, A. V., Chakrabarty, D., Mahapatra, S. Insights into the formation of hydroxyl ions in calcium carbonate: temperature dependent FTIR and molecular modelling studies. *Journal of Materials Chemistry*, 2000, 10 (8): 1835-1840.

Neagle, W., Rochester, C. H., Infrared study of the adsorption of water and ammonia on calcium carbonate. *Journal of the Chemical Society, Faraday Transactions* 1990, 86 (1), 181-183.

Stipp, S. L. S., Toward a conceptual model of the calcite surface: hydration, hydrolysis, and surface potential. *Geochimica et Cosmochimica Acta* 1999, 63 (19-20), 3121.

Stipp, S. L., Hochella Jr, M. F., Structure and bonding environments at the calcite surface as observed with X-ray photoelectron spectroscopy (XPS) and low energy electron diffraction (LEED). *Geochimica et Cosmochimica Acta* 1991, 55 (6), 1723-1736.

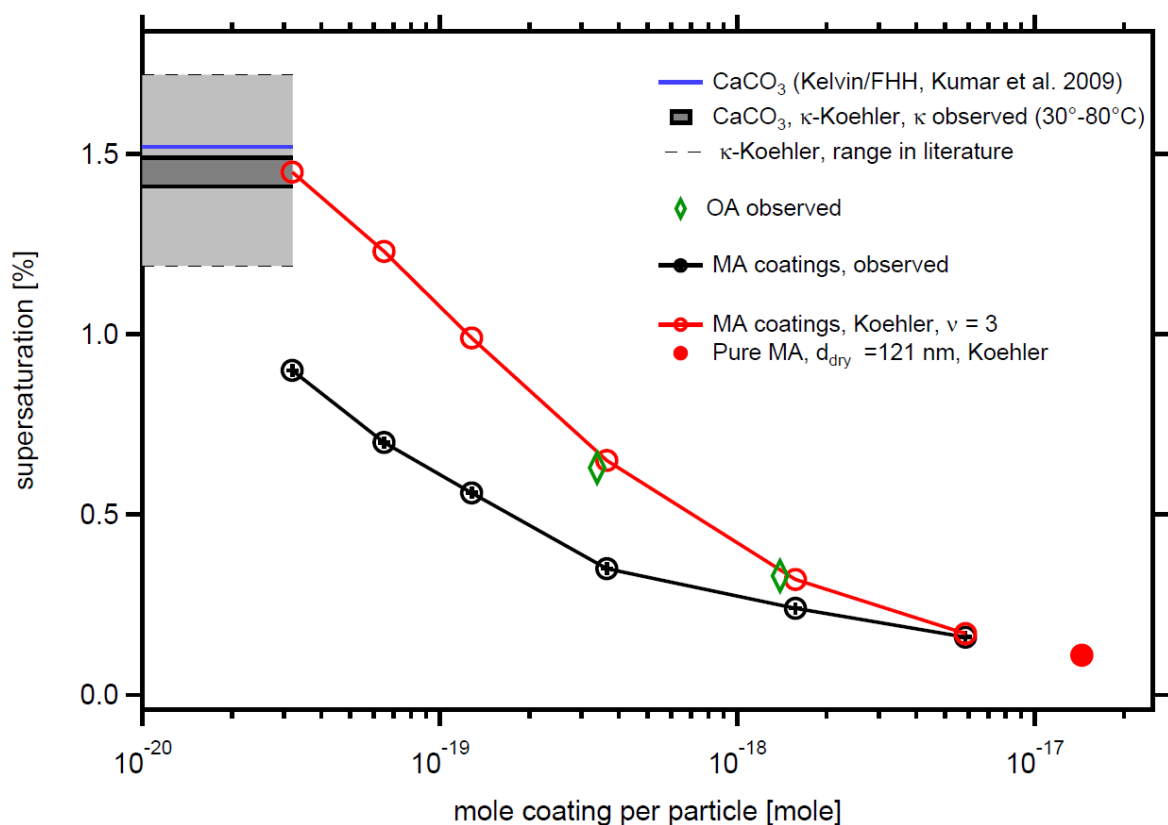


Figure S1: Comparison of SS_{crit} predicted by Köhler and Köhler/FHH theory with observations. The red circles are predictions by the Köhler theory for aqueous MA solutions assuming full dissociation, the black points present the observation. The red filled circle represents the Köhler prediction of SS_{crit} for 121.0 nm particles made of pure malonic acid. The horizontal lines give reference values for the bare $CaCO_3$ particles as calculated from our observed κ (black) and predicted by Köhler/FFH theory (blue). Light grey area between the thin dashed black lines indicates the range of SS_{crit} for 101.9 nm particles calculated from the range of κ in literature for wet generated $CaCO_3$ particles. Green diamonds show observed SS_{crit} for the two thickest OA coatings.

Cloud Condensation Nuclei Activity of CaCO₃ Particles with Oleic Acid and Malonic Acid Coatings

Mingjin Wang^{1,2}, Tong Zhu^{1*}, Defeng Zhao², Florian Rubach^{2,3}, Andreas Wahner², Astrid Kiendler-Scharr², and Thomas F. Mentel^{2*}

In this paper the effect of coating of oleic acid (low solubility in water) and malonic acid (water soluble) on the activation of particles to cloud drops is investigated. The CCNC experiments seem to be carried out according to present practice and the coating is done with great care.

It is thus disappointing that data evaluation does not meet the same standards. I have mainly identified two areas in which I would have liked to see a deeper analysis:

We thank the reviewer for the positive and critical remarks. We will address the critical remarks in the following.

Tables and Figures for illustration of the responses are given in an appended document.

CI. A full Koehler theory treatment based on the chemical composition of the particles would have been useful. A theoretical consideration of the expected changes in kappa values due to the reactions suggested and bilayer of oleic acid would improve the paper.

Response:

The advantage of using kappa approach (Petters and Kreidenweis, 2007) is that all differences in the (underdetermined) system are mapped to one parameter (i.e. the ratio of the partial molar volumes of water and the solute(s)) and thus CCN activation of differently composed particles becomes comparable. We would like to note, that in Figure 5 and 7 we show the observations in the domain critical supersaturation vs dry diameter relative to fixed kappa lines. For ideal solutions at activation the data in these plots should “parallel” the kappa lines, thus represent one kappa. Deviation from kappa lines indicates non-ideality and other limitations of the kappa approach.

The Koehler theory is described in details by Koehler (1936). For applying Koehler theory to CaCO₃ particles coated with malonic acid at dry condition (RH < 0.7%), we assume that the malonic acid coating will fully dissolve in water when droplets formed. This decreases the activity of water in solution, and thus increases the CCN activity. We assume that at the critical supersaturation (SS_{crit}) the solution is ideal, i.e. water activity coefficient is close to 1, and the partial molar volume of water equals the molar volume of pure water M_w/ρ_w. Since the solubility of CaCO₃ in water is very low (0.00058 g/100 g water, at 298 K), while the solubility of malonic acid (MA) is quite high (62 g/100 g water at 298 K), we apply the linearized approach (e.g. Seinfeld and Pandis 2006), to predict the saturation ratio as a function of the mole solute on a insoluble core:

$$\ln\left(\frac{P_w(D_p)}{P^\circ}\right) = \frac{A}{D_p} - \frac{B}{(D_p^3 - d_u^3)}$$

In this equation A represents the Kelvin effect while B contains the solute effect:

$$A = \frac{4M_w\sigma_w}{RT\rho_w} \cong \frac{0.66}{T} \quad (\text{in } \mu\text{m})$$

$$B = \frac{6n_s M_w}{\pi \rho_w} \cong \frac{3.44 \times 10^{13} v m_s}{M_s} \quad (\text{in } \mu\text{m}^3)$$

Herein $P_w(D_p)$ is the water vapor pressure over the droplet of diameter D_p ; P^o is the water vapor pressure over a flat surface at the same T ; D_p is droplet diameter; d_u is the diameter of insoluble particle fraction, in our case the CaCO_3 core; M_w is water molecular weight; σ_w is the air-water surface tension; ρ_w is the water density; T is in K; R is the universal gas constant; n_s is solute moles; v is the dissociation degree, i.e. the number of ions resulting from the dissociation of one solute molecule; m_s is solute mass per particle; M_s is solute molecular weight.

As the solubility of CaCO_3 in water is very low, activation of CaCO_3 and other mineral dust components is often predicted by a water adsorption approach, wherein the solute term B in the Köhler equation above is replaced by a water adsorption term. The equations show application of the Frenkel Halsey Hill adsorption isotherm (FHH, Sorjamaa and Laaksonen, 2007, Kumar et al. 2009):

$$B = -A_{FHH} \cdot \theta^{-B_{FHH}}$$

Therein we approach the water coverage θ by (Sorjamaa and Laaksonen, 2007):

$$\theta = \frac{D_p - d_u}{2 \cdot 2.75 \cdot 10^{-4}}$$

Therein A_{FHH} is a measure for the intermolecular interaction of water with the substrate surface whereas B_{FHH} characterizes the intermolecular interaction within higher adsorbed water layers. Kumar et al. (2009) gave parameter for CaCO_3 ($A_{FHH}=0.25$ and $B_{FHH}=1.19$, FHH approach) and we will use this later to yield SS_{crit} for bare CaCO_3 particles.

We applied Köhler theory to predict the CCN activation for the malonic acid coatings on the CaCO_3 particles at $T = 293$ K. We neglected the little dissolvable CaCO_3 and assumed that only malonic acid molecules contributed to the dynamic growth. The insoluble CaCO_3 core was set to $d_u = 0.1019 \mu\text{m}$ as measured. We further assume that CaCO_3 doesn't react with malonic acid and that the surface

tension of the solution at activation is that of pure water. The dissociation constants $\text{p}K_{A1}$ and $\text{p}K_{A2}$ of malonic acid are 2.8 and 5.7 in water, respectively. So MA will partly dissociate in water and in the limit of infinite dilute solutions the dissociation degree ν (van' Hoff factor) will be three for full dissociation. The amount of malonic acid coating m_s was taken from the AMS data in Table 1 (revised) in our manuscript and the mole MA solute was calculated applying the dissociation degree of $\nu = 3$ and the molecular mass of malonic acid of $M_s = 104.1 \text{ g mol}^{-1}$. The resulting Koehler curves, equilibrium supersaturation (SS) over the solution droplet as a function of the wet diameter D_p , are shown in Figure S1. In Figure S1, the maximum of each SS curve is the critical supersaturation (theory SS_{crit}). In Table S1 and Figure 2S we compare the SS_{crit} predicted by the Köhler approach (red) with the observed SS_{crit} (black). Köhler theory overpredicts SS_{crit} for thin coatings, but with increasing coating Köhler theory approaches the observed SS_{crit} and the SS_{crit} for a particle with 121 nm diameter composed of pure malonic acid is the limiting case (red filled circle).

In Figure S2 are also shown the $\text{SS}_{\text{crit}} = 1.49$ for bare CaCO_3 particles with $d_{\text{dry}} = 101.9 \text{ nm}$, calculated from the observed κ 's in our study, and the range of κ 's given in the literature for wet generated particles (Tang et al. 2016).

From the Köhler results we derived the predicted water content of the particles at point of activation and we calculated molality and mass fraction of the solute in the solution at the point of activation. The molality at minimum and maximum malonic acid load of $3.3 \cdot 10^{-12} \text{ ug/particle}$ and $610 \cdot 10^{-12} \text{ ug/particle}$ were $0.006 \text{ mol kg}^{-1}$ and $0.0015 \text{ mol kg}^{-1}$, respectively. We used these values in the AIOMFAC model (Zuend et al. 2011) to calculate the deviation from ideality for the solution at point of activation for a flat solution. The both solutions are highly non-ideal with respect to the MA ($a_x = 0.4$), wherein MA was treated as solute with reference state infinite dilution (mole fraction $x_{\text{solute}} \rightarrow 0$). However this did not affect much the activity coefficient of water, which is essentially 1, water treated as solvent with reference state pure liquid (mole fraction $x_{\text{water}} = 1$). Moreover, in this concentration range, the surface tension of aqueous malonic acid solutions is about 70 dyn/cm , thus the nearly same as for water (Table S2). One should expect that Köhler theory would predict SS quite well under such conditions.

One could imagine that a little CaCO_3 will dissolve in water and in the presence of malonic acid, CO_2 should be driven out, and a solution of CaMalonate could be formed. CaMalonate is still slightly soluble in water (0.365 g/100 g water, at 293 K, Linke and Seidell, 1958), ν for CaMalonate is 2. Solubility of CaMalonate converts into about 0.02 mol/kg water, would thus be in a range where the malonate would be fully dissolve. However, because of $\nu = 2$ for CaMalonate while $\nu = 3$ for the pure malonic acid, formation of CaMalonate will decrease the solute effect.

To bring Köhler theory in agreement with the observation for the thinnest coating, *more* solute entities would be required. Thus, disagreement cannot be caused by an ill determined van't Hoff factor as we used already maximum $\nu = 3$ and reducing ν will increase the deviation. (Note, that recent observations point to the importance of the surface effect by organic surface films over the solute effect for water soluble inorganics in presence of organics, including malonic acid (Ruehl et al., 2016). A lower surface tension will bring Koehler prediction and observation punctually in better agreement and still allow for smaller van't Hoff factors. As an example, at point of activation a surface tension of 55% of σ_w and a van't Hoff factor of one will bring Koehler theory and observation in agreement for the thinnest coating. However, a surface tension 55% of σ_w will cause disagreement for the thickest coating, because the solute term gains in importance. Probably, the findings for the mixed solutions of malonic acid and water soluble ammonium sulfate are not directly transferable to our system with insoluble inorganic core, where we expect dilute aqueous solutions of 0.006 mol/kg of malonic acid at the activation point. At such concentrations malonic acid does not reduce σ_w , moreover in the study of Ruehl et al. (2016) malonic acid was one of the more Koehler kappa behaving organics.)

If we turn back to Koehler theory with focus on the solute term, about 4-5 times the measured MA would be needed for the thinnest MA coating to bring prediction and observation in agreement. It cannot be due to a simple calibration error of 4-5, as that would apply to all coating amounts and would lead to mismatches at the thicker coatings. Moreover, a postulated missing mass of $14\text{-}17.5 \cdot 10^{-12}$ ug/particle will be detectable by AMS.

CaCO₃ aerosol in this study was generated by spraying saturated Ca(HCO₃)₂ solutions. The solubility of Ca(HCO₃)₂ in water is with 16.6 g/100g water sufficient that about 1% Ca(HCO₃)₂ would provide the missing amount of solute. However, we dry and temper the aerosol at 300°C and Ca(HCO₃)₂ in dry state is thermodynamically unstable (Zhao et al. 2010). As described in the manuscript, our wet generated CaCO₃ particles are more hygroscopic as Calcite and dry generated CaCO₃ particles. Larger κ for wet generated compared to dry generated CaCO₃ particles is a common phenomenon (e.g. Tang et al. 2016) and possibly related to the formation of Ca(OH)(HCO₃) structures at the surface (see below).

In Figure S2 we show the prediction of SS_{crit} 1.52% for activating CaCO₃ by the Kelvin/FHH theory with the CaCO₃ parameters taken from Kumar et al. (2009). SS_{crit} for our bare CaCO₃ particles is 1.49% and the lower SS_{crit} should be due to a more adsorptive surface, e.g. the presence of Ca(OH)(HCO₃) structures. According to classical Koehler theory the equivalent of $8.5 \cdot 10^{-20}$ moles of dissolvable entities would be needed to explain a drop from 1.52% to 1.3% supersaturation, which is only ¼ of the moles MA in the thinnest MA coating. Therefore, whatever makes our CaCO₃ particles wettable is not sufficient - in terms of Koehler theory - to explain the low SS_{crit} of 0.9 % at the thinnest MA coating.

We estimate monolayer coverage by MA at 2-3% volume fraction (vf), this would be achieved between the third and fourth MA mass load of $13 \cdot 10^{-12}$ - $38 \cdot 10^{-12}$ ug per particle, observed vf 1.5-4.1%. Thus a sub-monolayer coating of $3.3 \cdot 10^{-12}$ ug MA per particle caused a drop of SS_{crit} from 1.49 to 0.9 and increased kappa from 0.0028 to 0.012. Therefore we conclude that CaCO₃/MA coatings show a *non-Koehler* behavior at thin coatings and *approach* Koehler behavior with increasing MA load. This means there must be specific interactions between MA and the CaCO₃ surface which eases water adsorption and CCN activation.

Ca(OH)(HCO₃) structure exists commonly on the surface of CaCO₃ whenever the CaCO₃ surface has been exposed to gaseous water or liquid water. Ca(OH)(HCO₃) exist even at high vacuum condition and act as hydrophilic sites on the surface of CaCO₃ making the CaCO₃ surface more hydrophilic (Stipp, 1999; Stipp and Hochella, 1991; Neagle and Rochester, 1990). CaCO₃ aerosol in our study was generated by

spraying a $\text{Ca}(\text{HCO}_3)_2$ solution, so $\text{Ca}(\text{OH})(\text{HCO}_3)$ structures likely exist on the particle surface. When CaCO_3 particles are coated by malonic acid (or oleic acid) the hydrophilic sides can serve as polar surface active sites for accommodation of the acids. In case of MA there is a second carboxylic group which still could support the adsorption of water films.

If we think in terms of Kelvin/FHH theory to explain the observed low SS_{crit} for thin MA coatings, these coatings must have a net stronger interaction with water (higher A_{FHH}) and/or stronger interaction between the adsorbed water layers (lower B_{FHH}) than bare CaCO_3 . If coatings become thicker the Koehler solute effect starts increasingly to contribute and eventually controls the CCN activation. But our data are not sufficient to determine A_{FHH} and B_{FHH} . (The only system in the literature which comes close - in a far sense - is CaOxalate Monohydrate, with $A_{\text{FHH}} = 0.57$ and $B_{\text{FHH}} = 0.88$ (Kumar et al., 2009). Plug in these parameters will lead to $\text{SS}_{\text{crit}} = 0.53\%$ commensurable with our observed value of 0.56% for $13 \cdot 10^{-12}$ ug MA coating which represents an organic[^]vf of 1.6% , thus is close to monolayer.)

Oleic acid (OA) is not soluble in water. Pure oleic acid particles up to 333 nm do not activate at 0.87% SS. This data sets the upper limit of κ for pure oleic acid to < 0.0005 . With thin coatings of OA, CCN activity is smaller than bare CaCO_3 , however with thick coatings it becomes larger. This is not a classical Koehler behavior. Therefore adsorption e.g. described by Kelvin/FHH theory is a better approach to illustrate what could happen on coating with oleic acid.

Note that we are neither able to perform theoretical calculations nor is our data sufficient to determine e.g. FHH parameters. Both are clearly beyond this experimental work.

We again refer to $\text{Ca}(\text{OH})(\text{HCO}_3)$ structures at the surface which offer polar surface sites to bind the hydrophilic ends (the carboxyl groups) of the oleic acid molecules. Different to malonic acid, only hydrophobic ends of oleic acid molecules (the hydrocarbon chains) are then exposed on the particle surface hence increase the hydrophobicity of the particle surface. Such a formation of a hydrophobic layer

should be occurring until all polar sites are occupied or a monolayer coverage - maybe in form of a self-assembled layer - is reached. This can hinder the uptake of water, and in terms of Kelvin/FHH theory will lower A_{FHH} and/or likely increase B_{FHH} . The formation of a monolayer of OA on black carbon particles with the polar groups pointing outwards was postulated by Dalirian et al. (2017), which lead to increased activation of the black carbon particles. Thus, they observed a similar effect of layer formation, but with switched polarity.

When CaCO_3 particles are coated with more oleic acid (more than one monolayer) the first layer of oleic acid still combines with CaCO_3 surface. We suppose that a portion of the carboxyl groups of oleic acid molecules, which are not in the first layer, will be exposed on the particle surface in analogy to the formation of lipid bilayers, e.g. cells. The particle surface then becomes more hydrophilic and in terms of Kelvin/FHH theory the interaction of water with the OA surface becomes stronger, A_{FHH} increases and likely also the interaction between the higher water layers (B_{FHH} decreases). From this point of view water adsorption should become similar to thin malonic acid layers. In addition, when droplets form, oleic acid will transfer to the surface of the droplets and lower the surface tension of the solution (the surface tension of oleic acid is 0.033 J m^{-2} , which is much lower than that of pure water of 0.072 J m^{-2}). Thus, the activation of OA coated particles is probably a complex interaction between formation of specific hydrophobic layers and more hydrophilic multilayers, surface tension and for the largest coatings amount size effects. As shown in Figure S2, SS_{crit} for OA is lower than for thin malonic acid coatings, probably because of the surface tension effect, but higher than for thick MA coatings, because of the missing solute effect.

We will the discussion above implement in parts in the manuscript. This passages are highlighted in yellow in the revised manuscript.

C2. Focusing on the coating device temperature in the results section is a bit confusing and I am not convinced about the reproducibility of the experiment, given

that the experimental cases are identified mainly by the temperature of the coating device. Focusing more on presenting the mass of organics coated on the particles would improve the paper significantly. Does the coating thickness depend on the original particle size? Can this give more information towards understanding the observations?

Response:

First of all we would like to clarify that we did not mean that coating thickness depends only on temperature. Our intention was to use the coating temperature to classify our experiments, because the organic mass itself has some uncertainty, related to limitations of the measurements method. It means that we are convinced that for a given particle size (distribution) and fixed experimental conditions (flows, residence time etc.) will indeed lead to reproducible amounts of coatings for a given temperature.

In Table 1 (revised) in our manuscript we showed the organic mass per particle data. We will focus on the organic mass and organic volume fraction in the revision of our manuscript. Due to the Kelvin Effect, the amount of organic acid coating depends somewhat on the particle size of the core. In our study, we selected CaCO₃ particles at a diameter of 101.8nm and detailed discussion focus on the impact of coating thickness on the CCN activity of 101.8nm CaCO₃ particles. However, as shown in Figures polydisperse particles with a distribution of particle size and coatings behave similar.

C3. In the motivation of the chosen substances: is oleic acid really a good choice for a surface-active compound, considering its low solubility?

Response:

Yes, we think that the two acids are good choices as the water solubility of the two organic acids is complementary; it is high for malonic acid while it is very low for oleic acid, and we speculated in our planning that oleic acid would form kind of self-assembled layers. Surface active compounds do not need to be water soluble. Moreover, oleic acid is observed in the atmosphere.

C4. On line 179, the residence time in the flow tube is given. However in a laminar flow, the residence time varies with the position, i.e. whether the air passes at the center or near the walls. Is this effect considered and may it influence the results?

Response:

The flow tube was supposed to act as delay tube. The residence time of 23.7 s for the particles in the flow tube is the average residence time. This compares to the average residence time of only about 5.8 s for the particles in the coating device (including the water cooler). Thus average residence time in the flow tube is about 4 times of that in the coating device. 1.) In the way we sampled aerosol from the flow tube, the aerosol contains flow both from the center and near the walls. 2.) increasing of residence time (by 23.7 s) had no significant impact on CCN activity at all conditions, thus fact that particles travelling in center and particles travelling near the wall was not important.

C5. Lines 180 to 185: At first reading it sounds as if the relative humidities given are at 80 °C. However, in the case of 47% RH, the air would then be strongly supersaturated at 25 °C. Please clarify the temperature at which the RH is given. Also, if 47% RH refers to 25 °C, the RH at 80 °C will still be very low, just a few percent. How does this influence the experiments?

Response:

We thank the referee for the comment as our description maybe indeed misleading. RH experiments were performed at 60°C(MA) and 80°C(OA) coating temperature. The N₂ stream was passed through a bubbling device filled with Milli-Q water to saturate the N₂ stream and RH was measured to be >90% at T =25 °C (room temperature). The RH of the aerosol flow before entering the coating device is measured to be <10% at T =25 °C. The RH of the mixed stream should be about 50% at 25 °C, since the flow rate of the N₂ stream and the aerosol flow is the same. This corresponds to water vapor pressure of 1500 Pa. So, within the coating device at 60°C the RH will be >7% (MA experiment) and at 80°C >3% (OA experiment), still about an order of magnitude higher than the RH, when the stream is not humidified. In fact it will be a somewhat higher as the gas-phase may not reach the bath temperature which primarily served to warm up the coating agent and control its vapor pressure.

During passing through the cooler, RH increases to 47% at 25°C at the exit of the cooler.

We clarified this in the manuscript.

C6. In lines 228 to 231 proportionalities between AMS signals and organic particle mass and volume are described. Are they observations or assumptions? Also, determination of the amount of organic coating: If I read the table 1 correctly, and make some calculation, the change in diameter and the change in organic mass, do not agree. Is this correct? Why is that?

Response:

Yes, AMS determined mass and observed volume increase should be linearly related. This is the working hypothesis. There are apparent deviations from strict linearity, mainly because of limitations in determining the volume increase through coating, as the formed layers are thin, and growth is smaller than the bin width of the SMPS. The size resolution of the SMPS was set to maximum of 64 channels per decade.

AMS is obviously able to detect the smallest coating amounts, as described in the manuscript, but standard relative ionization efficiency (RIE = 1.4) for organics, which can be well applied to atmospheric systems, fails in our case as it underestimates the volume observed by SMPS for the thickest coating by more than a factor of two (applying the macroscopic densities). It is well known that application of average RIE for organics often fails for specific single compounds.

Therefore it seemed to us, a reasonable way out could be the procedure which we applied and described in the experimental section. We assume the particles with the thickest coating are spherical, coatings are bulk like, and can be measured by SMPS with sufficient accuracy. Then we calibrated the largest m/z observed by AMS as marker for the thickest coating, and apply the marker calibration to the thinner coatings. As can be seen from the STDEV the reproducibility is quite good but there are systematic errors. The bin width “uncertainty” in the range of diameters from 101.8 to 120.9 nm is 3.9 and 4.3 nm, respectively. At coating thicknesses of about 5 - 20 nm this introduces uncertainties of 32 to 12% already. If one recalculates the

expected diameter for the coated particle from core + coating volume

$$D_{coat} = \sqrt[3]{D_{core} \cdot \frac{6}{\pi} \cdot \frac{m_{org}}{\rho_{org}}}$$

the derived diameters D_{coat} fall in the bin-width of the channel noted in Table 1 (old) as mode diameter. As a consequence within these uncertainties the relation between SMPS volume and AMS mass agree. (These uncertainties of the coating mass was the reason why we use the operational coating temperature to classify our experiments).

We will show the relation between AMS data and SMPS data in Figure S1 in the supplement. See response to next comment.

C7. Line 234 to 235. Have you tried to account for mode shift within the bin, by fitting a function to the distribution?

Response:

Thanks for the suggestion. We now fitted the maxima of the SMPS number distribution by a lognormal function (considering 5 to 9 neighbor bins centered around the mode), and took the maximum of the fits as mode diameter. This led indeed to changes. The most significant changes were that for the thickest coating the fitted maxima shifted from 121.9 to 121 nm and from 121.9 to 124.3 nm for MA and OA respectively. This led to different calibration factors and thus to different coating amounts for the thinner coatings. The effects were -5% and +11% for OA and MA, respectively. By interpolating the mode position the linearity between SMPS volume and AMS also improved as indicated in Figure S3. In the Figure S3 also the mass range over the bin width is given as x error bars. (The error bars are different for MA and OA as the density ρ_{org} entered the calculation.) One can see that mass calculated with nominal mode position (old Table 1) is centered over the bin width bars. One can also recognize how much the mass calculated from the interpolated mode diameters

(Table 1(revised)) were shifted inside the bin width bar.

We will use the revised data in the revised manuscript. See previous comment.

C8. Line 293: You say “and our kappa value is somewhat higher but still in this range”. Isn’t it just in the range?

Response:

Yes, it is just in the range. We will correct in the manuscript and will mention that larger kappas for wet generated CaCO₃ has been found before.

C9. Line 298: You say “The increased kappa value of 0.0008”. Shouldn’t it be “The increase in kappa value of 0.0008”?

Response:

Yes, it should be “The increase in kappa value of 0.0008”. We will correct in the manuscript.

C10. Line 323: What do you mean by a “significant amount” of coating? Is a coating of less than 2 nm insignificant? In all aspects?

Response:

We will reformulate that section.

C11. Line 323-325: Unclear expression. Please specify that the sizing according to mobility diameter is referred to (if that is the case) and specify the temperature limit, instead of saying “a certain value”.

Response:

We will reformulate that section.

C12. Line 371: Why does the activated fraction level off at 83%? Did you make an intercalibration between numbers in the CCNC and CPC for other compounds?

Response:

The activation efficiency (i.e., the activated fraction when aerosol particles are completely activated) was 83% for our CCN instrument, determined using 150 nm (NH₄)₂SO₄ particles at SS=0.85%. In Figure 4 and Figure 6 in our manuscript, reaching the plateau of about 83% means that the aerosol particles were completely activated. Activation efficiency around 80% are typical compare the study of Abbatt et al. (2005). We prefer not to correct for better looks.

C13. In section 3.2 there is a lot of repetition, I think. Please see if the text can be made more efficient.

Response:

We will try to make the text more efficient and avoid repetition.

C14. Line 413, the sentence starting with “This suggestion is supported by very low CCN activity of pure oleic acid....” Is this based on some calculations? Please describe. Line 421 to 423: But the low surface tension does not seem to help the pure oleic acid particles to activate, according to your measurements as well as Kumar et al. (2003) and Broekhuizen et al. (2004). Also, the first “of” on line 422 should be removed.

Response:

Our CCN activity measurements show that oleic acid particles up to 333 nm do not activate at 0.87% SS, thus pure oleic acid particles have very low CCN activity ($\kappa < 0.0005$). The research of Kumar et al. (2003) and Broekhuizen et al. (2004) also showed pure oleic acid particles have very low CCN activity. In pure oleic acid particles micelle like structures are formed, with the hydrophilic ends (the carboxyl groups) of the oleic acid molecules tend to combine together by hydrogen bonds and the hydrophobic tail (the hydrocarbon chains) are exposed at the outside (Iwahashi et al., 2000; Garland et al., 2008). The arrangement of oleic acid molecules in pure oleic

acid particles should be similar to that in pure oleic acid liquid. This can increase the hydrophobicity of the particle surface and hinder the uptake of water. Even low surface tension cannot help the pure oleic acid particles to activate. And oleic acid is highly insoluble in water.

We will remove the first “of” on line 422.

C15. Figure 6: The fitted curves for 30-60 °C do not seem to follow the data very well. Why? Have you accounted for doubly charged particles? In my opinion there is a tendency to a two step-function, the first step reaching to CCN/CN of 0.15-0.2.

Response:

We can deduct the presence of doubly charged particles in the CN measurement, but we cannot deduct the activated doubly charged particles from CCN. One method for solving this problem is provided by Sullivan et al. (2009). In their paper they fitted the data from the “multiply-charged plateau” to the “completely-activated plateau” when the data had a clear “multiply-charged plateau”. But in our data, we don’t have a clear “multiply-charged plateau”, so we fitted from the beginning to the “completely-activated plateau”. This will lead to a systematic underestimate of the SS_{crit} . The underestimate is the largest when the malonic acid mass is the smallest (30 °C coating temperature), and we underestimate SS_{crit} by only about 0.02% (difference between fitting from the first point and fitting from the third point (multiply-charged plateau)). When the malonic acid mass is larger, the underestimate will be smaller. At the largest two malonic acid mass, the underestimate can be neglected.

We will also make that clearer in the revision in our manuscript.

References

Abbatt, J. P. D., Broekhuizen, K., Kumal, P. P., Cloud condensation nucleus activity of internally mixed ammonium sulfate/organic acid aerosol particles. *Atmos. Environ.* 2005, 39 (26), 4767-4778.

AIOMFAC model, <http://www.aiomfac.caltech.edu>

Broekhuizen, K. E., Thornberry, T., Kumar, P. P., and Abbatt, J. P. D., Formation of cloud condensation nuclei by oxidative processing: Unsaturated fatty acids, *J. Geophys. Res.-Atmos.*, 109, D24206, 10.1029/2004jd005298, 2004.

Dalirian, M., Ylisirniö, A., Buchholz, A., Schlesinger, D., Ström, J., Virtanen, A., and Riipinen, I.: Cloud droplet activation of black carbon particles coated with organic compounds of varying solubility, *Atmos. Chem. Phys. Discuss.*, 2017, 1-25, 10.5194/acp-2017-1084, 2017.

Garland, E. R.; Rosen, E. P.; Clarke, L. I.; Baer, T., Structure of submonolayer oleic acid coverages on inorganic aerosol particles: evidence of island formation. *Phys. Chem. Chem. Phys.* 2008, 10 (21), 3156-3161.

Iwahashi, M.; Kasahara, Y.; Matsuzawa, H.; Yagi, K.; Nomura, K.; Terauchi, H.; Ozaki, Y.; Suzuki, M., Self-diffusion, dynamical molecular conformation, and liquid structures of n-saturated and unsaturated fatty acids. *J. Phys. Chem. B* 2000, 104 (26), 6186-6194.

Koehler, H., The nucleus in and the growth of hygroscopic droplets. *Trans. Faraday Soc.* 1936, 32 (2), 1152-1161.

Kumar, P. P., Broekhuizen, K., and Abbatt, J. P. D., Organic acids as cloud condensation nuclei: Laboratory studies of highly soluble and insoluble species, *Atmos. Chem. Phys.*, 3, 509-520, 2003.

Kumar, P., Nenes, A., and Sokolik, I. N.: Importance of adsorption for CCN activity and hygroscopic properties of mineral dust aerosol, *Geophys. Res. Lett.*, 36, 10.1029/2009gl040827, 2009.

Linke W. F., Seidell A., *Solubilities: Inorganic and metal-organic compounds*, a compilation of solubility data from the periodical literature. Amer. Chem. Soc., 1958.

Neagle, W., Rochester, C. H., Infrared study of the adsorption of water and ammonia on calcium carbonate. *Journal of the Chemical Society, Faraday Transactions* 1990,

86 (1), 181-183.

Petters, M. D., Kreidenweis, S. M., A single parameter representation of hygroscopic growth and cloud condensation nucleus activity. *Atmos. Chem. Phys.* 2007, 7 (8), 1961-1971.

Ruehl, C. R., Davies, J. F., and Wilson, K. R.: An interfacial mechanism for cloud droplet formation on organic aerosols, *Science*, 351, 1447-1450, 10.1126/science.aad4889, 2016.

Seinfeld, J. H., Pandis, S. N., *Atmospheric Chemistry and Physics-From Air Pollution to Climate Change*, Second edition, Published by John Wiley & Sons, Inc., Hoboken, New Jersey, 773-776, 2006.

Sorjamaa, R., and Laaksonen, A.: The effect of H₂O adsorption on cloud drop activation of insoluble particles: a theoretical framework, *Atmos. Chem. Phys.*, 7, 6175-6180, 10.5194/acp-7-6175-2007, 2007.

Stipp, S. L. S., Toward a conceptual model of the calcite surface: hydration, hydrolysis, and surface potential. *Geochimica et Cosmochimica Acta* 1999, 63 (19-20), 3121.

Stipp, S. L., Hochella Jr, M. F., Structure and bonding environments at the calcite surface as observed with X-ray photoelectron spectroscopy (XPS) and low energy electron diffraction (LEED). *Geochimica et Cosmochimica Acta* 1991, 55 (6), 1723-1736.

Sullivan, R. C., Moore, M. J. K., Petters, M. D., Kreidenweis, S. M., Roberts, G. C., and Prather, K. A., Effect of chemical mixing state on the hygroscopicity and cloud nucleation properties of calcium mineral dust particles, *Atmos. Chem. Phys.*, 9, 3303-3316, 10.5194/acp-9-3303-2009, 2009.

Tang, M. J., Cziczo, D. J., and Grassian, V. H.: Interactions of Water with Mineral Dust Aerosol: Water Adsorption, Hygroscopicity, Cloud Condensation, and Ice Nucleation, *Chemical Reviews*, 116, 4205-4259, 10.1021/acs.chemrev.5b00529, 2016.

Zhao, D. F., Buchholz, A., Mentel, T. F., Müller, K. P., Borchardt, J., Kiendler-Scharr, A., Spindler, C., Tillmann, R., Trimborn, A., Zhu, T., and Wahner, A., Novel method of generation of $\text{Ca}(\text{HCO}_3)_2$ and CaCO_3 aerosols and first determination of hygroscopic and cloud condensation nuclei activation properties, *Atmos. Chem. Phys.*, 10, 8601-8616, 10.5194/acp-10-8601-2010, 2010.

Zuend, A., Marcolli, C., Booth, A. M., Lienhard, D. M., Soonsin, V., Krieger, U. K., Topping, D. O., McFiggans, G., Peter, T., and Seinfeld, J. H.: New and extended parameterization of the thermodynamic model AIOMFAC: calculation of activity coefficients for organic-inorganic mixtures containing carboxyl, hydroxyl, carbonyl, ether, ester, alkenyl, alkyl, and aromatic functional groups, *Atmospheric Chemistry and Physics*, 11, 9155-9206, 10.5194/acp-11-9155-2011, 2011.

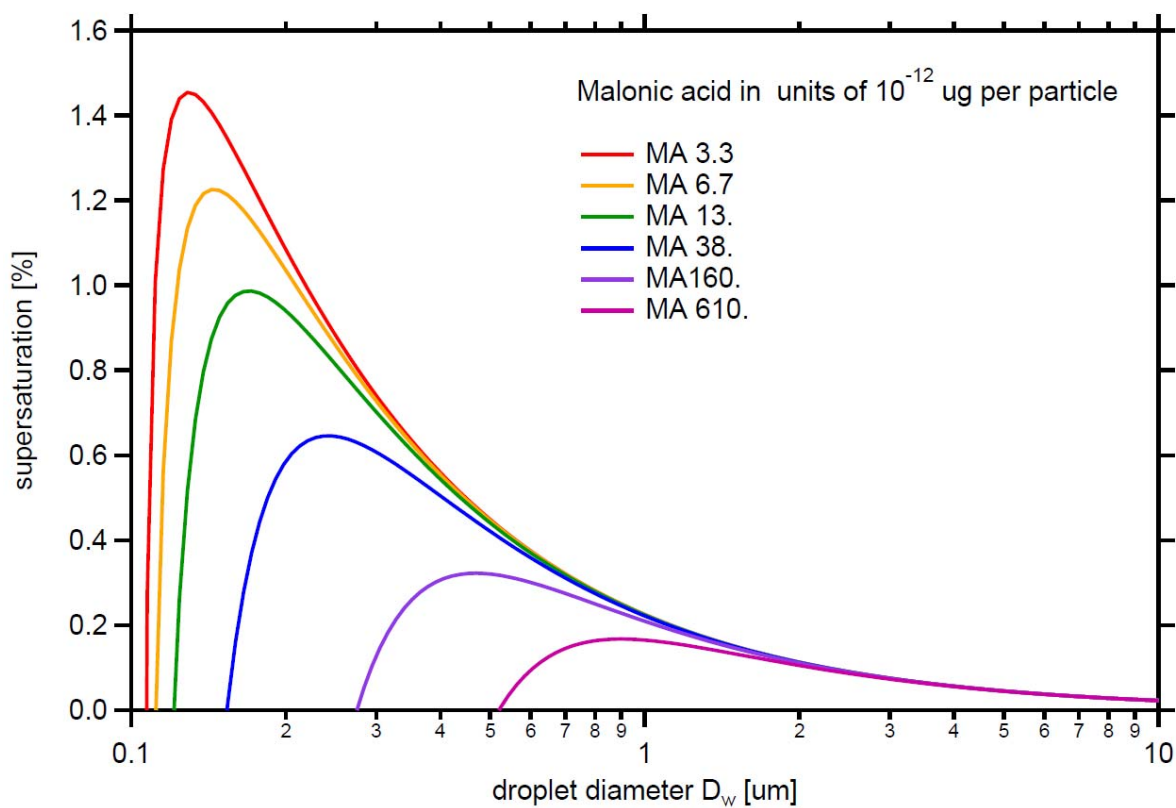


Figure S1. Variation of the equilibrium supersaturation over aqueous solution drops containing CaCO_3 and different mass of malonic acid at 293 K, assuming CaCO_3 is insoluble and doesn't react with malonic acid and the solution is dilute (water activity coefficient is close to 1). The diameter of insoluble CaCO_3 is 101.8 nm. Malonic acid mass per particle is 3.3, 6.7, 13, 38, 160, and 610 ($\times 10^{-12}$ μg , different color curves in the figure).

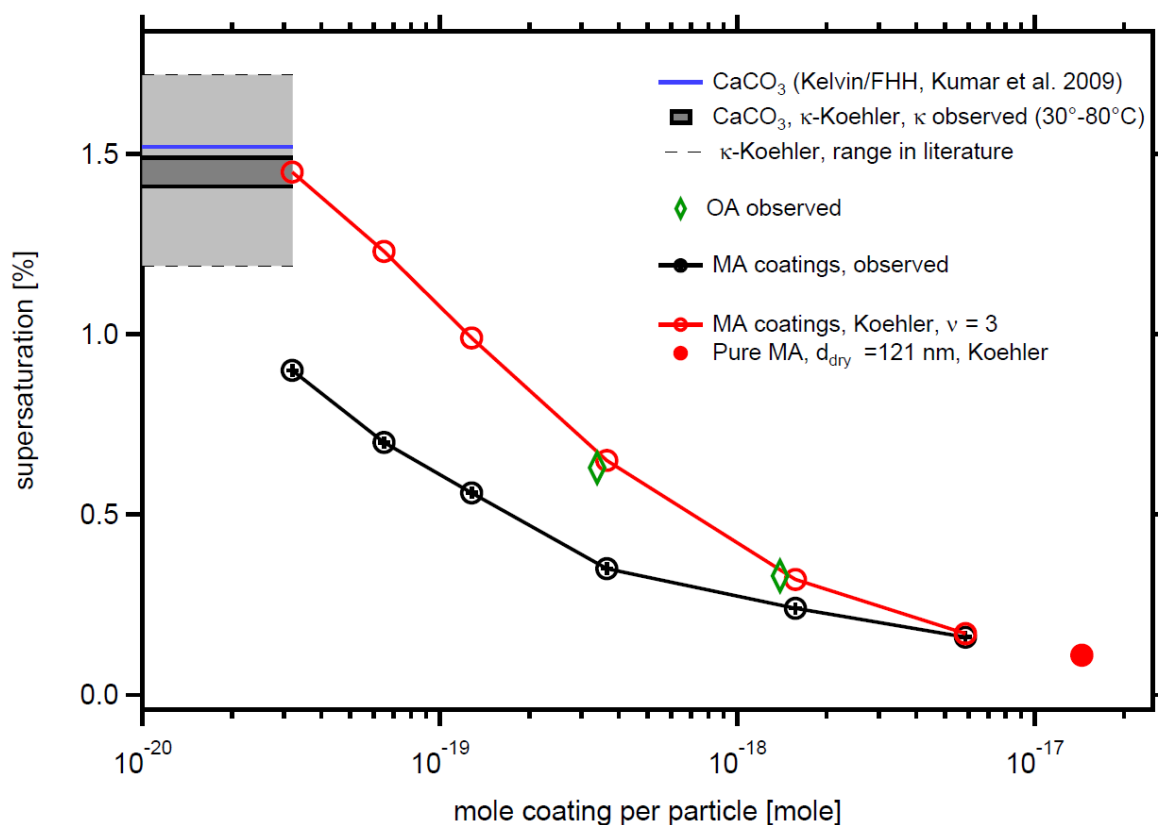


Figure S2: Comparison of SS_{crit} predicted by Koehler and Koehler/FHH theory with observations. The red circles are predictions by the Köhler theory for aqueous MA solutions assuming full dissociation, the black points present the observation. The red filled circle represents the Koehler prediction of SS_{crit} for 121.0 nm particles made of pure malonic acid. The horizontal lines give reference values for the bare $CaCO_3$ particles as calculated from our observed κ (black) and predicted by Koehler/FFH theory (blue). Light grey area between the thin dashed black lines indicates the range of SS_{crit} for 101.9 nm particles calculated from the range of κ in literature for wet generated $CaCO_3$ particles. Green diamonds show observed SS_{crit} for the two thickest OA coatings.

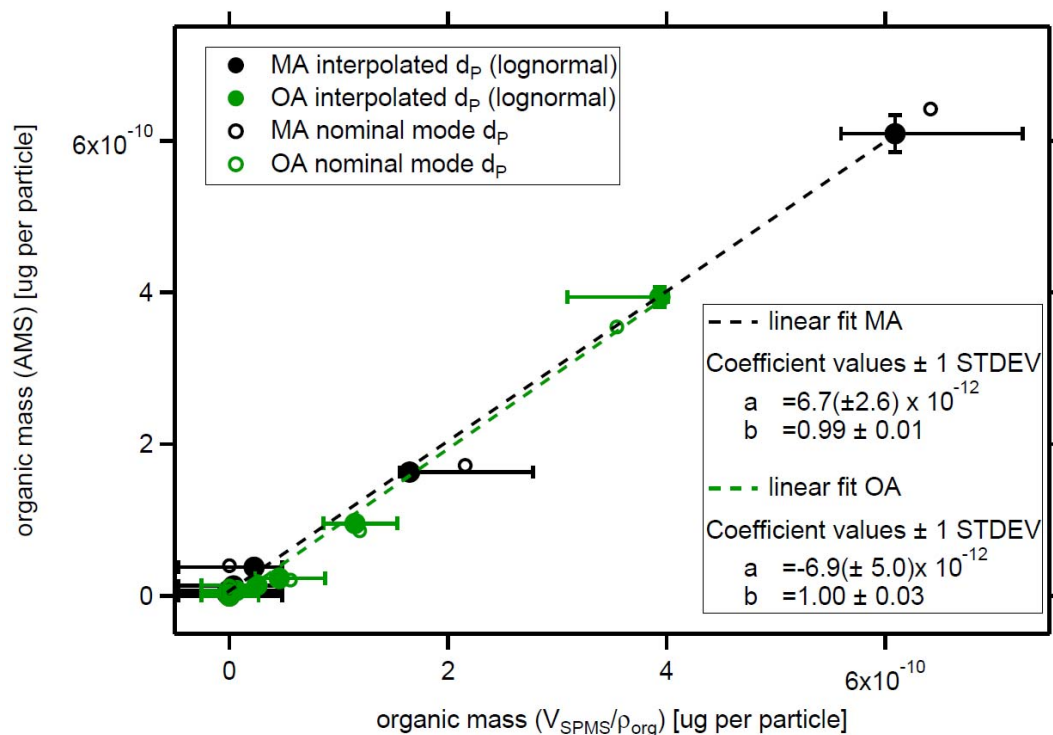


Figure S3: Linear relation between organic mass of the coating (AMS) and the organic coating mass calculated from the SMPS measurements for oleic acid coatings (green) and maleic acid coatings (black). For full circles the organic mass was calculated from the interpolated mode diameters (new). For interpolation we fitted a lognormal function in the range of the nominal mode diameter (considering 5-7 bins). The open circles are the data from the manuscript, where the nominal mode diameters were used to calculate the organic mass expected from SMPS measurements. Error bars in y give the reproducibility of the AMS measurement, error bars in x indicate the mass range (volume range) spanned by the SMPS bin width for the respective nominal mode diameter that entered the mass calculation. Note that the highest values must be the same as they were used to calibrate AMS organic mass vs SMPS volume.

Table S1. Theory and experimental SS_{crit} and κ values of $CaCO_3$ particles with different mass of MA coating.

Dry diam. (nm)	MA per particle ($\times 10^{-12}$ μg)	Theory SS_{crit} (%)	Experimental SS_{crit} (%)	Theory κ	Experimental κ
102.0	3.3 \pm 0.3	1.44	0.90	0.0024	0.0123 \pm 0.0005
102.1	6.8 \pm 1.2	1.20	0.70	0.0053	0.0231 \pm 0.0008
102.2	13 \pm 1.8	0.97	0.56	0.0107	0.0380 \pm 0.0012
102.7	38 \pm 1.6	0.63	0.35	0.0315	0.1063 \pm 0.0023
107.8	160 \pm 8.1	0.31	0.24	0.1110	0.1907 \pm 0.0031
121.0	610 \pm 24	0.16	0.16	0.3001	0.3126 \pm 0.0062

Table 2. Properties of investigated compounds.

Name	Formula	Molecular weight (g mol ⁻¹)	Density (g cm ⁻³)	Solubility (g/100 g water, at 298K)	Surface tension (dyn/cm)
Calcite	CaCO ₃	100.1	2.71	0.00058	- ^a
Malonic acid	C ₃ H ₄ O ₄	104.1	1.62	62	69 ^b
Oleic acid	C ₁₈ H ₃₄ O ₂	282.5	0.89	Very low	33 ^c

Values are taken from: Handbook of Chemistry and Physics, the 82nd Edition; Handbook of aqueous solubility data, Samuel H. Yalkowsky and Yan He, 2003; Chumpitaz et al., 1999; Hyvarinen et al., 2006.

a: no data

b: Surface tension of 0.01 mole fraction malonic acid aqueous solution at 298K

c: Surface tension of pure oleic acid at 293K

Chumpitaz, L. D. A., Coutinho, L. F., and Meirelles, A. J. A.: Surface tension of fatty acids and triglycerides, *J. Am. Oil Chem. Soc.*, 76, 379-382, 10.1007/s11746-999-0245-6, 1999.

Hyvarinen, A. R.; Lihavainen, H.; Gaman, A.; Vairila, L.; Ojala, H.; Kulmala, M.; Viisanen, Y., Surface tensions and densities of oxalic, malonic, succinic, maleic, malic, and cis-pinonic acids. *Journal of Chemical and Engineering Data* 2006, 51 (1), 255-260.

1 **Cloud Condensation Nuclei Activity of CaCO₃ Particles**
2 **with Oleic Acid and Malonic Acid Coatings**

3 **Mingjin Wang^{1,2}, Tong Zhu^{1*}, Defeng Zhao², Florian Rubach^{2,3}, Andreas**
4 **Wahner², Astrid Kiendler-Scharr², and Thomas F. Mentel^{2*}**

5 ¹BIC-ESAT and SKL-ESPCI, College of Environmental Sciences and Engineering,
6 Peking University, Beijing 100871, China.

7 ²Institut für Energie- and Klimaforschung (IEK-8), Forschungszentrum Jülich GmbH,
8 52425 Jülich, Germany.

9 ³Klimageochemie, Max Planck Institut für Chemie, 55128 Mainz, Germany

10

11 * To whom correspondence should be addressed: tzhu@pku.edu.cn;
12 t.mentel@fz-juelich.de

13

14 **Abstract.**

15 Condensation of carboxylic acids on mineral particles will lead to coatings, and
16 impact on the particles' potential to act as cloud condensation nuclei (CCN). To
17 determine how the CCN activity of mineral particles is impacted by carboxylic acid
18 coatings, the CCN activity of CaCO₃ particles and CaCO₃ particles with oleic acid
19 and malonic acid coatings were compared in this study. The results revealed that small

20 amounts of oleic acid coating (volume fraction (vf) \leq 4.3%) decreased the CCN
21 activity of CaCO₃ particles, while more oleic acid coating (vf \geq 16%) increased the
22 CCN activity of CaCO₃ particles. This phenomenon has not been reported before. On
23 the other hand, the CCN activity of CaCO₃ particles coated with malonic acid
24 increased with the thickness of the malonic acid coating (vf = 0.4 - 40%). Even
25 smallest amounts of malonic acid coating (vf = 0.4%) significantly enhanced the CCN
26 activity of CaCO₃ particles from $\kappa = 0.0028 \pm 0.0001$ to $\kappa = 0.0123 \pm 0.0005$. This
27 supports that a small amount of water-soluble organic acid coating may significantly
28 enhance the CCN activity of mineral particles. The presence of water vapor during the
29 coating process with malonic acid additionally increased the CCN activity of the
30 coated CaCO₃ particles, probably because more CaCO₃ reacts with malonic acid if
31 sufficient water is available.
32

33 **1 Introduction**

34 Atmospheric aerosols serve as cloud condensation nuclei and change the radiative
35 properties (cloud albedo effect) and lifetime (cloud lifetime effect) of clouds, thus
36 affecting the Earth's climate indirectly (Liu and Wang, 2010; Gantt et al., 2012;
37 Penner et al., 2004; Haywood and Boucher, 2000). Mineral aerosol is one of the most
38 abundant components of the atmospheric aerosol. It is estimated that 1500-2600 Tg of
39 mineral aerosol particles with radii between 0.1 and 8 μm are emitted annually into
40 the atmosphere on a global scale (Cakmur et al., 2006). Mineral aerosol particles are
41 mainly composed of substances that are slightly soluble or insoluble in water. Cloud
42 condensation nuclei (CCN) activity measurements show that the hygroscopicity
43 parameter κ (Petters and Kreidenweis, 2007) varies between 0.001 and 0.08 for
44 mineral aerosols, including CaCO_3 aerosol, clay aerosols and mineral dust aerosols
45 generated in the laboratory or sampled from various locations worldwide (Garimella
46 et al., 2014; Yamashita et al., 2011; Zhao et al., 2010; Koehler et al., 2009; Sullivan et
47 al., 2010; Herich et al., 2009). The low κ indicates that the CCN activity of mineral
48 aerosol is much lower than the CCN activity of water soluble salts like $(\text{NH}_4)_2\text{SO}_4$ (κ
49 = 0.61) and NaCl ($\kappa = 1.28$), which are also common in atmospheric aerosols (Petters
50 and Kreidenweis, 2007). Tang et al. (2016) reviewed recently the interaction of
51 mineral dust particles with water.

52 Mineral aerosol particles can be coated by organic vapors during their residence and
53 transport in the atmosphere. Many individual particle measurements have shown that
54 mineral components and organic matter can coexist in the same individual aerosol

55 particle in the real atmosphere (Falkovich et al., 2004; Falkovich et al., 2001; Russell
56 et al., 2002; Li and Shao, 2010). Carboxylic acids ($R(C=O)OH$) are abundant species
57 among the organic matter that coexists with mineral particles. Russell et al. (2002)
58 found that carbonyls ($R(C=O)R$), alkanes, and $R(C=O)OH$ are present in individual
59 mineral (and sea salt) aerosol particles, with enhanced concentration of $R(C=O)OH$.
60 They also found that Ca^{2+} , CO_3^{2-} , $R(C=O)OH$ and $R(C=O)R$ coexisted in some
61 individual mineral aerosol particles with a strong correlation between CO_3^{2-} and
62 $R(C=O)OH$. These particles could be formed by $CaCO_3$ particles (partly) coated with
63 organic film. Falkovich et al. (2004) also found that organic and inorganic
64 components coexisted in individual mineral aerosol particles with the organic
65 component consisting of various short-chain (C_1 - C_{10}) mono- and dicarboxylic acids
66 (MCA and DCA). The concentration of short-chain carboxylic acids in mineral
67 aerosol particles increased with the increase of the ambient relative humidity. A
68 possible explanation for such observations could be that when more water is
69 condensed onto mineral particles at higher ambient relative humidity, the adsorbed
70 carboxylic acids are ionized in the aqueous environment and react with mineral
71 particles forming organic acid salts. Of the major components of mineral aerosol
72 particles (clay, calcite ($CaCO_3$), quartz, mica, feldspar, etc.), only $CaCO_3$ with
73 alkaline character can react with carboxylic acids in this way. Thus $CaCO_3$ may play a
74 key role in the uptake of carboxylic acids by mineral aerosol particles.

75 Carboxylic acid coatings on mineral aerosol particles change their chemical
76 composition and thus may have an impact on their CCN activity. Many previous
77 studies have investigated the CCN activity of pure mineral aerosol (Garimella et al.,
78 2014; Yamashita et al., 2011; Zhao et al., 2010; Koehler et al., 2009; Sullivan et al.,
79 2010; Herich et al., 2009) and pure carboxylic acid aerosol (Kumar et al., 2003; Hori

80 et al., 2003; Cruz and Pandis, 1997; Hartz et al., 2006), but only a few studies have
81 investigated the CCN activity of mineral aerosol particles with carboxylic acid
82 coatings (Tang et al., 2015; Hatch et al., 2008; Gierlus et al., 2012).

83 In this study we used malonic acid and oleic acid as coating materials and CaCO_3
84 particles as cores, and investigated the CCN activity of the coated CaCO_3 particles.
85 Herein we varied the coating thickness and the relative humidity during the coating
86 process. Malonic acid is a representative of the class of dicarboxylic acids and oleic
87 acid is an example of surfactant like compounds. Dicarboxylic acids are ubiquitous in
88 the atmosphere (Kawamura et al., 1996; Kawamura and Ikushima, 1993; Ho et al.,
89 2007; Mkoma and Kawamura, 2013; Kawamura and Bikkina, 2016) and formed by
90 photochemical reactions and ozonolysis (Chebbi and Carlier 1996; Kawamura and
91 Bikkina, 2016; Kawamura et al., 1996; Khare et al. 1999; Mellouki et al., 2015). It has
92 been reported that dicarboxylic acids ($\text{C}_2\text{-C}_{10}$) account for 0.06-1.1% of the total
93 aerosol mass, with higher values in the summer, and 1.8% of the total aerosol carbon
94 (TC) in urban aerosol, in which oxalic acid, malonic acid, and succinic acid are the
95 most abundant species (Kawamura et al., 1996; Kawamura and Ikushima, 1993; Ho et
96 al., 2007; Mkoma and Kawamura, 2013). Oleic acid, which is emitted into the
97 atmosphere by the cooking of meat, wood burning, and automobile source (Schauer et
98 al., 1999; Rogge et al., 1998; Rogge et al., 1993), is present in atmospheric aerosols of
99 urban, rural, and forest areas (Cheng et al., 2004; Ho et al., 2010). The water
100 solubility of the two organic acids is complementary; it is high for malonic acid while
101 it is very low for oleic acid. Coatings of malonic acid and oleic acid could thus have
102 different effects on CCN activity of mineral particles.

103

104

105 **2 Experimental**

106 As general procedure, CaCO₃ aerosol was generated according to Zhao et al. (2010),
107 and then poly- or monodisperse CaCO₃ aerosol particles were coated by malonic or
108 oleic acid in a coating device. A flow tube was optionally applied to extend the
109 residence time. The particle size, chemical composition, and CCN activity of the
110 CaCO₃ particles were measured before and after coating. Figure 1 shows the
111 schematic of the experimental set up.

112 **2.1 Generation of CaCO₃ aerosol**

113 CaCO₃ aerosol was generated by spraying a saturated Ca(HCO₃)₂ solution. A sample
114 of CaCO₃ powder (2 g, pro analysis, ≥99%, Merck, Darmstadt, Germany) was
115 suspended in 1-L Milli-Q water (18.2 MΩcm, TOC <5 ppb). Then about 1.5 L min⁻¹
116 CO₂ (purity ≥99.995%, Praxair Industriegase GmbH & Co. KG, Magdeburg,
117 Germany) was bubbled into the suspension at room temperature for 3 h, while the
118 suspension was stirred using a magnetic stirrer. During bubbling, CO₂ reacted with
119 CaCO₃ to produce Ca(HCO₃)₂. After bubbling, the suspension was allowed to settle
120 for 10 min, the supernatant clear Ca(HCO₃)₂ solution was decanted and used for
121 spraying by a constant output atomizer (Model 3076, TSI, Shoreview, MN, USA)
122 using 1.75 L min⁻¹ high-purity N₂ (Linde LiPur 6.0, purity 99.9999%, Linde AG,
123 Munich, Germany).

124

125 The major portion (0.9 L min^{-1}) of the aerosol flow generated by spraying was dried
126 in a diffusion drier filled with silica gel. The relative humidity was below 10% after
127 drying. The remainder of the aerosol flow was drawn off by a pump and discarded.
128 The dry aerosol was passed through a tube furnace (Model RS 120/1000/12,
129 Nabertherm GmbH, Lilienthal, Germany) set at $300 \text{ }^\circ\text{C}$. The residence time of the
130 aerosol in the furnace was 5.2 s. Zhao et al. (2010) described this method for
131 generating CaCO_3 aerosol in detail. At room temperature dry $\text{Ca}(\text{HCO}_3)_2$ is
132 thermodynamically unstable and decays into CaCO_3 , CO_2 , and H_2O (Keiser and
133 Leavitt, 1908). With this method the aerosol still contained some $\text{Ca}(\text{HCO}_3)_2$ after
134 drying, but after heating at $300 \text{ }^\circ\text{C}$ it was completely converted into CaCO_3 (Zhao et
135 al., 2010). The CaCO_3 aerosol generated was either first size selected by a Differential
136 Mobility Analyzer (DMA, TSI 3081) with a neutralizer on the inlet or entered the
137 coating device directly as poly-disperse aerosol.

138 Figure 2 (upper panel) shows the total number concentration and mean size of the
139 bare CaCO_3 aerosol particles generated at different spraying time, which were
140 measured with the SMPS described below. The mean size (mode diameter) stabilized
141 after about 50 min in the range 49.8-55.5 nm. Over the 232 min spraying time, the
142 total number concentration varied in the range 1.8×10^6 – $4.5 \times 10^6 \text{ cm}^{-3}$. The total
143 number concentration decreased by about 1/3 in the initial 70 min. The decrease
144 became slower after 70 min and the total number concentration tended to stabilize
145 after 155 min. After 70 min the total number concentration varied in a smaller range
146 of 1.8×10^6 – $2.9 \times 10^6 \text{ cm}^{-3}$, therefore, the measurements in this study typically started

147 after 70 min spraying. The typical size distribution of the CaCO₃ aerosol particles
148 after 70 min spraying is shown in Fig. 2 (lower panel). The CaCO₃ particles showed a
149 single mode distribution with a mode diameter at 32.2 nm. The number concentration
150 was more than 100 cm⁻³ for particles between 9.82 and 346 nm.

151 **2.2 Organic acid coating**

152 The coating device (Fig. 1, right hand side) used in this study was designed by Roselli
153 (2006), and showed good reproducibility, controllability, and stability. The glass
154 apparatus consisted of a small storage bulb (100 ml) holding the organic coating
155 substances which was directly connected to a mixing cell (about 35 ml). The storage
156 bulb and mixing cell were fully immersed in a flow-through water heater connected to
157 a thermostatic bath (F25, Julabo GmbH, Seelbach, Germany). The temperature range
158 of the thermostatic bath used in this study was 30-80 °C. An extra N₂ stream could be
159 passed through the storage bulb in order to enhance the organic vapors flowing into
160 the mixing cell. The outflow of the coating device was connected to a Liebig type
161 water cooler. The water cooler was controlled by another thermostatic bath (F25,
162 Julabo GmbH, Seelbach, Germany) operated at 25 °C throughout all of the
163 experiments.

164 The bottom of the storage bulb was filled with either 5.0 g malonic acid powder
165 (assay ≥98%(T), Fluka Chemika, Sigma-Aldrich, St Louis, MO, USA) or 10.0 ml
166 oleic acid (chemical purity (GC) 99.5%, Alfa Aesar, Ward Hill, MA, USA). A flow of
167 0.9 L min⁻¹ high purity N₂ was used to carry the organic acid vapor up into the mixing
168 cell. The flow of 0.9 L min⁻¹ CaCO₃ aerosol was passed through the mixing cell and
169 mixed with the 0.9 L min⁻¹ N₂ flow carrying the organic acid vapor. The mixed flow

170 then entered the water cooler. The organic acid vapor was condensed on CaCO₃
171 aerosol particles in both the mixing cell and the water cooler. The residence time of
172 the aerosol in the coating device including the cooler was about 6 seconds Three
173 identical coating devices, with the same heating and cooling thermostatic bath, were
174 used: one for malonic acid coating, one for oleic acid coating, and a blank one without
175 organic acid for assessing the impact caused by heating the CaCO₃ aerosol in the
176 coating device without organic acid (Roselli, 2006).

177 The aerosol could enter the measuring instruments directly, or after passing through a
178 flow tube to increase its residence time. The flow tube was made of a straight circular
179 glass tube with a 2.5 cm internal diameter. The aerosol flow in the flow tube was
180 laminar flow. The residence time of the aerosol in the flow tube was 23.7 s.

181 For the coating process we mixed flows of 0.9 L min⁻¹ of dry N₂ and of aerosol dried
182 to <10% relative humidity (RH) at room temperature (RT). As a consequence RH at
183 the outlet of the coating device was <5% at RT. To investigate the impact of water on
184 the coating process and CCN activity, organic coating at a higher relative humidity
185 was also performed. For that a bubbling device filled with Milli-Q water was utilized
186 to saturate the N₂ stream with water vapor before it entered the storage bulb (RH>90%
187 at RT). After mixing with the aerosol stream at RH ≈10%, the water concentration in
188 the mixing cell corresponded to RH ≈ 50% at RT or a partial pressure of ≈1500 Pa.
189 The relative humidity of the aerosol at the outlet of the coating device at RT was
190 indeed ~47% when humidification was applied. For the partial water vapor pressure
191 of 1500 Pa we calculated RH >7% at 60°C (for MA), and RH >3% at 80°C (for OA)
192 which is about an order of magnitude higher than RH in the dry cases. In fact RH will
193 be somewhat higher as the gas-phase may not reach the bath temperature which

194 primarily serves to warm up the coating agent and control its vapor pressure.

195 **2.3 Size and chemical composition measurements**

196 The number size distribution of the aerosol particles was measured using a Scanning
197 Mobility Particle Sizer (SMPS, TSI 3080 Electrostatic Classifier with TSI 3081 DMA,
198 TSI 3786 UWCPC). The sample flow was set to 0.6 L min^{-1} and the sheath flow was
199 set to 6.0 L min^{-1} . The size range measured was 9.82-414.2 nm with a size resolution
200 of 64 channels per decade and the time resolution was 3 min for a complete scan.
201 Despite the maximum resolution of the SMPS the size bin width was still substantial
202 compared to the observed growth by coating. We therefore derived the diameter of the
203 coated (and the respective bare CaCO_3 particles) by interpolating in between the size
204 bins. For that we considered 5-9 size bins around the size bin of nominal mode and
205 fitted a lognormal distribution to these data. The fitted mode positions are listed in
206 Table 1. The error bars in x direction in Figure S1 in the supplement, show the shifts
207 of the fitted mode position relative to the nominal size bin.

208 The chemical composition and the vacuum aerodynamic diameter of the aerosol
209 particles were measured using a High-Resolution Time-of-Flight Aerosol Mass
210 Spectrometer (HR-ToF-AMS, Aerodyne Research Inc., Billerica, MA, USA (DeCarlo
211 et al., 2006)). The aerosol particles were vaporized at $600 \text{ }^\circ\text{C}$ and ionized by electron
212 impact ionization at 70 eV, i.e. we focused on the measurements of the organic
213 coatings and sacrificed a direct CaCO_3 determination by AMS (compare Zhao et al.
214 2010). The AMS was routinely operated in V-mode in two alternating modes: 1 min
215 MS mode to measure the chemical composition and 2 min PToF mode. Only MS
216 mode data were analyzed. AMS measurements and SMPS measurements were
217 synchronous and both were repeated at least four times for each sample. Size

218 information for bare CaCO₃ was taken from SMPS data in the blank coating device.

219 We used specific marker m/z to derive the amount of organic coating. For pure oleic
220 acid the signal at $m/z41$ (C₃H₅⁺) was reported to be the strongest signal in the mass
221 spectrum measured by Q-AMS at EI energy of 70 eV and vaporizer temperature of
222 600 °C (Sage et al., 2009). The signal at $m/z41$ was also strongest for oleic acid
223 coatings in our HR mass spectra. In order to get a high signal to noise ratio we choose
224 the signal at $m/z41$ in the MS mode of the AMS measurement as a marker for oleic
225 acid in the coated CaCO₃ particles. There was no significant signal at $m/z41$ for the
226 uncoated CaCO₃ particles. The average background signal at $m/z41$ per single aerosol
227 particle corresponded to $2.4 \pm 0.79 \cdot 10^{-12}$ µg for bare CaCO₃. The average value
228 presented the baseline of the mass spectra and the standard deviation was derived
229 from the noise of the mass spectra at $m/z41$. Similarly, the signal at $m/z42$ (C₂H₂O⁺)
230 was one of the strongest signals in the mass spectrum of pure malonic particles
231 measured by Q-AMS with EI energy of 70 eV and vaporizer temperature of 600 °C
232 (Takegawa et al., 2007). That signal was also observed for malonic acid coatings in
233 our HR mass spectra and used as marker for malonic acid coatings. The average
234 background signal per aerosol particle at $m/z42$ for bare CaCO₃ particles was
235 $1.4 \pm 0.42 \cdot 10^{-12}$ µg. The average value represented the baseline of the mass spectra at
236 $m/z42$ and the standard deviation was derived from the noise in the mass spectra.

237 The coating amount for both organic compounds was derived as follows. The
238 observed signal at the respective marker m/z was corrected for the background signal
239 from bare CaCO₃ and then scaled to the volume increase (per particle) calculated
240 from the shift of the particle diameter D_p for the largest coating amount achieved at 80
241 °C coating temperature. Because of the relative large bin width compared to the

242 growth by coating we used the D_p 's, interpolated between the nominal size bins of the
243 SMPS (see above). This assumed spherical core shell morphology, based on Zhao et
244 al. (2011) where we showed that the CaCO_3 particles generated by our spray drying
245 method are spherical. The relation between AMS derived organic mass (baseline
246 corrected marker signals at $m/z41$ or $m/z42$ per particle) and SMPS derived organic
247 mass ($\pi/6 \cdot (D_p)^3 / \rho_{\text{org}}$) is linear within the limits of the method (see Figure S1 in the
248 supplement). For discussion we will refer to the AMS results, as we are able to detect
249 amounts of organic coatings as small as few time 10^{-12} ug per particle with the AMS,
250 while these could be not be detected by the SPMS.

251 **2.4 CCN activity measurement**

252 The aerosol was dried to RH <3% by another diffusion drier before the CCN activity
253 was measured. To determine the CCN activity of the aerosol, the number
254 concentration of the cloud condensation nuclei (CCN) of the aerosol was measured
255 with a continuous flow CCN counter (CCNC, DMT-100, Droplet Measurement
256 Technologies, Boulder, CO, USA). The total number concentration (CN) of the
257 aerosol particles was synchronously measured using an ultrafine water-based
258 condensation particle counter (UWCPC, TSI 3786, cf. Zhao et al., 2010). The ratio of
259 CCN to CN (CCN/CN) is called the activated fraction (a_f). In cases where
260 poly-disperse aerosol was coated, the coated aerosol particles were size selected by
261 scanning a DMA between 10.6 and 478.3 nm , and the CCN and CN concentrations
262 were determined for each size bin while the super-saturation (SS) kept constant
263 (known as 'Scanning Mobility CCN Analysis (SMCA)', Moore et al., 2010). The
264 activated fraction was calculated after the CCN and CN concentrations were corrected
265 for the multiple charged particles.

266 The activated fraction as a function of the particle size was fitted with a cumulative
267 Gaussian distribution function (Rose et al., 2008). The turning point of the function is
268 the critical dry diameter (D_{crit} or D_{50}) at the set SS. The activation efficiency (i.e., the
269 activated fraction when aerosol particles are completely activated) was 83% for the
270 CCN instrument, determined using 150 nm $(\text{NH}_4)_2\text{SO}_4$ particles at $\text{SS}=0.85\%$.
271 Besides CaCO_3 and coated CaCO_3 particles, the CCN activity of malonic acid
272 particles, oleic acid particles, and mixed particles of CaCO_3 and malonic acid was
273 also measured. The oleic acid particles were generated by heating 10.0 ml oleic acid
274 to 97 °C in the storage bulb and then cooling the vapor to 2 °C in the water cooler in a
275 clean coating device. 1.75 L min^{-1} high-purity N_2 was used as carrying gas and went
276 into the storage bulb through '1 N_2 in' entrance in Fig. 1; the '3 Aerosol in' entrance in
277 Fig. 1 was closed. This way, pure oleic acid particles with diameters up to 333 nm
278 were generated. Mixed CaCO_3 /malonic acid particles were generated by spraying the
279 supernatant clear solutions which were prepared by settling suspensions containing
280 CaCO_3 and malonic acid in molar ratios of about 1:1 and 3:1. The suspensions were
281 prepared with 0.020 g malonic acid and 0.021 g CaCO_3 and 0.025 g malonic acid and
282 0.076 g CaCO_3 in 1000 ml Milli-Q water, respectively. The suspensions were allowed
283 to stand for 24h.

284 For aerosols where monodisperse aerosol particles with a dry diameter D_p were
285 coated, the CCN concentration was measured at different SS and the CN
286 concentration was measured synchronously. Similarly, the activated fraction as a
287 function of SS was fitted with a sigmoidal function. The turning point of the function
288 is the critical supersaturation (SS_{crit}) and the corresponding to the dry diameter D_p is
289 also called the critical diameter, D_{crit} . The hygroscopicity parameter κ (Petters and
290 Kreidenweis, 2007) was then calculated from the $D_p(D_{\text{crit}})\text{-SS}_{\text{crit}}$ or $\text{SS}(\text{SS}_{\text{crit}})\text{-}D_{\text{crit}}$ data

291 set. The SS settings of the CCN counter were calibrated weekly using $(\text{NH}_4)_2\text{SO}_4$
292 aerosol based on the theoretic values in the literature (summarized by Rose et al.,
293 2008).

294 **3 Results and discussion**

295 **3.1 CCN activity of CaCO_3 aerosol**

296 Before the coating experiments we determined the CCN activity of the bare CaCO_3
297 aerosol particles. It was measured by the scanning method (SMCA) using
298 poly-disperse CaCO_3 aerosol particles. The value of the hygroscopicity parameter κ of
299 the CaCO_3 aerosol was 0.0028 ± 0.0001 derived by the least-square-fitting of D_{crit} as a
300 function of SS (SS_{crit}). This κ value is quite small, indicating that the CCN activity of
301 the CaCO_3 aerosol is low. Our κ is well within the range of κ 's of 0.0011 ± 0.0004 to
302 0.0070 ± 0.0017 found in previous studies for wet generated CaCO_3 particles (Zhao et
303 al., 2010; Sullivan et al., 2009; Gierlus et al., 2012, Tang et al., 2016), but larger than
304 κ for dry generated CaCO_3 aerosols (0.008-0.0018, Sullivan et al., 2009).

305 The CCN activity for CaCO_3 aerosol passed through the blank coating device and
306 exposed to temperatures of 60 °C and 80 °C was determined using the same method.
307 The κ value remained 0.0028 ± 0.0001 up to 60 °C and increased to 0.0036 ± 0.0001
308 at 80 °C. The increased κ value of 0.0008 at 80 °C was lower than the differences of
309 reported κ values for CaCO_3 aerosol in various studies, and much lower than the
310 changes of κ values measured in this study when the CaCO_3 aerosol particles were
311 coated by malonic or oleic acid. So the effect of heating the CaCO_3 aerosol during the

312 coating process on the CCN activity of the CaCO₃ aerosol was neglected. The D_{crit} at
 313 different supersaturations (SS_{crit}) for the CaCO₃ aerosol and for the CaCO₃ aerosol
 314 passed through a blank coating device at heating temperatures of 60 °C and 80 °C are
 315 shown in Fig. 5 (red, yellow and green circles).

316 As the solubility of CaCO₃ in water is very low, droplet activation of CaCO₃ (and
 317 other mineral dust components) is often described by a water adsorption approach,
 318 wherein the solute term B in the Köhler equation (Köhler 1936, Seinfeld and Pandis,
 319 2006, see eq. (S1-S3) in the supplement) is replaced by a water adsorption term. The
 320 equations (1) and (2) show application of the Frenkel Halsey Hill adsorption isotherm
 321 (FHH) as proposed by Sorjamaa and Laaksonen (2007) and Kumar et al. (2009):

$$322 \quad B = -A_{\text{FHH}} \cdot \theta^{-B_{\text{FHH}}} \quad (1)$$

323 Therein the water coverage θ by (Sorjamaa and Laaksonen, 2007) is given as:

$$324 \quad \theta = \frac{D_w - d_u}{2 \cdot 2.75 \cdot 10^{-4}} \quad [\mu\text{m}] \quad (2)$$

325 and D_w and d_u are the diameter of the wet particles and the insoluble core. We applied
 326 the FHH parameter for CaCO₃ (AFHH=0.25 and BFHH=1.19, Kumar et al. 2009) and
 327 derived a critical supersaturation of 1.52% for CaCO₃ particles with d_u = 101.9 nm
 328 (Figure 7, blue line). In comparison κ-Koehler theory predicts SS_{crit}=1.49% for
 329 κ=0.0028. Such an SS_{crit}=1.49% would also be achieved by 8.5·10⁻²⁰ mole solute per
 330 particle (Figure 7, black line). Figure 7 also shows the SS_{crit} for the bare CaCO₃
 331 particles processed at 80°C coating temperature and the range of SS_{crit} for 101.9nm

332 particles calculated from the range of κ 's given in the literature (Tang et al., 2016 and
333 references therein) for wet generated CaCO₃ particles.

334 We conclude that the surface of our CaCO₃ particles is a little more wettable than the
335 dry generated particles studied by Kumar et al. (2009). We presume formation of
336 Ca(OH)(HCO₃) structures on the surface during the spray-drying generation process
337 as commonly observed whenever the CaCO₃ surface has been exposed to gaseous
338 water or liquid water (Stipp, 1999; Stipp and Hochella, 1991; Neagle and Rochester,
339 1990). In case of soluble components causing the lower SS_{crit} their amount must be of
340 the order of $1 \cdot 10^{-19}$ mole per particles.

341 **3.2 CCN activity of CaCO₃ particles with oleic acid coating**

342 For the coating with oleic acid, we selected monodisperse CaCO₃ aerosol particles of
343 101.8 nm diameter using the DMA, and measured the size and chemical composition
344 of the particles before (uncoated) and after (coated) coating with oleic acid. The
345 results are listed in the upper part of Table 1.

346 The mode diameters of number size distribution for the uncoated CaCO₃ particles at
347 30-80 °C remained in the 101.8 nm size bin, identical to that selected by the DMA.
348 Interpolation in between the size bins as described in the experimental section led to
349 an average dry diameters of bare CaCO₃ of $d_u = 101.9$ nm. The mode diameters of the
350 CaCO₃ particles after coating with oleic acid in the range of 30-50 °C stayed in the
351 pre-selected size bin at 101.8 nm, which means that the layers were too thin to

352 effectively grow the particles to the next size bin; the mode diameters increased
353 distinctively in the temperature range of 60-80 °C (Fig. 3, upper panel). However, the
354 bin-interpolated diameters D_p which are shown in Table 1 increased monotonically
355 over the whole temperature range.

356 The values of $m/z41$ [μg per particle] originating from the oleic acid coating for the
357 coated CaCO_3 particles at 30-80 °C were at all temperatures significantly larger than
358 for the bare CaCO_3 particles, and increased with the increasing coating temperature
359 ($3.7 \cdot 10^{-12}$ - $390 \cdot 10^{-12}$ μg per particle, compare Table 1 and Fig. 3, bottom panel, red
360 circles). The AMS detected increase at $m/z41$ showed that the CaCO_3 particles already
361 contained small amounts of oleic acid after coating with oleic acid at temperatures
362 below 60 °C although the D_p shifted less than a size bin.

363 The organic volume fraction (vf) in the aerosol particles, $V_{\text{OA}}/V_{\text{par}}$ [%], was calculated.
364 Herein $V_{\text{par}} = (V_{\text{OA}} + V_{\text{CaCO}_3})$, V_{OA} is the oleic acid volume derived by AMS and
365 V_{CaCO_3} the volume of the bare CaCO_3 before coating (101.9 nm). $V_{\text{OA}}/V_{\text{par}}$ for the
366 uncoated CaCO_3 particles is by definition zero. The vf for the coated CaCO_3 particles
367 at 30-80 °C increased with the increase in the coating temperature from 0.8% at 30 °C
368 to 44% at 80 °C (Fig. 3, bottom panel, red crosses and Table 1). The CaCO_3 particles
369 were indeed coated with a significant amount of oleic acid and the amount of oleic
370 acid coating increased with the increase in the coating temperature. The experiments
371 were repeated at least four times. The according standard deviations for the oleic acid
372 mass per particle in Table 1 demonstrate that the reproducibility of the experiments

373 was good and the performance of the coating device was stable.

374 The activated fractions at different SS for monodisperse CaCO₃ particles with d_u =
375 101.9 nm before and after oleic acid coating at 30-80 °C are shown in Fig. 4. The top
376 panel in Fig. 4 shows the results at 30-60 °C with up to $23 \pm 1.2 \cdot 10^{-12}$ ug of coating
377 material deposited on the CaCO₃ particles (vf = 4.3%). At the lowest SS of 0.17% and
378 0.35%, the activated fractions were very low and independent of the presence of the
379 coating material within the errors. When the SS increased to 0.52%, 0.70%, and
380 0.87%, the activated fractions for the coated CaCO₃ particles were *lower* than those
381 for the uncoated particles. Notably the activated fractions for the coated CaCO₃
382 particles *decreased* with the increase in the coating material in the range of vf
383 0.8-2.7%. The activated fractions for the CaCO₃ particles with different amounts of
384 coating spread with larger SS applied. However this trend reversed at the coating
385 temperature of 60 °C and an oleic acid vf of 4.3%, and the activated fractions at vf =
386 4.3% became higher than those at 2.7% at the three largest SS. In summary, we found
387 that the CCN activity of the coated CaCO₃ particles with vf of OA in a range 0.8-4.3%
388 was lower than that of the uncoated CaCO₃ particles. The CCN activity of the coated
389 CaCO₃ particles decreased with the increasing vf in between 0.8-2.7%, i.e. the CCN
390 activity became lower when more coating material deposited on the CaCO₃ particles.
391 This trend turned somewhere at a vf somewhere between 2.7 and 4.3%. As the D_p also
392 increased at 60 °C we cannot differentiate if the increase in the activated fractions is
393 due to increasing size or because of increasing wettability.

394 The activated fractions of CaCO₃ particles after coating with oleic acid with vf of 16%
395 and 44% (coating temperatures of 70 and 80 °C , respectively) were considerably
396 higher than that before coating, as shown in Fig. 4 (bottom panel). The increased
397 activated fractions resulted from both the increase in particle size (Fig. 3) and the
398 increase of the OA volume fraction of particles. At vf of 16% and 44%, the activated
399 fractions of the CaCO₃ particles after coating increased with the increase of SS and
400 reached complete activation. (Note, because the activation efficiency is 83%, the
401 activated fractions appear at values less than 100% at the points of full activation.)
402 For vf of 16% and 44% SS_{crit} was determined by fitting a sigmoidal function to the
403 activated fraction as a function of SS. The particle dry diameter D_P which is D_{crit} in
404 these cases is given as in Table 1. The hygroscopicity parameter κ was determined
405 from D_P (D_{crit}) and the corresponding SS_{crit}. The κ values of the CaCO₃ particles
406 coated with vf of oleic acid of 16% and 44% were 0.0237 ± 0.0006 and 0.0673 ±
407 0.0016, respectively. The respective κ values for the CaCO₃ particles with a diameter
408 of 101.9 nm without coating and after coating with oleic acid at 30-60 °C (oleic acid
409 vf ≤4.1%) could not be determined by this method because these particles could not
410 be fully activated at the highest SS reachable by the CCN counter. Therefore we give
411 as upper limit κ = 0.0028 ± 0.0001 for the uncoated CaCO₃ particles determined by
412 scanning the size of the poly-disperse CaCO₃ aerosol particles as described above (see
413 Fig. 5).

414 So we conclude that for vf of oleic acid of 0.8-2.7% the CCN activity of CaCO₃
415 particles after coating is lower than that of uncoated CaCO₃ particles and decreases

416 with the fraction of oleic acid. The trend turns at a vf between 2.7 and 4.3%. CCN
417 activity was higher than that of the bare CaCO₃ particles at vf of oleic acid of 16%
418 (70°C) and 44% (80°C) with CCN activity $\kappa = 0.0237 \pm 0.0006$ and $\kappa = 0.0673 \pm$
419 0.0016), respectively. The enhanced and reduced CCN activity of CaCO₃ particles
420 coated with oleic acid at 80 °C and 60 °C, respectively, was also evident from the
421 CCN activity measurement using *poly-disperse* aerosols (Fig. 5).

422 A possible explanation for our observation can be based on the amphiphilic character
423 of oleic acid, namely that one end of the oleic acid molecule is hydrophobic (the
424 hydrocarbon chain), while the other is hydrophilic (the carboxyl group).

425 We refer to Ca(OH)(HCO₃) structures at the surface which offer polar surface sites to
426 bind the hydrophilic ends (the carboxyl groups) of the oleic acid molecules. The
427 hydrophobic ends of oleic acid molecules (the hydrocarbon chains) are then exposed
428 on the particle surface hence increase the hydrophobicity of the particle surface. Such
429 a formation of a hydrophobic layer should be occurring until all polar sites are
430 occupied or monolayer coverage - maybe in form of a self-assembled layer - is
431 reached. This can hinder the uptake of water. Activation of CaCO₃ particles can be
432 described by the Kelvin term and a water absorption term, e.g. Frenkel Halsey Hill
433 isotherm (Sorjamaa and Laaksonen, 2007, Kumar et al. 2009). In terms of
434 Kelvin/FHH theory the hydrophobic OA coating will lower A_{FHH} and/or likely
435 increase B_{FHH} . (The formation of a monolayer of OA on black carbon particles with
436 the polar groups pointing outwards was postulated by Dalirian et al. (2017), which

437 lead to increased activation of the black carbon particles. Thus, they observed a
438 similar effect of layer formation, but with switched polarity.)

439 Garland et al. (2008) suggested that OA at sub-monolayer coverage form
440 self-associated islands rather than uniformly covering the surfaces, and OA molecules
441 are oriented vertically, with polar heads facing to the surface. This is in support of our
442 working hypothesis: the formation of a hydrophobic surface film. We conclude that
443 all hygroscopic sides on the CaCO_3 surface are covered at OA vf somewhere between
444 2.7% and 4.3%, as here the trend turns and droplet activation starts to increase again.
445 This would place the monolayer coverage above 3%, organic volume fraction.
446 According to the measurements and calculations of the length of oleic acid molecule,
447 the thickness of oleic acid sub-monolayer on solid surfaces, and the thickness of
448 deuterated oleic acid monolayers at the air-water interface (Garland et al., 2008; King
449 et al., 2009; Iwahashi et al., 2000), we estimate 2.3 nm as the likely thickness of oleic
450 acid monolayer on CaCO_3 particles, accordingly a monolayer would be achieved at
451 about 12-13% organic volume fraction. As a consequence the re-increase of
452 hygroscopicity starts at sub-monolayer coverage and we propose that a fraction of
453 oleic acid binds to already adsorbed oleic acid tail by tail such that carboxylic groups
454 are facing outwards.

455 For CaCO_3 particles coated with more than an OA monolayer (vf = 16% and 44% at
456 70 and 80 °C coating temperatures), OA in the first layer should still combine with the
457 CaCO_3 surface, the heads pointing downwards. We suppose that now a portion of the

458 carboxyl groups of the oleic acid molecules, which are not in the first layer, will be
459 exposed to the particle surface, in analogy to the formation of lipid bilayers, e.g. in
460 cells, though the structure of this part of oleic acid is not known. The particle surface
461 then becomes more hydrophilic.

462 When carboxylic groups of OA are exposed at the surface, the interaction of water
463 with the OA layer becomes stronger, and the surface becomes wettable. In terms of
464 the Kelvin/FHH approach, the surface water interaction becomes stronger and A_{FHH}
465 increases and likely also the interaction between the higher water layers (B_{FHH}
466 decreases). From this point of view water adsorption by the “OA bilayer” should
467 become similar to thin malonic acid layers (compare next section). In addition, when
468 droplets form, oleic acid will transfer to the surface of the droplets and lower the
469 surface tension of the solution (the surface tension of oleic acid is 0.033 J m^{-2} , which
470 is much lower than that of pure water of 0.072 J m^{-2}). Thus, the activation of OA
471 coated particles is probably a complex interaction between formation of a specific
472 hydrophobic layers and more hydrophilic multilayers, surface tension effects and for
473 the largest coating amounts, simple size effects. As shown in Figure 7, SS_{crit} for OA is
474 lower than for thin malonic acid coatings, probably because of the surface tension
475 effect, but higher than for thick MA coatings, because of the missing solute effect.

476 The CCN activity of all oleic coated particles is higher than the CCN activity of pure
477 oleic acid. Our CCN activity measurement showed that pure oleic acid particles up to
478 333 nm did not activate at 0.87% SS; this sets an upper limit for CCN activity of oleic

479 acid particles ($\kappa < 0.0005$), in agreement with Kumar et al. (2003) and Broekhuizen et
480 al. (2004). In liquid state oleic acid (OA) forms micelle like structures, the hydrophilic
481 ends (the carboxyl groups) of oleic acid molecules tend to combine together by
482 hydrogen bonds and the hydrophobic tails (the hydrocarbon chains) are exposed at the
483 outside (Iwahashi et al., 2000; Garland et al., 2008). The arrangement of oleic acid
484 molecules in pure oleic acid particles should be similar. Hydrophobic tails facing
485 outwards can explain the hydrophobicity of the particle surface and the hindrance of
486 the uptake of water, making the CCN activity of pure oleic acid particles very low.
487 For sub-monolayer coatings of OA of v_f 0.8 - 2.7% the CCN activity seem to
488 approach that of pure OA. However, the arrangement of oleic acid molecules in these
489 thin coatings will be influenced by the CaCO_3 core with its polar, hydrophilic sides
490 differing from pure oleic acid particles and can thus be less hydrophobic

491 Even at the largest coating with an organic volume fraction of 44%, the coating
492 thickness is about 10 nm, which corresponds to about only 4 monolayers of oleic acid
493 (assuming the thickness of oleic acid monolayer on CaCO_3 particles is about 2.3 nm).
494 And the arrangement of oleic acid molecules will still be likely influenced by the
495 CaCO_3 core. Water can probably adsorb at the carboxylic groups facing outward
496 (“bilayer” type structure) and diffuse through the thin oleic acid coatings. It may form
497 an adsorbed water phase near the CaCO_3 surface. This could push the oleic acid out to
498 act as surfactant which lowers the Kelvin term. Such processes should also happen in
499 pure oleic acid particles. Because of the presence of CaCO_3 core the SS to achieve
500 this is lower than for pure OA.

501 The phenomenon described above is reported for the first time in the studies on the
502 CCN activity of multicomponent aerosols. This phenomenon also shows a limitation
503 of the otherwise very useful mixing rule (Petters and Kreidenweis, 2007) for
504 multicomponent aerosols with specific morphologies.

505 In Fig. 5 we additionally show the influence of water vapor on CCN activity of
506 CaCO_3 particles coated with oleic acid for the highest coating temperature (80 °C)
507 and thus largest oleic acid amount. Herein we determined D_{crit} at different
508 super-saturations (SS_{crit}) for *poly-disperse* CaCO_3 aerosol particles (by SMCA). The
509 experiments were performed at RH 0.3% and at RH 3% at the coating temperature of
510 80 °C on cooling to room temperature the RH increased to 47%. The presence of
511 more water vapor (1500 Pa) in the coating process increased κ somewhat and
512 enhanced the CCN activity. This is of importance since often RH will larger than 0.3%
513 if coating appears in the atmosphere. This will be discussed further in context of
514 malonic acid coatings at enhanced water vapor.

515 **3.3 CCN activity of CaCO_3 particles with malonic acid coating**

516 For the study with malonic acid coatings, the CaCO_3 particles were also size selected
517 with a diameter of 101.8 nm. The size D_p and chemical composition of CaCO_3 aerosol
518 particles are listed in Table 1 before and after coating with malonic acid (MA) at
519 temperatures in a range of 30-80 °C. The mode diameter did not shift after coating in a
520 temperature range of 30-60 °C, but it increased for coatings at 70 and 80 °C with
521 increasing coating temperature. The size bin interpolated particle diameter D_p of the

522 MA coated particles increased monotonically with the coating temperature. The
523 average of the interpolated diameter of bare CaCO₃ particles in the temperature range
524 30°C-80°C was $d_u = 101.9$ nm.

525 Values of the malonic acid marker $m/z42$ per particle were significantly larger for
526 CaCO₃ particles after coating at 30-80 °C and the MA mass increased from $3.3 \cdot 10^{-12}$
527 to $610 \cdot 10^{-12}$ ug per particle with the coating temperature (Table 1, Figure 3, bottom
528 panel). The organic volume fraction vf of malonic acid ($V_{MA}/(V_{MA}+V_{CaCO_3})[\%]$) was
529 calculated as in the case of the oleic acid and ranged from 0.4 to 40%. As for oleic
530 acid the malonic acid experiments were repeated at least four times and the
531 reproducibility and stability were good (see standard deviations in Table 1).

532 The activated fractions at different SS for 101.9 nm CaCO₃ particles before and after
533 coating with malonic acid at 30-80 °C are shown in Fig. 6. SS_{crit} was determined by
534 fitting a sigmoidal function to the data and the κ value was calculated from the
535 $D_p(D_{crit})$ and the corresponding SS_{crit} . The results are listed in Table 1. In this
536 procedure we had to neglect the contribution of double charged particles as the step in
537 the CN/CCN vs SS data in Fig.6 is not sufficiently expressed to separate a plateau for
538 multiply charged particles (e.g. Sullivan et al. 2009). The exception is the MA coating
539 with $vf = 0.04\%$. For this case we compared a sigmoidal fitting both from the
540 beginning (the first point) and from the multiply-charged plateau (the third point) to
541 the “completely-activated plateau” (Figure S3, supplement). We yield $SS_{crit} =$
542 $0.887 \pm 0.005\%$ for fitting from the beginning and $SS_{crit} = 0.900 \pm 0.013\%$ for fitting

543 from the multiply-charged plateau, a difference of 0.013%. The underestimate in SS_{crit}
544 is the largest (0.013%) when the MA mass is the smallest ($vf = 0.04\%$) and the
545 underestimate will be reduced with increasing vf of MA. At the largest two MA vf it
546 can be neglected. We have to concede a systematic error in SS_{crit} , but it is distinctively
547 less than 0.02%

548 The κ values of the $CaCO_3$ particles after coating with malonic acid at 30-80 °C were
549 higher than the κ value of the uncoated $CaCO_3$ particles ($\kappa = 0.0028 \pm 0.0001$), and
550 increased with the increasing coating MA mass per particle and increasing MA vf .
551 The CCN activity of the $CaCO_3$ particles increased monotonically after coating with
552 increasing malonic acid mass. This result differs from that of oleic acid which is not
553 surprising since malonic acid is easily soluble in water.

554 The κ value for the $CaCO_3$ particles after coating with a mass of malonic acid as small
555 as $3.3 \cdot 10^{-12}$ ug per particle and vf of MA of only 0.4% was 0.0123 ± 0.0005 thus
556 considerably larger than the κ value for the uncoated $CaCO_3$ particles ($\kappa = 0.0028 \pm$
557 0.0001). This suggests that already a small amount of malonic acid can significantly
558 enhance the CCN activity of $CaCO_3$ particles. Such phenomenon, that traces of water
559 soluble substances can strongly affect droplet activation has been reported before
560 (Bilde and Svenningsson, 2004).

561 We applied Koehler theory to $CaCO_3$ particles coated with malonic acid assuming
562 that the malonic acid coating will fully dissolve in water when droplets form (see
563 supplement eq. (S1-S3). Increasing MA solute decreases the activity of water in

564 solution, and lowers the critical supersaturation SS_{crit} for droplet activation.

565 The resulting Koehler curves, i.e. equilibrium supersaturation (SS) over the solution
566 droplet as a function of the wet diameter D_w , are shown in Figure S2. Therein the
567 maximum of each SS curve is the critical supersaturation (theory SS_{crit}). In Table S1
568 and Figure 7 we compare the SS_{crit} predicted by the Köhler approach (red) with the
569 observed SS_{crit} (black). Koehler theory overpredicts SS_{crit} for thin coatings
570 substantially, meaning it underestimates the hygroscopicity of the thinly coated
571 particles. But with increasing coating Koehler theory approaches the observed SS_{crit}
572 and SS_{crit} for a particle of 121 nm diameter composed of pure malonic acid is the
573 limiting case (red circle).

574 From the Koehler results we derived the water content of the particles at SS_{crit} and we
575 calculated molality and mass fraction of the solute in the solution at the point of
576 activation. The molality at minimum and maximum malonic acid load of $3.3 \cdot 10^{-12}$
577 $\mu\text{g}/\text{particle}$ and $610 \cdot 10^{-12}$ $\mu\text{g}/\text{particle}$ were $0.006 \text{ mol kg}^{-1}$ and $0.0015 \text{ mol kg}^{-1}$,
578 respectively. We used these values in the AIOMFAC model (Zuend et al. 2011) to
579 calculate the deviation from ideality for the solution at point of activation for a flat
580 solution. The both solutions are highly non-ideal with respect to the MA ($a_x = 0.4$),
581 wherein MA was treated as solute with reference state infinite dilution (mole fraction
582 $x_{solute} \rightarrow 0$). However this did not affect much the activity coefficient of water, which
583 is essentially 1, water treated as solvent with reference state pure liquid (mole fraction
584 $x_{water} = 1$). Moreover, in this concentration range, the surface tension of aqueous

585 malonic acid solutions is about 0.070 J m^{-2} , thus the nearly same as for water (Table
586 S2 in the supplement). One should expect that Koehler theory would predict SS quite
587 well under such conditions.

588 To bring Köhler theory in agreement with the observation for the thinnest coating,
589 *more* solute entities would be required. Thus, disagreement cannot be caused by an ill
590 determined van't Hoff factor as we used already maximum $\nu = 3$ and reducing ν will
591 increase the deviation. Note, that recent observations point to the importance of the
592 surface effect by organic surface films over the solute effect for water soluble
593 inorganics in presence of organics, including malonic acid (Ruehl et al., 2016). A
594 lower surface tension will bring Koehler prediction and observation punctually in
595 better agreement and still allow for smaller van't Hoff factors. As an example, a
596 surface tension of 55% of σ_w and a van't Hoff factor of one will bring SS_{crit} predicted
597 by Koehler theory and observation in agreement for the thinnest coating. However, a
598 surface tension 55% of σ_w will cause disagreement for the thickest coating, because
599 the solute term gains in importance. Probably, the findings for the mixed solutions of
600 malonic acid and water soluble ammonium sulfate are not directly transferable to our
601 systems with insoluble inorganic core, where we expect dilute aqueous solutions of
602 0.006 mol/kg of malonic acid at the activation point. At such concentrations malonic
603 acid does not reduce σ_w , moreover in the study of Ruehl et al. (2016) malonic acid
604 was one of the more Koehler κ behaving organics.

605 In Figure 7 we show the prediction of $SS_{crit}=1.52\%$ for activating CaCO_3 by the

606 Kelvin/FHH theory with the CaCO_3 parameters taken from Kumar et al. (2009). SS_{crit}
607 for our bare CaCO_3 particles is 1.49% and the lower SS_{crit} should be due to a more
608 adsorptive surface, e.g. the presence of $\text{Ca(OH)(HCO}_3\text{)}$ structures. According to
609 classical Koehler theory the equivalent of $8.5 \cdot 10^{-20}$ moles of dissolvable entities
610 would be needed to explain a κ of 0.0028 and SS_{crit} of 1.49%, which is only about $\frac{1}{4}$
611 of the moles MA in the thinnest MA coating. Therefore, whatever makes our CaCO_3
612 particles wettable is not sufficient to explain the low SS_{crit} of 0.9 % at the thinnest MA
613 coating - in terms of Koehler theory.

614 We estimate monolayer coverage by MA at 2-3% vf; this would be achieved in
615 between MA mass loads of $13 \cdot 10^{-12}$ - $38 \cdot 10^{-12}$ ug per particle. Thus a sub-monolayer
616 coating of $3.3 \cdot 10^{-12}$ ug MA per particle caused a drop of SS_{crit} from 1.49 to 0.9 and
617 increased κ from 0.0028 to 0.012. Therefore we conclude that CaCO_3/MA coatings
618 show a non-Koehler behavior at thin coatings, but approach Koehler behavior with
619 increasing MA load.

620 This means there must be specific interactions between MA and the CaCO_3 surface
621 which eases water adsorption and CCN activation. We refer to the $\text{Ca(OH)(HCO}_3\text{)}$
622 structures that likely exist on the particle surface. When CaCO_3 particles are coated by
623 malonic acid (or oleic acid) the hydrophilic sides can serve as polar surface active
624 sites for accommodation of the acids. In case of MA there is no long hydrophobic
625 organic chain, but a second carboxylic group which still could support the adsorption
626 of water films.

627 In terms of Kelvin/FHH theory one could explain the observed low SS_{crit} for thin MA
628 coatings by net stronger interaction with water (higher A_{FHH}) and/or stronger
629 interaction between the adsorbed water layers (lower B_{FHH}) compared to bare $CaCO_3$.
630 If coatings become thicker the Koehler solute effect starts increasingly to contribute
631 and eventually controls the CCN activation. Our data are not sufficient to determine
632 A_{FHH} and B_{FHH} . (The only system in the literature which comes close - in a far sense -
633 is CaOxalate Monohydrate, with $A_{FHH} = 0.57$ and $B_{FHH} = 0.88$ (Kumar et al., 2009).
634 Plug in these FHH parameters will lead to $SS_{crit} = 0.53\%$ commensurable with our
635 observed value of 0.56% for $13 \cdot 10^{-12}$ ug MA coating which represents an organic
636 volume fraction of 1.6% , thus is close to monolayer.)

637 The D_{crit} at different super-saturations (SS_{crit}) for *poly-disperse* $CaCO_3$ aerosol
638 particles before and after coating with malonic acid are shown in Fig. 8. Our
639 observation of $\kappa = 0.25 \pm 0.04$ for pure malonic is consistent with the κ derived from
640 the data of Kumar et al. (2003) ($\kappa = 0.20-0.25$) and Prenni et al. (2001) ($\kappa = 0.24$), but
641 significantly lower than the κ derived from the data of Giebl et al. (2002) ($\kappa =$
642 $0.41-1.04$). The behavior of poly-disperse coated aerosol was similar to the result
643 obtained from the monodisperse $CaCO_3$ aerosol particles.

644 In Fig. 8 we added results for coating in presence of enhanced water vapor (1500 Pa)
645 and aerosols generated by spraying mixtures of malonic acid and $CaCO_3$. At the
646 coating temperature of $60^\circ C$, when the RH increased from 0.7% to 7% and eventually
647 to 47% at room temperature, the CCN activity of the coated $CaCO_3$ particles

648 increased substantially (compare “dry” (blue triangles) and “wet” (lilac triangles) in
649 Fig. 8). The effect is more distinct than for the oleic acid coating shown in Fig. 5, and
650 κ increases by about an order of magnitude. At a wet conditions, the reaction between
651 CaCO_3 and malonic acid maybe more efficient and formation of calcium malonate
652 will reduce d_u , i.e. the diameter of the insoluble core and according to eq, (S1) this
653 may be the reason for the higher CCN activity at the higher RH. The hypothesis of
654 malonate formation is supported by the CCN activity of “calcium malonate” aerosols,
655 generated by spraying solutions containing CaCO_3 and malonic acid with molar ratios
656 of about 1:1 and 3:1. Here the CCN activity is similar to that arising in the coating
657 process in presence of water vapor. The change of the Ca/malonate ratio from 3:1 to
658 1:1 had no large effects. But taking the data of pure malonic acid particles also into
659 account there is a trend to lower κ with increasing Ca in the initial solution.

660 The increasing of residence time (by 23.7 s) had no significant impact on CCN
661 activity for both oleic acid coating and malonic acid coating at both dry and enhanced
662 water vapor conditions, probably because the coating process was already completed
663 in the coating device and no further reactions occurred in the flow tube.

664 Our findings may be important for aging processes of mineral particles in the
665 atmosphere. The dependence of CCN activity of the coated particles on RH during the
666 coating process will help to enhance the increase of the CCN activity by the coating
667 process as water will be abundant in many instances. The effect probably will be
668 relatively small for oleic acid and similar organics, which are hardly water soluble,

669 but strong for malonic acid and similar organic acids, which are highly water soluble.

670 **4 Conclusions**

671 The CCN activity of CaCO₃ particles with oleic acid and malonic acid coatings was
672 investigated in this study. The results show that oleic acid coating and malonic acid
673 coating have different impacts on the CCN activity of CaCO₃ particles. This can be
674 attributed to the amphiphilic property of oleic acid in contrast to the high water
675 solubility of malonic acid. Small amounts of oleic acid coating ($vf \leq 4.3\%$) decreased
676 the CCN activity of the CaCO₃ particles, while more oleic acid coating ($vf \geq 16\%$)
677 increased it. This phenomenon was reported here for the first time, and attributed to
678 stepwise passivating the active sites of CaCO₃ by oleic acid. Once all active sites are
679 occupied we suggest the formation of a lipid like bilayer with the carboxylic groups
680 facing outwards.

681 On the other hand, malonic acid coating (0.4-40%) increased the CCN activity of
682 CaCO₃ particles regardless of the amount of the coating. The CCN activity of CaCO₃
683 particles with malonic acid coating increased with the amount of the coating. Even a
684 small amount of malonic acid coating ($vf = 0.4\%$) significantly enhanced the CCN
685 activity of CaCO₃ particles from $\kappa = 0.0028 \pm 0.0001$ to $\kappa = 0.0123 \pm 0.0005$.
686 Increasing the relative humidity during the coating increased the CCN activity of the
687 CaCO₃ particles with malonic acid coating, probably because more CaCO₃ reacted
688 with malonic acid to soluble CaMalonate. This process will help to increase the CCN
689 activity.

690 Although malonic acid is well soluble in water, SS_{crit} for MA coated particles was
691 overpredicted by Köhler theory. Our results indicate that thin MA coatings provide a
692 wettable particle surface, which favors adsorption of water. For thicker coatings the
693 coated particles approached Köhler behavior, because of increasing importance of the
694 solute effect.

695 Mineral aerosol is one of the most abundant components of the atmospheric aerosol,
696 but its low water solubility limits its CCN activity. This study showed that
697 water-soluble organic acid coating might significantly enhance the CCN activity of
698 mineral aerosol particles. This could lead to mineral aerosol playing a more important
699 role in cloud formation.

700

701 **Acknowledgments**

702 This study was supported by Forschungszentrum Jülich, the National Natural Science
703 Foundation Committee of China (41421064, 21190051, 41121004), and the China
704 Scholarship Council.

705

706

707 **References**

- 708 AIOMFAC model, <http://www.aiomfac.caltech.edu>
- 709 Broekhuizen, K. E., Thornberry, T., Kumar, P. P., and Abbatt, J. P. D.: Formation of cloud
710 condensation nuclei by oxidative processing: Unsaturated fatty acids, *J. Geophys.*
711 *Res.-Atmos.*, 109, D24206, 10.1029/2004jd005298, 2004.
- 712 Cakmur, R. V., Miller, R. L., Perlwitz, J., Geogdzhayev, I. V., Ginoux, P., Koch, D., Kohfeld,
713 K. E., Tegen, I., and Zender, C. S.: Constraining the magnitude of the global dust cycle by
714 minimizing the difference between a model and observations, *J. Geophys. Res.-Atmos.*, 111,
715 D06207, 10.1029/2005jd005791, 2006.
- 716 Charbouillot, T., Gorini, S., Voyard, G., Parazols, M., Brigante, M., Deguillaume, L., Delort,
717 A. M., and Mailhot, G.: Mechanism of carboxylic acid photooxidation in atmospheric
718 aqueous phase: Formation, fate and reactivity, *Atmos. Environ.*, 56, 1-8,
719 10.1016/j.atmosenv.2012.03.079, 2012.
- 720 Chebbi, A. and P. Carlier (1996). "Carboxylic acids in the troposphere, occurrence, sources,
721 and sinks: A review." *Atmospheric Environment* 30(24): 4233-4249.
- 722 Cheng, Y., Li, S. M., Leithead, A., Brickell, P. C., and Leitch, W. R.: Characterizations of
723 cis-pinonic acid and n-fatty acids on fine aerosols in the Lower Fraser Valley during Pacific
724 2001 Air Quality Study, *Atmos. Environ.*, 38, 5789-5800, 10.1016/j.atmosenv.2004.01.051,
725 2004.
- 726 Chumpitaz, L. D. A., Coutinho, L. F., and Meirelles, A. J. A.: Surface tension of fatty acids
727 and triglycerides, *J. Am. Oil Chem. Soc.*, 76, 379-382, 10.1007/s11746-999-0245-6, 1999.
- 728 Cruz, C. N., and Pandis, S. N.: A study of the ability of pure secondary organic aerosol to act
729 as cloud condensation nuclei, *Atmos. Environ.*, 31, 2205-2214,
730 10.1016/s1352-2310(97)00054-x, 1997.
- 731 Dalirian, M., Ylisirniö, A., Buchholz, A., Schlesinger, D., Ström, J., Virtanen, A., and
732 Riipinen, I.: Cloud droplet activation of black carbon particles coated with organic
733 compounds of varying solubility, *Atmos. Chem. Phys. Discuss.*, 2017, 1-25,
734 10.5194/acp-2017-1084, 2017.
- 735 DeCarlo, P. F., Kimmel, J. R., Trimborn, A., Northway, M. J., Jayne, J. T., Aiken, A. C.,
736 Gonin, M., Fuhrer, K., Horvath, T., Docherty, K. S., Worsnop, D. R., and Jimenez, J. L.:
737 Field-deployable, high-resolution, time-of-flight aerosol mass spectrometer, *Anal. Chem.*, 78,
738 8281-8289, 10.1021/ac061249n, 2006.
- 739 Falkovich, A. H., Ganor, E., Levin, Z., Formenti, P., and Rudich, Y.: Chemical and
740 mineralogical analysis of individual mineral dust particles, *J. Geophys. Res.-Atmos.*, 106,
741 18029-18036, 10.1029/2000jd900430, 2001.
- 742 Falkovich, A. H., Schkolnik, G., Ganor, E., and Rudich, Y.: Adsorption of organic
743 compounds pertinent to urban environments onto mineral dust particles, *J. Geophys.*
744 *Res.-Atmos.*, 109, D02208, 10.1029/2003jd003919, 2004.

745 Gantt, B., Xu, J., Meskhidze, N., Zhang, Y., Nenes, A., Ghan, S. J., Liu, X., Easter, R., and
746 Zaveri, R.: Global distribution and climate forcing of marine organic aerosol - Part 2: Effects
747 on cloud properties and radiative forcing, *Atmos. Chem. Phys.*, 12, 6555-6563,
748 10.5194/acp-12-6555-2012, 2012.

749 Garimella, S., Huang, Y. W., Seewald, J. S., and Cziczo, D. J.: Cloud condensation nucleus
750 activity comparison of dry- and wet-generated mineral dust aerosol: the significance of
751 soluble material, *Atmos. Chem. Phys.*, 14, 6003-6019, 10.5194/acp-14-6003-2014, 2014.

752 Garland, E. R., Rosen, E. P., Clarke, L. I., and Baer, T.: Structure of submonolayer oleic acid
753 coverages on inorganic aerosol particles: evidence of island formation, *Phys. Chem. Chem.
754 Phys.*, 10, 3156-3161, 10.1039/b718013f, 2008.

755 Giebl, H., Berner, A., Reischl, G., Puxbaum, H., Kasper-Giebl, A., and Hitzemberger, R.:
756 CCN activation of oxalic and malonic acid test aerosols with the University of Vienna cloud
757 condensation nuclei counter, *J. Aerosol Sci.*, 33, 1623-1634, Pii s0021-8502(02)00115-5,
758 10.1016/s0021-8502(02)00115-5, 2002.

759 Gierlus, K. M., Laskina, O., Abernathy, T. L., and Grassian, V. H.: Laboratory study of the
760 effect of oxalic acid on the cloud condensation nuclei activity of mineral dust aerosol, *Atmos.
761 Environ.*, 46, 125-130, 10.1016/j.atmosenv.2011.10.027, 2012.

762 Hartz, K. E. H., Tischuk, J. E., Chan, M. N., Chan, C. K., Donahue, N. M., and Pandis, S. N.:
763 Cloud condensation nuclei activation of limited solubility organic aerosol, *Atmos. Environ.*,
764 40, 605-617, 10.1016/j.atmosenv.2005.09.076, 2006.

765 Hatch, C. D., Gierlus, K. M., Schuttlefield, J. D., and Grassian, V. H.: Water adsorption and
766 cloud condensation nuclei activity of calcite and calcite coated with model humic and fulvic
767 acids, *Atmos. Environ.*, 42, 5672-5684, 10.1016/j.atmosenv.2008.03.005, 2008.

768 Haywood, J., and Boucher, O.: Estimates of the direct and indirect radiative forcing due to
769 tropospheric aerosols: A review, *Reviews of Geophysics*, 38, 513-543,
770 10.1029/1999rg000078, 2000.

771 Herich, H., Tritscher, T., Wiacek, A., Gysel, M., Weingartner, E., Lohmann, U.,
772 Baltensperger, U., and Cziczo, D. J.: Water uptake of clay and desert dust aerosol particles at
773 sub- and supersaturated water vapor conditions, *Phys. Chem. Chem. Phys.*, 11, 7804-7809,
774 10.1039/b901585j, 2009.

775 Ho, K. F., Cao, J. J., Lee, S. C., Kawamura, K., Zhang, R. J., Chow, J. C., and Watson, J. G.:
776 Dicarboxylic acids, ketocarboxylic acids, and dicarbonyls in the urban atmosphere of China,
777 *J. Geophys. Res.-Atmos.*, 112, D22s27, 10.1029/2006jd008011, 2007.

778 Ho, K. F., Lee, S. C., Ho, S. S. H., Kawamura, K., Tachibana, E., Cheng, Y., and Zhu, T.:
779 Dicarboxylic acids, ketocarboxylic acids, alpha-dicarbonyls, fatty acids, and benzoic acid in
780 urban aerosols collected during the 2006 Campaign of Air Quality Research in Beijing
781 (CAREBeijing-2006), *J. Geophys. Res.-Atmos.*, 115, D19312, 10.1029/2009jd013304, 2010.

782 Hori, M., Ohta, S., Murao, N., and Yamagata, S.: Activation capability of water soluble
783 organic substances as CCN, *J. Aerosol Sci.*, 34, 419-448, 10.1016/s0021-8502(02)00190-8,

784 2003.

785 Iwahashi, M., Kasahara, Y., Matsuzawa, H., Yagi, K., Nomura, K., Terauchi, H., Ozaki, Y.,
786 and Suzuki, M.: Self-diffusion, dynamical molecular conformation, and liquid structures of
787 n-saturated and unsaturated fatty acids, *J. Phys. Chem. B*, 104, 6186-6194,
788 10.1021/jp000610l, 2000.

789 Kawamura, K., and Ikushima, K.: Seasonal-changes in the distribution of dicarboxylic-acids
790 in the urban atmosphere, *Environ. Sci. Technol.*, 27, 2227-2235, 10.1021/es00047a033, 1993.

791 Kawamura, K., Kasukabe, H., and Barrie, L. A.: Source and reaction pathways of
792 dicarboxylic acids, ketoacids and dicarbonyls in arctic aerosols: One year of observations,
793 *Atmos. Environ.*, 30, 1709-1722, 10.1016/1352-2310(95)00395-9, 1996.

794 Kawamura, K., and Bikkina, S.: A review of dicarboxylic acids and related compounds in
795 atmospheric aerosols: Molecular distributions, sources and transformation, *Atmospheric*
796 *Research*, 170, 140-160, 10.1016/j.atmosres.2015.11.018, 2016.

797 Keiser, E. H., and Leavitt, S.: On the preparation and the composition of the acid carbonates
798 of calcium and barium, *J. Am. Chem. Soc.*, 30, 1711-1714, 10.1021/ja01953a008, 1908.

799 Khare, P., et al. (1999). "Atmospheric formic and acetic acids: An overview." *Reviews of*
800 *Geophysics* 37(2): 227-248.

801 King, M. D., Rennie, A. R., Thompson, K. C., Fisher, F. N., Dong, C. C., Thomas, R. K.,
802 Pfrang, C., and Hughes, A. V.: Oxidation of oleic acid at the air-water interface and its
803 potential effects on cloud critical supersaturations, *Phys. Chem. Chem. Phys.*, 11, 7699-7707,
804 10.1039/b906517b, 2009.

805 Koehler, H.: The nucleus in and the growth of hygroscopic droplets, *Trans. Faraday Soc.*, 32,
806 1152-1161, 10.1039/tf9363201152, 1936.

807 Koehler, K. A., Kreidenweis, S. M., DeMott, P. J., Petters, M. D., Prenni, A. J., and Carrico,
808 C. M.: Hygroscopicity and cloud droplet activation of mineral dust aerosol, *Geophys. Res.*
809 *Lett.*, 36, L08805, 10.1029/2009gl037348, 2009. Kumar, P. P., Broekhuizen, K., and Abbatt,
810 J. P. D.: Organic acids as cloud condensation nuclei: Laboratory studies of highly soluble and
811 insoluble species, *Atmos. Chem. Phys.*, 3, 509-520, 2003.

812 Kumar, P. P., Broekhuizen, K., and Abbatt, J. P. D.: Organic acids as cloud condensation
813 nuclei: Laboratory studies of highly soluble and insoluble species, *Atmos. Chem. Phys.*, 3,
814 509-520, 2003.

815 Kumar, P., Nenes, A., and Sokolik, I. N.: Importance of adsorption for CCN activity and
816 hygroscopic properties of mineral dust aerosol, *Geophys. Res. Lett.*, 36,
817 10.1029/2009gl040827, 2009.

818 Li, W. J., and Shao, L. Y.: Mixing and water-soluble characteristics of particulate organic
819 compounds in individual urban aerosol particles, *J. Geophys. Res.-Atmos.*, 115, D02301,
820 10.1029/2009jd012575, 2010.

821 Liu, X. H., and Wang, J. A.: How important is organic aerosol hygroscopicity to aerosol

822 indirect forcing?, *Environ. Res. Lett.*, 5, 044010, 10.1088/1748-9326/5/4/044010, 2010.

823 Mkoma, S. L., and Kawamura, K.: Molecular composition of dicarboxylic acids,
824 ketocarboxylic acids, alpha-dicarbonyls and fatty acids in atmospheric aerosols from
825 Tanzania, East Africa during wet and dry seasons, *Atmos. Chem. Phys.*, 13, 2235-2251,
826 10.5194/acp-13-2235-2013, 2013.

827 Moore, R. H., Nenes, A., and Medina, J.: Scanning Mobility CCN Analysis-A Method for
828 Fast Measurements of Size-Resolved CCN Distributions and Activation Kinetics, *Aerosol*
829 *Sci. Technol.*, 44, 861-871, 10.1080/02786826.2010.498715, 2010.

830 Neagle, W., and Rochester, C. H., Infrared study of the adsorption of water and ammonia on
831 calcium carbonate. *Journal of the Chemical Society, Faraday Transactions*, 86, 181-183,
832 1990.

833 Penner, J. E., Dong, X. Q., and Chen, Y.: Observational evidence of a change in radiative
834 forcing due to the indirect aerosol effect, *Nature*, 427, 231-234, 10.1038/nature02234, 2004.

835 Petters, M. D., and Kreidenweis, S. M.: A single parameter representation of hygroscopic
836 growth and cloud condensation nucleus activity, *Atmos. Chem. Phys.*, 7, 1961-1971, 2007.

837 Rogge, W. F., Hildemann, L. M., Mazurek, M. A., Cass, G. R., and Simoneit, B. R. T.:
838 Sources of fine organic aerosol .2. Noncatalyst and catalyst-equipped automobiles and
839 heavy-duty diesel trucks, *Environ. Sci. Technol.*, 27, 636-651, 10.1021/es00041a007, 1993.

840 Rogge, W. F., Hildemann, L. M., Mazurek, M. A., Cass, G. R., and Simoneit, B. R. T.:
841 Sources of fine organic aerosol. 9. Pine, oak and synthetic log combustion in residential
842 fireplaces, *Environ. Sci. Technol.*, 32, 13-22, 10.1021/es960930b, 1998.

843 Rose, D., Gunthe, S. S., Mikhailov, E., Frank, G. P., Dusek, U., Andreae, M. O., and Pöschl,
844 U.: Calibration and measurement uncertainties of a continuous-flow cloud condensation
845 nuclei counter (DMT-CCNC): CCN activation of ammonium sulfate and sodium chloride
846 aerosol particles in theory and experiment, *Atmos. Chem. Phys.*, 8, 1153-1179, 2008.

847 Rühl, C. R., Davies, J. F., and Wilson, K. R.: An interfacial mechanism for cloud droplet
848 formation on organic aerosols, *Science*, 351, 1447-1450, 10.1126/science.aad4889, 2016.

849 Russell, L. M., Maria, S. F., and Myneni, S. C. B.: Mapping organic coatings on atmospheric
850 particles, *Geophys. Res. Lett.*, 29, 1779, 10.1029/2002gl014874, 2002.

851 Sage, A. M., Weitkamp, E. A., Robinson, A. L., and Donahue, N. M.: Reactivity of oleic acid
852 in organic particles: changes in oxidant uptake and reaction stoichiometry with particle
853 oxidation, *Phys. Chem. Chem. Phys.*, 11, 7951-7962, 10.1039/b904285g, 2009.

854 Schauer, J. J., Kleeman, M. J., Cass, G. R., and Simoneit, B. R. T.: Measurement of emissions
855 from air pollution sources. 1. C-1 through C-29 organic compounds from meat charbroiling,
856 *Environ. Sci. Technol.*, 33, 1566-1577, 10.1021/es980076j, 1999.

857 Sorjamaa, R., and Laaksonen, A.: The effect of H₂O adsorption on cloud drop
858 activation of insoluble particles: a theoretical framework, *Atmos. Chem. Phys.*, 7, 6175-6180,
859 10.5194/acp-7-6175-2007, 2007.

860 Stipp, S. L. S.: Toward a conceptual model of the calcite surface: hydration, hydrolysis, and
861 surface potential. *Geochimica et Cosmochimica Acta*, 63, 3121-3131, 1999.

862 Stipp, S. L., Hochella Jr, M. F.: Structure and bonding environments at the calcite surface as
863 observed with X-ray photoelectron spectroscopy (XPS) and low energy electron diffraction
864 (LEED). *Geochimica et Cosmochimica Acta*, 55, 1723-1736, 1991.

865 Sullivan, R. C., Moore, M. J. K., Petters, M. D., Kreidenweis, S. M., Roberts, G. C., and
866 Prather, K. A.: Effect of chemical mixing state on the hygroscopicity and cloud nucleation
867 properties of calcium mineral dust particles, *Atmos. Chem. Phys.*, 9, 3303-3316,
868 10.5194/acp-9-3303-2009, 2009.

869 Sullivan, R. C., Moore, M. J. K., Petters, M. D., Kreidenweis, S. M., Qafoku, O., Laskin, A.,
870 Roberts, G. C., and Prather, K. A.: Impact of Particle Generation Method on the Apparent
871 Hygroscopicity of Insoluble Mineral Particles, *Aerosol Sci. Technol.*, 44, 830-846,
872 10.1080/02786826.2010.497514, 2010.

873 Takegawa, N., Miyakawa, T., Kawamura, K., and Kondo, Y.: Contribution of selected
874 dicarboxylic and omega-oxocarboxylic acids in ambient aerosol to the m/z 44 signal of an
875 aerodyne aerosol mass spectrometer, *Aerosol Sci. Technol.*, 41, 418-437,
876 10.1080/02786820701203215, 2007.

877 Tang, M. J., Cziczo, D. J., and Grassian, V. H.: Interactions of Water with Mineral Dust
878 Aerosol: Water Adsorption, Hygroscopicity, Cloud Condensation, and Ice Nucleation,
879 *Chemical Reviews*, 116, 4205-4259, 10.1021/acs.chemrev.5b00529, 2016.

880 Tang, M. J., Whitehead, J., Davidson, N. M., Pope, F. D., Alfarra, M. R., McFiggans, G., and
881 Kalberer, M.: Cloud condensation nucleation activities of calcium carbonate and its
882 atmospheric ageing products, *Phys. Chem. Chem. Phys.*, 17, 32194-32203,
883 10.1039/c5cp03795f, 2015.

884 Yamashita, K., Murakami, M., Hashimoto, A., and Tajiri, T.: CCN Ability of Asian Mineral
885 Dust Particles and Their Effects on Cloud Droplet Formation, *Journal of the Meteorological
886 Society of Japan*, 89, 581-587, 10.2151/jmsj.2011-512, 2011.

887 Zhao, D. F., Buchholz, A., Mentel, T. F., Muller, K. P., Borchardt, J., Kiendler-Scharr, A.,
888 Spindler, C., Tillmann, R., Trimborn, A., Zhu, T., and Wahner, A.: Novel method of
889 generation of Ca(HCO₃)₂ and CaCO₃ aerosols and first determination of hygroscopic
890 and cloud condensation nuclei activation properties, *Atmos. Chem. Phys.*, 10, 8601-8616,
891 10.5194/acp-10-8601-2010, 2010.

892 Zuend, A., Marcolli, C., Booth, A. M., Lienhard, D. M., Soonsin, V., Krieger, U. K., Topping,
893 D. O., McFiggans, G., Peter, T., and Seinfeld, J. H.: New and extended parameterization of
894 the thermodynamic model AIOMFAC: calculation of activity coefficients for
895 organic-inorganic mixtures containing carboxyl, hydroxyl, carbonyl, ether, ester, alkenyl,
896 alkyl, and aromatic functional groups, *Atmospheric Chemistry and Physics*, 11, 9155-9206,
897 10.5194/acp-11-9155-2011, 2011.

Table 1. Mode diameters, chemical compositions, and κ values of CaCO₃ aerosol particles (size selected by DMA at 101.8 nm) before (uncoated) and after coating with oleic (OA) or malonic acid (MA) at 30-80 °C.

	D_p [nm]	Organic mass per particle [10 ⁻¹² μg]	Mole organics per particle [10 ⁻²⁰ mole]	Org. volume fraction [%]	κ
Oleic acid					
Uncoated CaCO₃ 30-80 °C	101.9	(backgr. <i>m/z</i> 41: 2.7±0.9)	0	0.0	0.0028±0.0001
CaCO₃+Oleic acid 30 °C	102.1	3.7±1.9	1.3	0.8	
CaCO₃+Oleic acid 40 °C	102.5	7.0±2.8	2.5	1.4	
CaCO₃+Oleic acid 50 °C	103.7	14±3.7	5.1	2.7	
CaCO₃+Oleic acid 60 °C	104.9	23±1.2	8.3	4.3	
CaCO₃+Oleic acid 70 °C	109.2	96±3.7	34	16	0.0241±0.0006
CaCO₃+Oleic acid 80 °C	123.7	390±14	140	44	0.0649±0.0008
Malonic acid					
Uncoated CaCO₃ 30-80 °C	101.9	(backgr. <i>m/z</i> 42: 1.4±0.4)	0	0.0	0.0028±0.0001
CaCO₃+Malonic acid 30 °C	102.0	3.3±0.3	3.2	0.4	0.0123±0.0005
CaCO₃+Malonic acid 40 °C	102.1	6.8±1.2	6.5	0.8	0.0231±0.0008
CaCO₃+Malonic acid 50 °C	102.2	13±1.8	13	1.5	0.0380±0.0012
CaCO₃+Malonic acid 60 °C	102.7	38±1.6	36	4.1	0.1063±0.0023
CaCO₃+Malonic acid 70 °C	107.8	160±8.1	160	15	0.1907±0.0031
CaCO₃+Malonic acid 80 °C	121.0	610±24	590	40	0.3126±0.0062

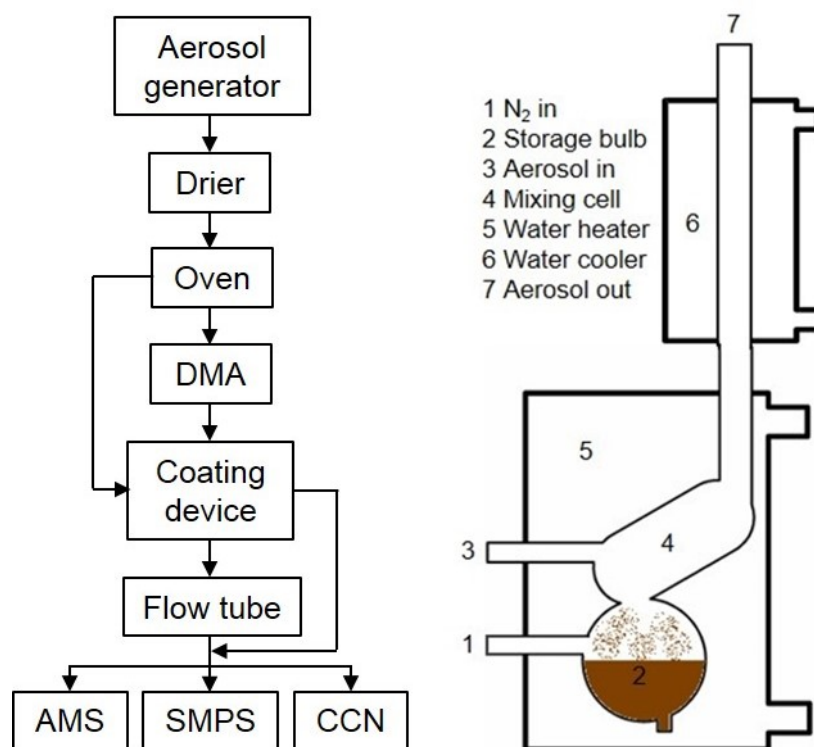


Figure 1. Schematics of the experimental set up (left side). CaCO_3 aerosol is generated by spray-drying of saturated $\text{Ca}(\text{HCO}_3)_2$ solutions and tempering the aerosol passing through an oven at 300°C . The *poly-disperse* CaCO_3 aerosol is either led directly to the coating device (right side, after Roselli, 2006) or led to a differential mobility Analyzer (DMA) for size selection first. Optional, a flow tube can be switched into the pass to enhance the reaction time of the coated particles. The stream of coated particles is finally split to the analytical instruments, namely aerosol mass spectrometer (AMS), scanning mobility particle sizer (SMPS) and CCN counter.

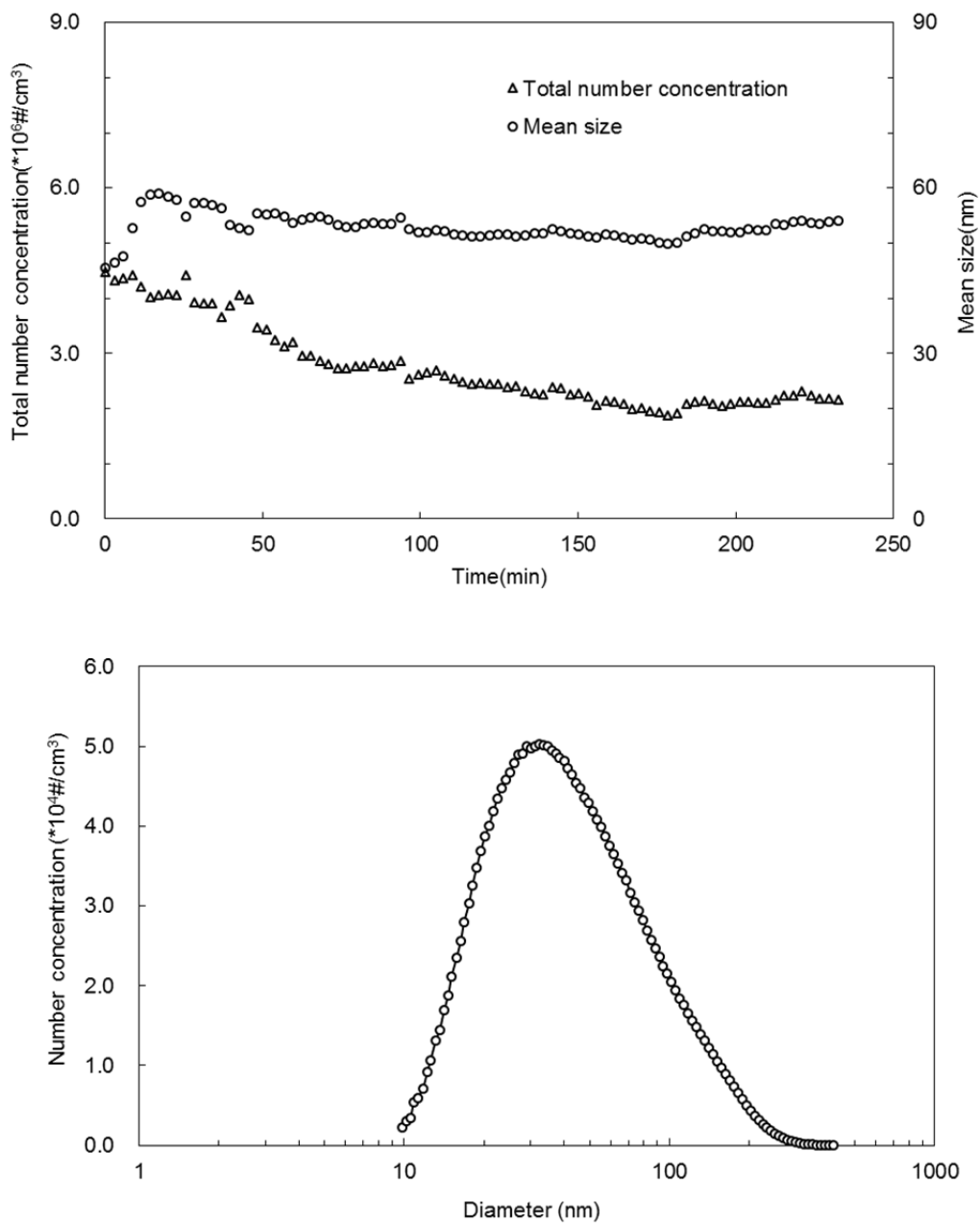


Figure 2. Total number concentration and mean diameter of CaCO₃ aerosol particles generated as a function of the spraying time (upper panel). Typical size distribution of the CaCO₃ aerosol after 70 min spraying (lower panel).

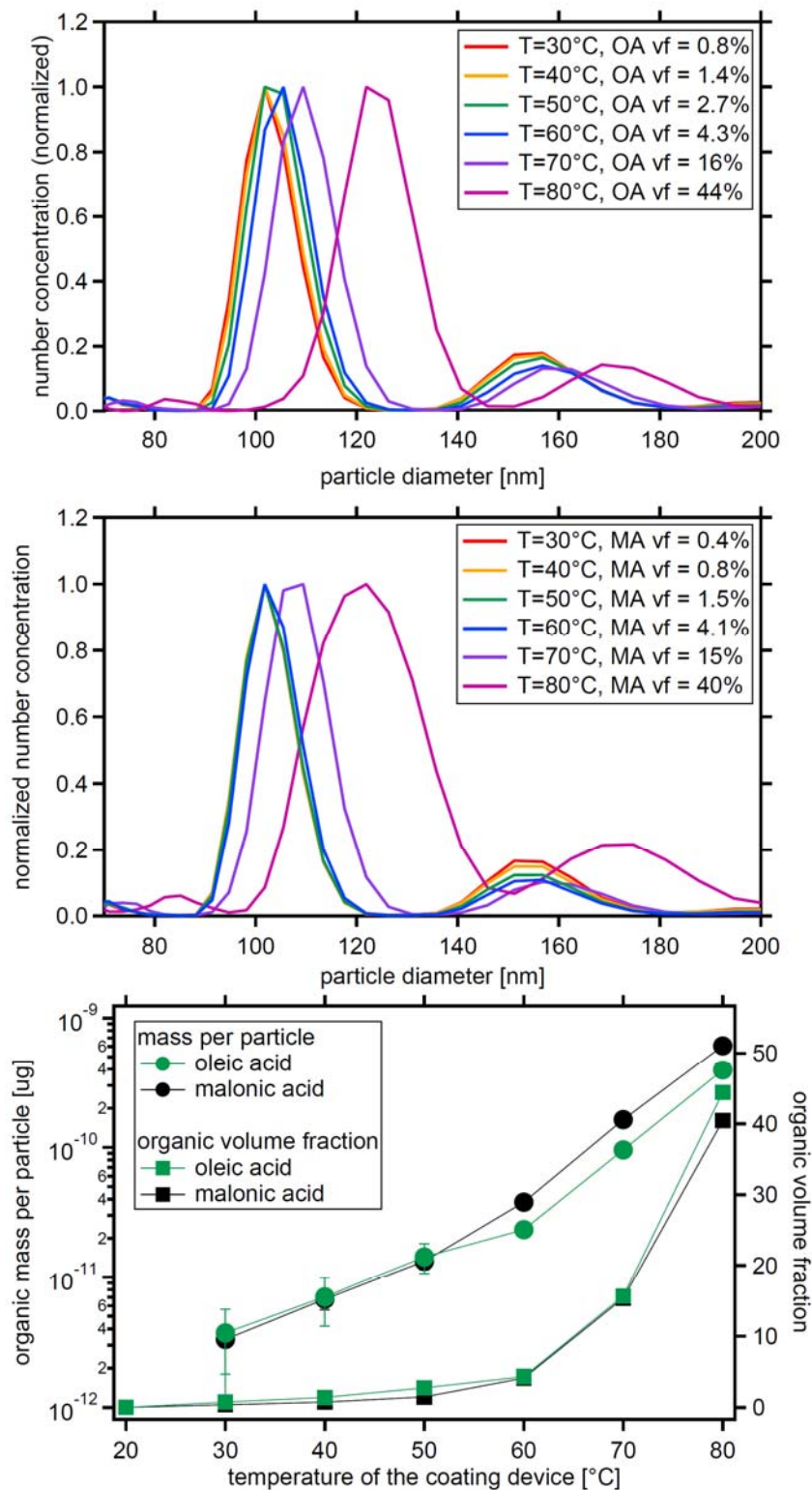


Figure 3. Size distribution of monodisperse CaCO_3 aerosol particles after coating with oleic acid (top panel) or malonic acid (middle panel). Coating amount and organic volume fraction for oleic and malonic acid as a function of the coating temperature for the same experiments (bottom panel, data in Table 1).

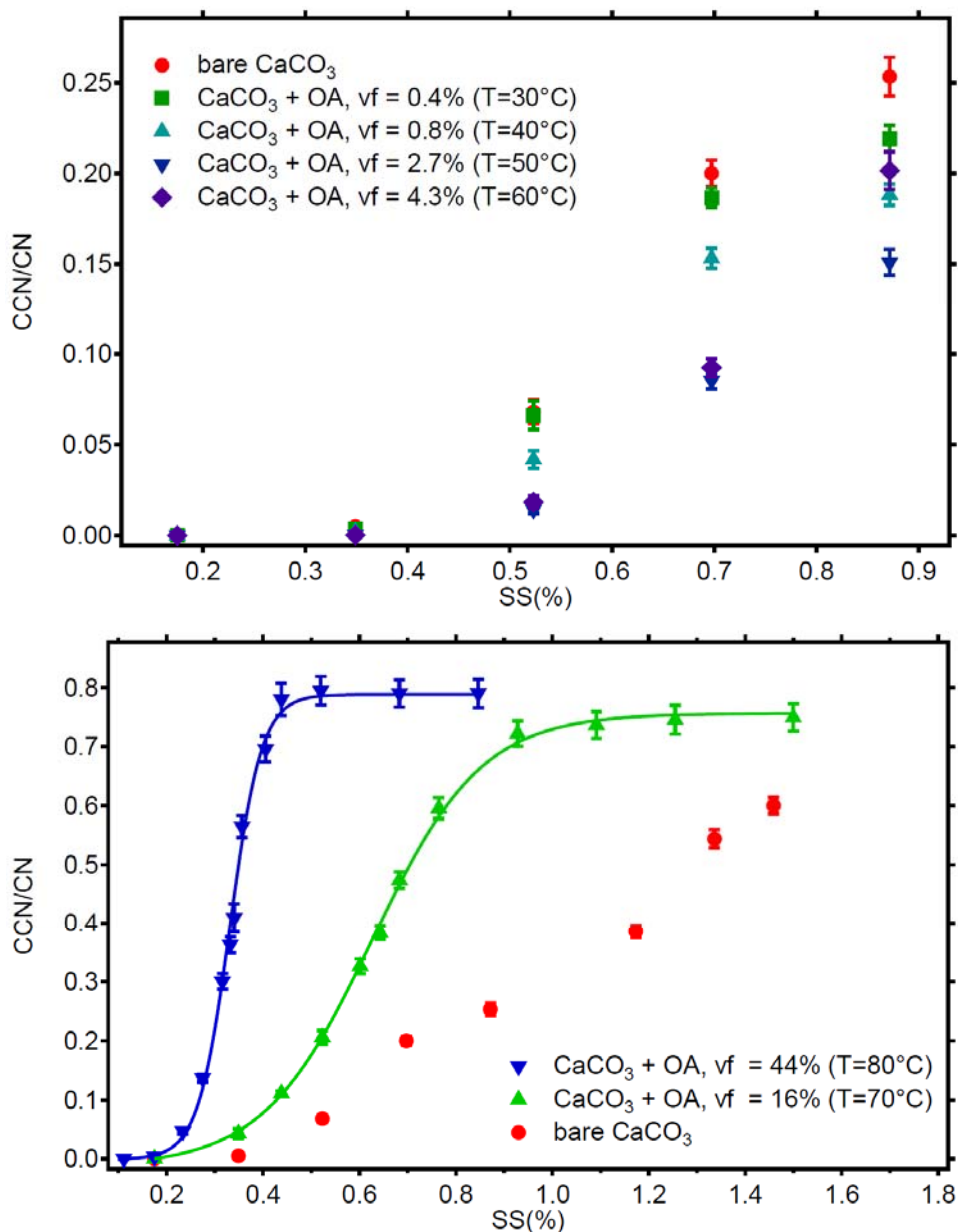


Figure 4. Activated fractions (CCN/CN) of *monodisperse* CaCO₃ aerosol particles (diameter $d_u = 101.9$ nm) at different supersaturations before and after oleic acid coating. With increasing coating temperatures of 30-50 °C the activated fraction decreases despite the increase of organic vf from 0.8% - 2.7%. At vf = 4.3% at 60°C this trend turns. Considering the invariant particle diameter at 30-50 °C, the increased particle diameter at 60 °C, and the reduced activated fraction simultaneously, the CCN activity of the coated CaCO₃ particles at 30-60 °C was lower than that of the uncoated CaCO₃ particles (top panel). At coating vf of 16% and 44% (T= 70-80 °C) the activated fractions, thus CCN activities, are higher than for bare CaCO₃ and increase with coating vf. In these two cases all particles are activated at the highest SS and SS_{crit} and κ can be determined from the turning point of the sigmoidal fit (bottom panel, compare Table 1).

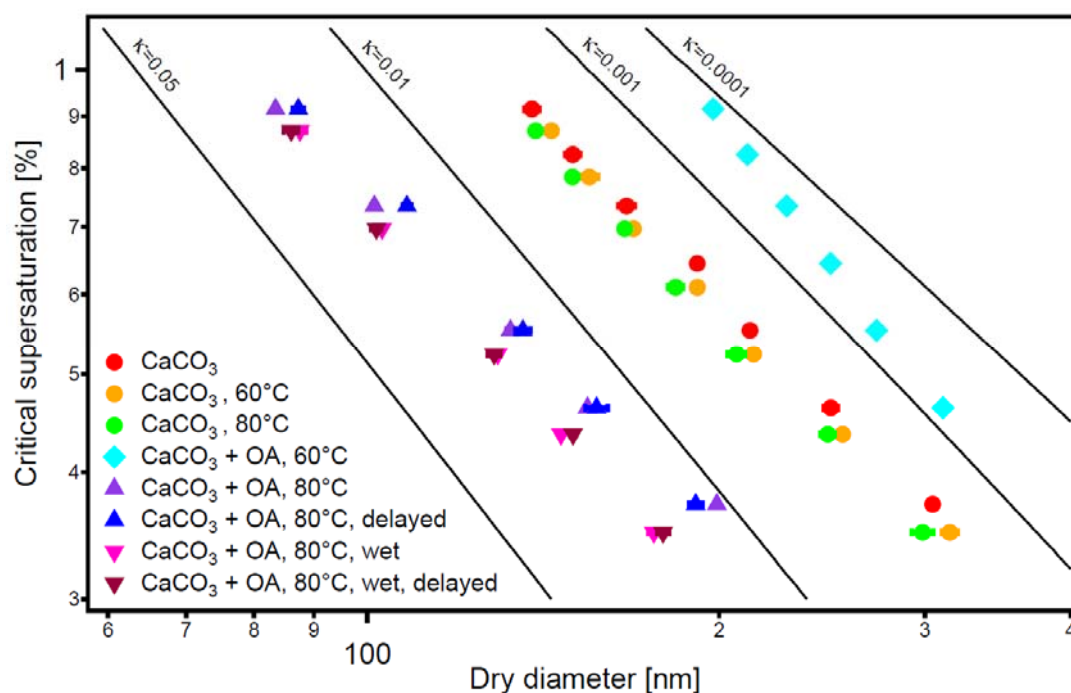


Figure 5. Critical dry diameters at different supersaturations (SS) of *poly-disperse* CaCO₃ aerosol before (circles) and after oleic acid coating. Experiments were performed at 60°C (turquoise diamond) and 80°C (triangles) coating temperatures. The flow tube experiments at 80° C were performed (indicated by ‘delayed’) at dry conditions (normal, blue triangles) and at enhanced water vapor (‘wet’, brown triangles). The effect of the temperature in the coating device on the CaCO₃ core is negligible (red, green, and orange circles). As for the monodisperse case in Figure 4, at 60° coating temperature the particles are less CCN active than bare CaCO₃ while at 80°C the coated particle more CCN active. The presence of water vapor (1500 Pa) in the coating process enhances CCN activity. The increasing of residence time (23.7 s) of the coated aerosol in the flow tube had no significant effect on CCN activity in both experiments.

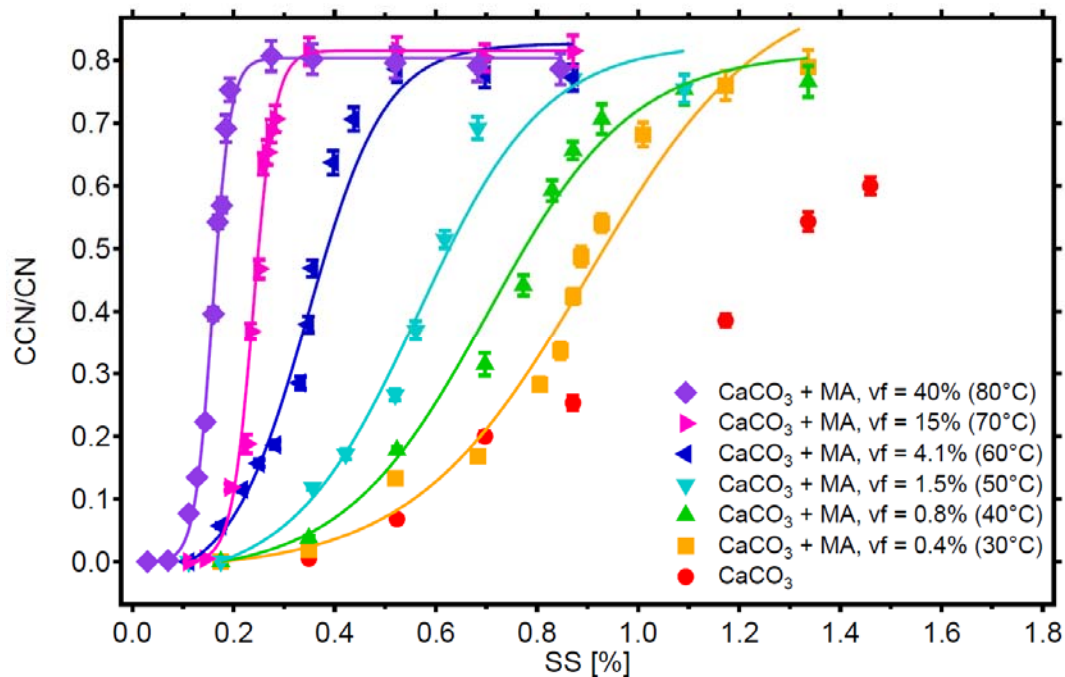


Figure 6. Activated fractions (CCN/CN) of *monodisperse* $CaCO_3$ aerosol particles (with $CaCO_3$ core, $d_u = 101.9$ nm) at different supersaturations before (red circles) and after malonic acid coating. With increasing coating, i.e. MA volume fraction vf the activated fraction, thus CCN activity, increase compared to bare $CaCO_3$ particles. All coated particles can be activated at sufficiently high SS and SS_{crit} and κ was determined (see Table 1).

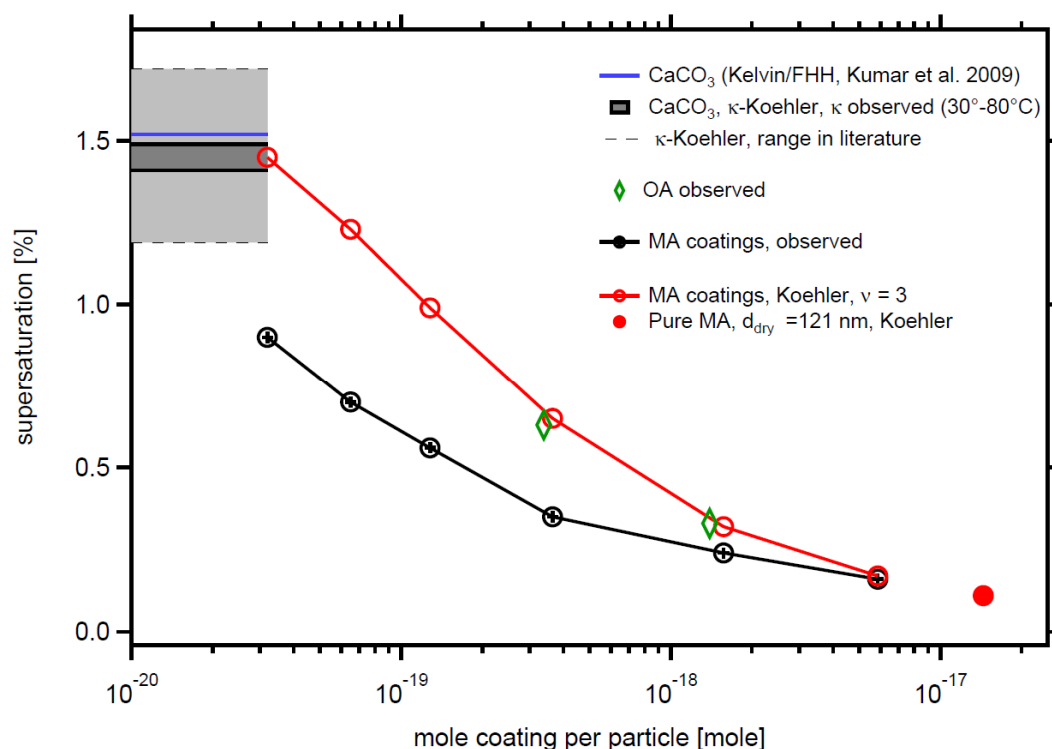


Figure 7: Comparison of SS_{crit} predicted by Koehler theory with observations. Koehler theory for aqueous MA solutions assuming full dissociation overpredicts SS_{crit} (red circles) compared to the observation (black circles). With increasing coating amount Koehler theory approaches the observation, with the limiting SS_{crit} for 121.0 nm particles made of pure malonic acid. For comparison we show observed SS_{crit} for the two thickest OA coatings (diamonds show). The horizontal lines indicate SS_{crit} of the bare CaCO₃ particles as calculated from our observed κ observed (black) and predicted by Kelvin/FFH theory (blue). Light grey area between the thin dashed grey lines shows the range of SS_{crit} for 101.9 nm particles calculated from the range of κ in literature for wet generated CaCO₃ particles (compare Tang et al. 2016).

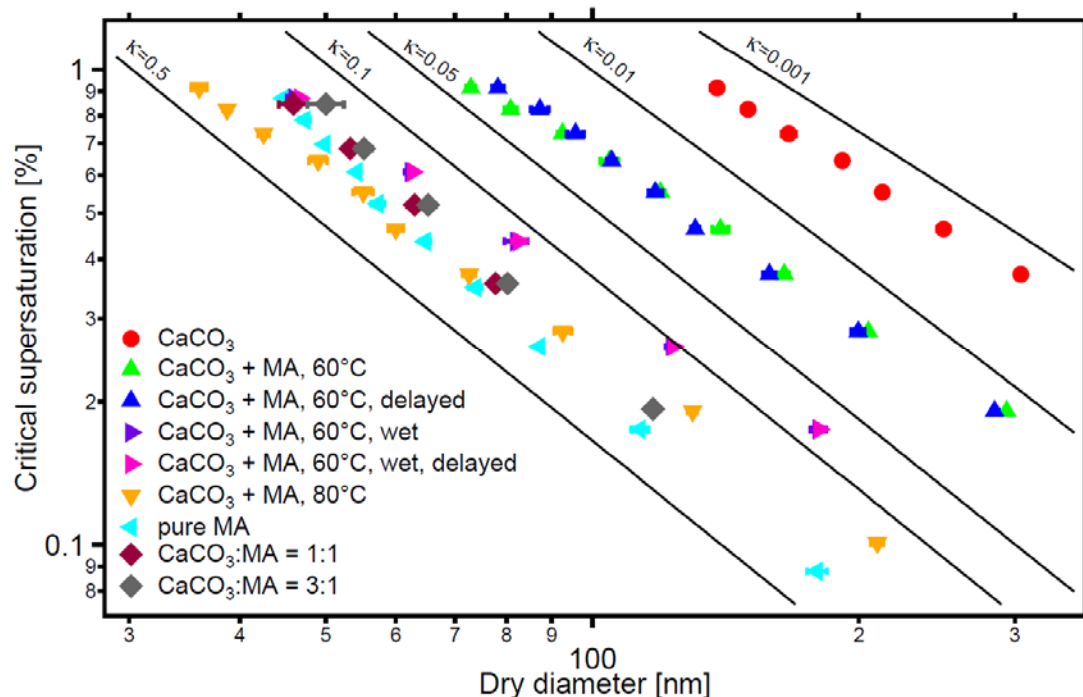


Figure 8. Critical dry diameters at different super-saturations (SS) of *poly-disperse* CaCO_3 aerosol before (circles) and after malonic acid coating (triangles). Experiments were performed at 60°C and 80°C coating temperatures. The results are similar to the monodisperse case in Figure 6. Critical dry diameters as a function of SS are also shown for malonic acid particles and particles that were generated by spraying mixed solution with molar ratios of CaCO_3 /malonic acid of 1:1 and 3:1. The CCN activity decreases with increasing CaCO_3 content. The flow tube experiments at 60 °C were performed (indicated by ‘delayed’) at dry condition (blue triangles) and in presence of 1500 Pa water vapor (magenta triangles). The presence of water in the coating process substantially enhanced κ and CCN activity. The increasing of residence time (23.7 s) of the coated aerosol in the flow tube had no significant effect on CCN activity in both experiments.

Supplement to

**Cloud Condensation Nuclei Activity of CaCO₃ Particles with
Oleic Acid and Malonic Acid Coatings**

**Mingjin Wang^{1,2}, Tong Zhu^{1*}, Defeng Zhao², Florian Rubach^{2,3}, Andreas Wahner²,
Astrid Kiendler-Scharr², and Thomas F. Mentel^{2*}**

¹BIC-ESAT and SKL-ESPCI, College of Environmental Sciences and Engineering, Peking University, Beijing 100871, China.

²Institut für Energie- and Klimaforschung (IEK-8), Forschungszentrum Jülich GmbH, 52425 Jülich, Germany.

³Klimageochemie, Max Planck Institut für Chemie, 55128 Mainz, Germany

* To whom correspondence should be addressed: tzhu@pku.edu.cn; t.mentel@fz-juelich.de

Experimental

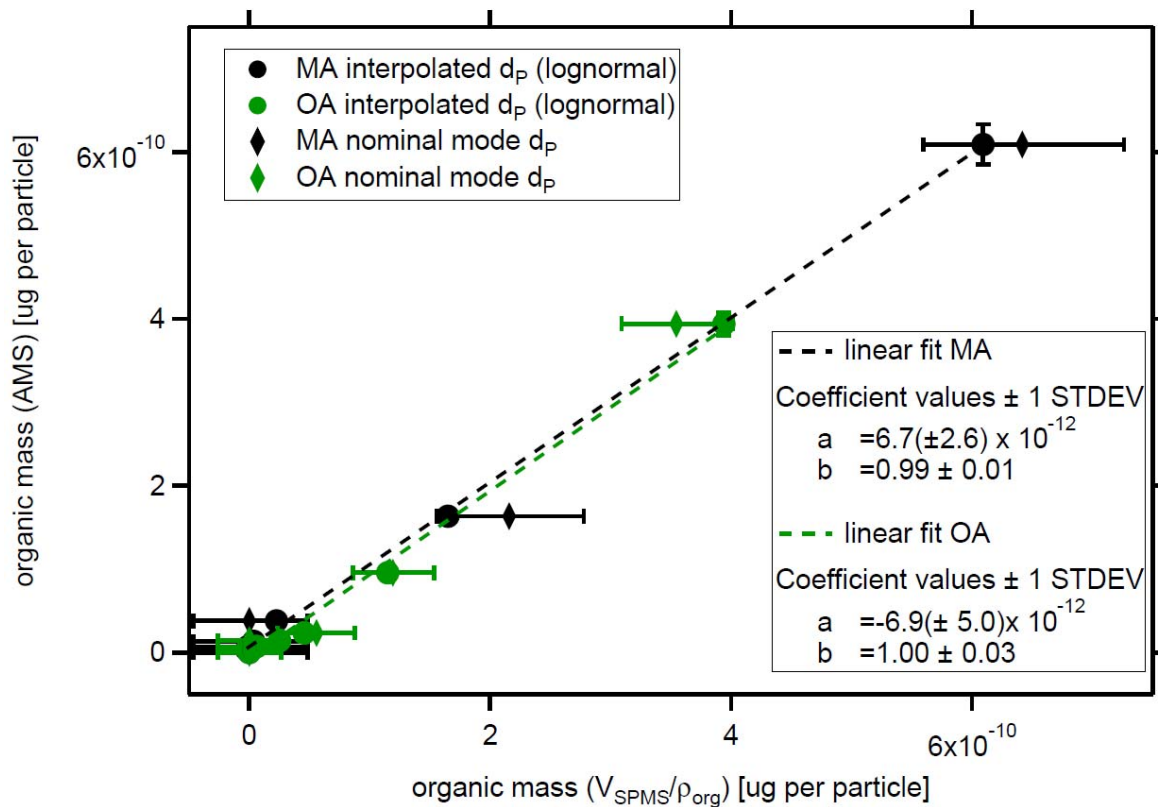


Figure S1: Linear relation between organic mass of the coating derived by AMS measurements and the organic coating mass calculated from the SMPS measurements for oleic acid coatings (green) and maleic acid coatings (black). For full circles the organic mass derived by SMPS was calculated from interpolated mode diameters given in Table 1. Error bars in y direction give the reproducibility of the AMS measurements; error bars in x direction indicate the mass span by considering the SMPS bin width for the respective nominal mode diameter. Note that the highest values must be the same as they were used to calibrate the marker m/z of AMS to the SMPS derived organic mass.

Koehler theory

We assume that at the critical supersaturation (SS_{crit}) the solution is ideal, i.e. water activity coefficient is close to 1, and the partial molar volume of water equals the molar volume of pure water M_w/ρ_w . Since the solubility of $CaCO_3$ in water is very low (0.00058 g/100 g water, at 298 K), while the solubility of malonic acid (MA) is quite high (62 g/100 g water at 298 K), we apply the linearized approach (e.g. Seinfeld and Pandis 2006), to predict the saturation ratio as a function of the mole solute on a insoluble core:

$$\ln\left(\frac{P_w(D_w)}{P^\circ}\right) = \frac{A}{D_p} - \frac{B}{(D_w^3 - d_u^3)} \quad (S1)$$

In this equation A represents the Kelvin effect while B contains the solute effect:

$$A = \frac{4M_w\sigma_w}{RT\rho_w} \cong \frac{0.66}{T} \quad (in \mu m) \quad (S2)$$

$$B = \frac{6n_s M_w}{\pi\rho_w} \cong 3.44 \times 10^{13} v \times n_s \quad (in \mu m^3) \quad (S3)$$

Herein $P_w(D_w)$ is the water vapor pressure over the droplet of diameter D_w ; P° is the water vapor pressure over a flat surface at the same T ; d_u is the diameter of insoluble particle fraction, in our case the $CaCO_3$ core; M_w is water molecular weight; σ_w is the air-water surface tension; ρ_w is the water density; T is in K; R is the universal gas constant; n_s is solute moles = m_s/M_s , with M_s as solute molecular weight. v is the dissociation degree, i.e. the number of ions resulting from the dissociation of one solute molecule.

We neglected the little dissolvable $CaCO_3$ and considered only malonic acid molecules for the dynamic growth. The insoluble $CaCO_3$ core was set to $d_u = 0.1019 \mu m$ as observed. We further assume that $CaCO_3$ doesn't react with malonic acid and that the surface tension of the solution at

activation is that of pure water. The dissociation constants $\text{p}K_{\text{A}1}$ and $\text{p}K_{\text{A}2}$ of MA are 2.8 and 5.7 in water, respectively. So MA will partly dissociate in water and in the limit of infinite dilute solutions the dissociation degree ν (van' Hoff factor) will be three for full dissociation. The moles of malonic acid coating n_s was taken from the AMS data in Table 1 and we applied $\nu = 3$.

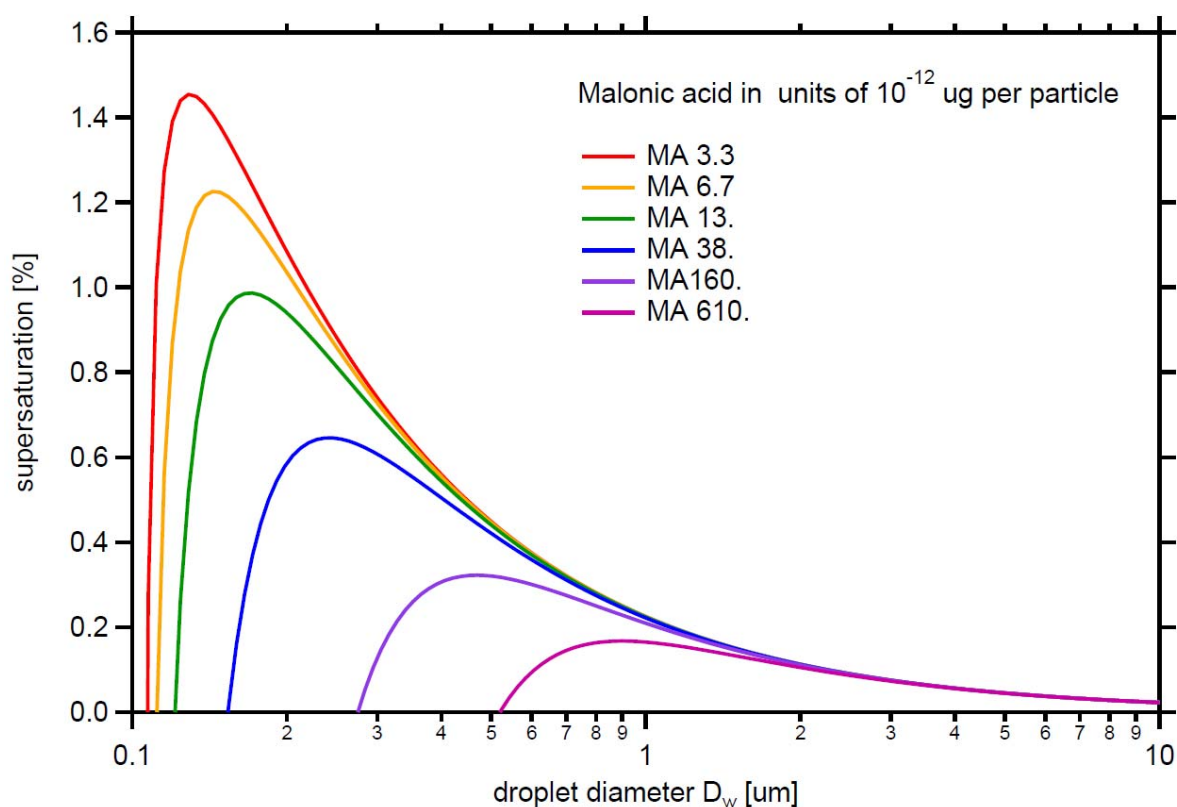


Figure S2. Variation of the equilibrium supersaturation over aqueous solution drops containing CaCO_3 and different mass of malonic acid at 293 K, assuming CaCO_3 is insoluble and doesn't react with malonic acid and the solution is dilute (water activity coefficient is close to 1). The diameter of insoluble CaCO_3 is 101.9 nm.

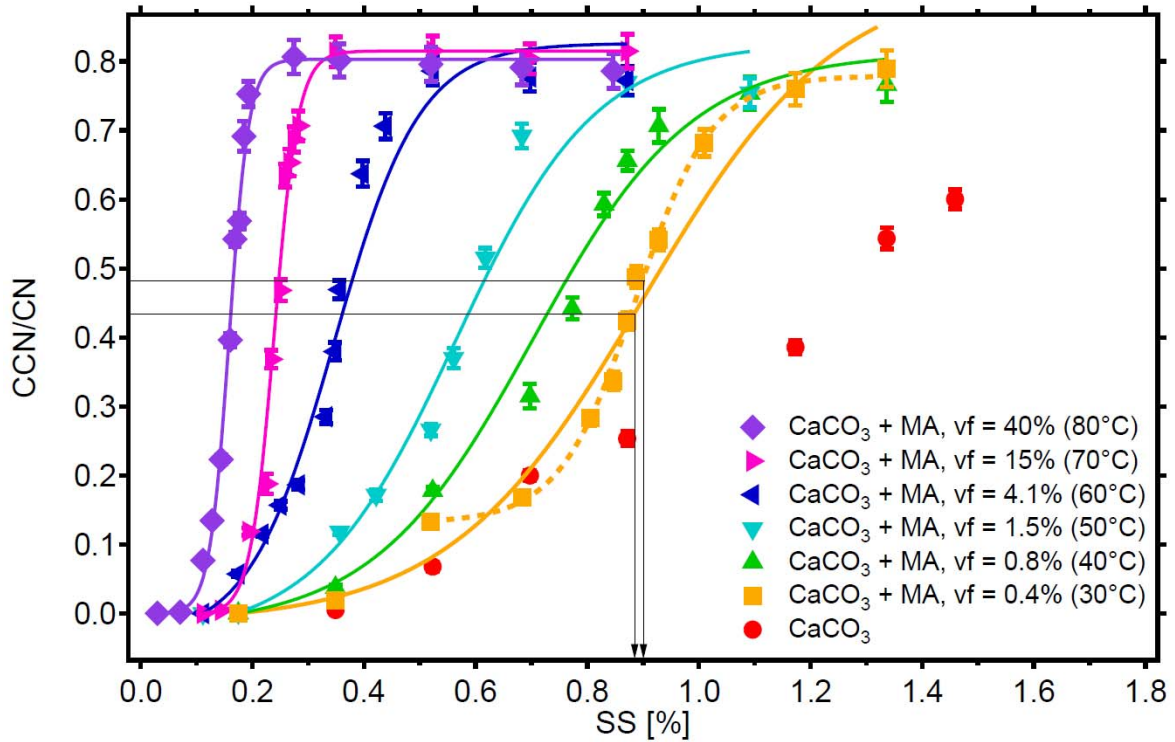


Figure S3: Systematic error introduced by neglecting the contribution of multiple charged particles in determining SS_{crit} by single sigmoidal fits. The multiple charge plateau is best recognizable for the MA coating with the smallest $vf=0.04\%$ (orange). The difference in SS_{crit} considering the plateau (0.900% dashed orange line) and neglecting it (0.887% solid orange line) is only 0.013%. The importance of the effect is largest for the smallest vf and disappears for the largest vf 's.

Table S1. Koehler theory and experimental SS_{crit} and κ values of $CaCO_3$ particles with different mass of MA coating.

Dry diam. (nm)	MA per particle ($\times 10^{-12}$ μg)	Theory SScrit (%)	Experimental SScrit (%)	Theory κ	Experimental κ
102.0	3.3 \pm 0.3	1.44	0.90	0.0024	0.0123 \pm 0.0005
102.1	6.8 \pm 1.2	1.20	0.70	0.0053	0.0231 \pm 0.0008
102.2	13 \pm 1.8	0.97	0.56	0.0107	0.0380 \pm 0.0012
102.7	38 \pm 1.6	0.63	0.35	0.0315	0.1063 \pm 0.0023
107.8	160 \pm 8.1	0.31	0.24	0.1110	0.1907 \pm 0.0031
121.0	610 \pm 24	0.16	0.16	0.3001	0.3126 \pm 0.0062

Table S2. Properties of investigated compounds.

Name	Formula	Molecular weight (g mol ⁻¹)	Density (g cm ⁻³)	Solubility (g/100 g water, at 298K)	Surface tension (dyn/cm)
Calcite	CaCO ₃	100.1	2.71	0.00058	- ^a
Malonic acid	C ₃ H ₄ O ₄	104.1	1.62	62	69 ^b
Oleic acid	C ₁₈ H ₃₄ O ₂	282.5	0.89	Very low	33 ^c

a: no data

b: Surface tension of 0.01 mole fraction malonic acid aqueous solution at 298K

c: Surface tension of pure oleic acid at 293K

Handbook of Chemistry and Physics, the 82nd Edition; Handbook of aqueous solubility data, Samuel H. Yalkowsky and Yan He, 2003; Chumpitaz et al., 1999; Hyvarinen et al., 2006.

Chumpitaz, L. D. A., Coutinho, L. F., and Meirelles, A. J. A.: Surface tension of fatty acids and triglycerides, J. Am. Oil Chem. Soc., 76, 379-382, 10.1007/s11746-999-0245-6, 1999.

Hyvarinen, A. R.; Lihavainen, H.; Gaman, A.; Vairila, L.; Ojala, H.; Kulmala, M.; Viisanen, Y., Surface tensions and densities of oxalic, malonic, succinic, maleic, malic, and cis-pinonic acids. Journal of Chemical and Engineering Data 2006, 51 (1), 255-260.